sciendo

DOI: 10.2478/ahr-2021-0018
Acta hort regiotec, 24, 2021(1): 1–8

Research Article

Influence of infiltration on soil erosion in green infrastructures

Janarul Shaikh[1]*, Sudheer Kumar Yamsani[2], Manash Jyoti Bora[3], Sanjeet Sahoo[1], Sreedeep Sekharan[4], Ravi Ranjan Rakesh[5]
[1]*C.V Raman Global University, Bhubaneswar, Odisha, India*
[2]*National Institute of Technology, Warangal, Telangana, India*
[3]*Indian Institute of Technology Guwahati, Assam, India*
[4]*Indian Institute of Technology Guwahati, Assam, India*
[5]*Bhabha Atomic Research Centre, Mumbai, Maharashtra, India*

Article Details: Received: 2021-01-04 | Accepted: 2021-03-04 | Available online: 2021-05-31

Licensed under a Creative Commons Attribution 4.0 International License

SCREENED BY iThenticate Professional Plagiarism Prevention

Rainwater-induced erosion in green geotechnical infrastructures such as a multilayered landfill cover system (MLCS) is a severe concern in the current era. Although vegetation is a proven measure to control erosion in the MLCS, there are other factors such as infiltration rate which influence the control of the phenomenon. Most of the existing studies are limited to understand influence of vegetation on erosion control or infiltration rate alone. In this study, an attempt is made to incorporate infiltration measurements alongside vegetation cover to understand erosion in surface layer of the MLCS. For this purpose, a pilot MLCS was constructed, and erosion of its surface soil was temporally evaluated through soil loss depth of eroded cover surface under the influence of natural as well as simulated rainfall conditions. Alongside erosion, the amount of vegetated cover was evaluated through photographic image analyses and infiltration rate was measured by mini disk infiltrometer. From the observed results, it is understood that soil erosion and infiltration rate depict a contrasting behaviour with growing vegetation. Antecedent moisture contents were observed to show greater influence on such erosion behaviour which was observed during the testing period. Such studies may be helpful to researchers and practicing engineers for understanding performance of various green geotechnical infrastructures and scheduling the maintenance services to increase the longevity of their layered soil systems.

Keywords: erosion, vegetation, infiltration, surface soil, multilayered landfill cover system

1 Introduction

Rainfall-induced erosion is one of the most important concerns involved with layered soil system of different geotechnical green infrastructures such as a multilayered landfill cover system (MLCS) (Xue et al., 2016). It needs prime attention particularly if environmental influence of uncovered waste is considered (Shaikh et al., 2019a; Yamsani et al., 2017). Shaikh et al. (2021) investigated seepage characteristics of MLCSs under an extreme ponding condition through detailed laboratory column tests and finite-element seepage analyses. Their study suggested that erosion can be controlled by managing surface-water runoff, minimizing seepage flow, and selecting a surface layer material that can withstand anticipated erosive stresses. Swope (1975) studied 24 landfill cover systems in the USA and found that 33% had slight erosion, 40% had moderate erosion, and more than 20% had severe erosion. In the United States of America, most landfill cover system top decks are designed to have an inclination in the range of 2 to 5%, after accounting for settlement, to promote surface runoff (Nyhan, 2005). Based on the literature, slopes flatter than 2% may cause water to be ponded on the surface (Anderson & Stormont, 1997). Slopes greater than 5% likely promote erosion, unless preventive measures are taken (Gross et al., 2002). Excessive erosion or slope instability rises as the cover system inclination increases (Morris & Stormont, 1998). The soil surface should be uniformly graded and sloped at about 3% to prevent ponding of rainwater (Koerner & Daniel, 1997). According to Sherard et al. (1976), erosion potential of soil is primarily a function of the size of soil particles, inter-particle cohesive forces, and velocity of transporting fluid (air or water). Erosion-resistant materials such as soil-gravel mixtures, gravel, riprap,

***Corresponding Author:** Janarul Shaikh, Raman Global University, Bhubaneswar, Odisha, India; e-mail: jshaikh@cvrce.edu.in

and geo-synthetic erosion control materials, may be utilized to help in reducing erosion (Gray & Sotir, 1996). In addition to these, use of asphalt concrete, articulated block systems, construction and demolition wastes, and lightweight manufactured aggregates can also be used (Barnswell & Dwyer, 2012).

Landreth et al. (1991) recommends a minimum cover soil thickness of 900 mm or greater for a few specific types of MLCSs such as evapotranspiration or capillary barrier cover system. The minimum thickness of surface layer is established based on consideration of rooting depth of surface vegetation, anticipated erosion rate, and construction tolerances (Øygarden et al., 1997). For shallow-rooted plants such as certain grasses, a 150 mm thick layer of soil usually provides adequate rooting depth (Zhan et al., 2007). Thus, the minimum thickness of a vegetated surface layer is generally 150 mm (USEPA, 1989). If plants with deeper roots are considered, thickness of topsoil should be increased to accommodate the excess root growth (Blight, 2009). The most common material used to construct the surface layer is locally available topsoil which contains adequate organic matter and plant nutrients (Hoor and Rowe, 2013). It helps to promote growth of vegetation (Khapre et al., 2017). Thus, previous researchers (Schnabel et al., 2012; Song et al., 2017) have had diverse opinions on the relation between erosion and infiltration in vegetated soils. Climatic factors affect the types of vegetation that grow on MLCS surface layers (Bonaparte et al., 2002). Climatic criteria for designing MLCSs may include quantity and seasonal distribution of precipitation, intensity and duration of specific storm events, seasonal temperature variations, depth of frost penetration, quantity of snow melt, wind speed and direction, solar radiation, and humidity (Jarvis et al., 2011). Heavy rainfall for a prolonged period leads to increase in rainwater infiltration and erosion of MLCS (Maqsoud et al., 2011). Drier climate results in shrinkage and desiccation cracks in MLCS surface layer (Landreth et al., 1991). Cracks may also develop due to the effects of freeze-thaw cycles in cold regions (Dune et al., 2011). Repeated cycles of wetting and drying can induce fatigue stress in the geomaterials, thereby deteriorating its performance (Nyhan et al., 1990). As a result, hydraulic conductivity may increase in surface layers because of cracks and root growth (Sinnathamby et al., 2014). The effect of climate change on functioning of MLCS has been rarely investigated from the purview of geotechnical engineering. Most of the existing studies solely discuss the influence of rainfall on surface erosion of vegetated cover soil (Shaikh et al., 2019b) without much emphasis on the infiltration happening simultaneously. Some studies (Gadi et al., 2017; Ghosh et al., 2019) attempted for understanding the infiltration rate through vegetated soils without considering the erosion. Limited studies (Zhang et al., 2014) attempted for evaluating the combined effects of infiltration and vegetation on rain induced erosion of surface soils of the MLCS.

This study attempts to address this issue by monitoring the infiltration of surface soils alongside the vegetation and erosion due to rainfall activity. The prime objective of the study is to access the temporal variation in erosion, infiltration, and vegetation characteristics of surface layer in a pilot Multilayered landfill cover system (MLCS) under natural and controlled rainfall simulation events.

2 Materials and methods

2.1 Study area

As understood from the above-mentioned literature, field monitoring programmes might solve such problems involving MLCS erosion. Hence for this study, a pilot MLCS was constructed in the backyard of the civil engineering department, Indian Institute of Technology Guwahati, India. Configuration and individual layer material of field model were selected in accordance with the

Table 1 Basic characteristics of soils used in the study

Properties	Clayey silt (ML)
Specific gravity	2.65
Hygroscopic water content (%)	5
Saturated hydraulic conductivity (m.s^{-1})	2.9E-8
Specific surface area (m^2.g^{-1})	55
Linear shrinkage (%)	2
Free swell index (%)	10
% mass of gravel (>4.75 mm)	0
% mass of coarse sand (2.0–4.75 mm)	17
% mass of medium sand (0.425–2.0 mm)	16
% mass of fine sand (0.075–0.425 mm)	16
% mass of silt (0.002–0.075 mm)	19
% mass of clay (<0.002mm)	32
Liquid limit (% mass)	42
Plastic limit (% mass)	22
Shrinkage limit (% mass)	21
Plasticity index (%)	20
Optimum moisture content (% mass)	20
Maximum dry density (g.cm^{-3})	1.73
Soil pH value with water (at 28.5 °C)	6.85
Organic content (% mass)	0.48
Cation exchange capacity (meq.100 g^{-1})	8

recommendations of the United States Environmental Protection Agency (USEPA, 1989). Soils used for the MLCS model were locally collected from a nearby hill. The MLCS is made of the conventional layers: hydraulic barrier, drainage system, and surface protection layer along with various geosynthetic inclusions as additional barrier, drainage, and filter layers for superior performance. Locally available hill soil, reddish in colour, was selected for its use as a surface protection layer. Geotechnical characterization of this surface soil was evaluated using standard procedures in the ASTM guidelines (ASTM standard D422-63 (2007); ASTM standard D854 (2014); ASTM standard D5084 (2014); ASTM standard D4318 (2017)), and corresponding results are summarized in Table 1. It was low plastic clayey silt soil (ML according to the Unified soil classification system (ASTM standard D2487, 2017)). This soil would depict moderate infiltration and good resistance to erosion as understood from its plasticity and density characteristics. However, a detailed study would show an exact performance of the surface soil with growing vegetation.

2.2 Experimental set-up

The construction of the pilot cover system, filling up with materials, compacting every layer, erecting rainfall simulator, and installation of weather monitoring systems have been done with extreme care to avoid any kind of experimental errors. The coefficient of uniformity for 100 mm rainfall was found to be around 90% (Shaikh et al., 2019a). About 8,000 kilograms of soils were used for preparing the setup. The usual recommendation of cover slope angle is 3 to 7°, however, to understand the worst probable performance a slope of 10° is adopted in this study. The photograph of operational field set-up under simulated rainfall is presented in Fig. 1. The properties of rainfall simulator are in accordance with Shaikh et al. (2019b). A micro weather station equipped with rain gauge (ECRN 100 high-resolution double-spoon tipping bucket type rain gauge, Meter Group Inc. (2019a)) is installed in the vicinity of field pilot MLCS. The weather monitoring during the test period is summarized in Fig. 2. The rainfall simulation experiments are started after finishing the regular monsoon for understanding the maximum possible erosion scenario.

The surface area is categorized into small grids for quantifying spatial heterogeneity in vegetation growth, infiltration, and soil loss depth. The grid size was selected based on the initial measurements of vegetation and infiltration. Fig. 3. illustrates the layout of 81 locations, where the vegetation percentage, infiltration rate, and eroded depth of soil surface are measured on surface protection layer of MLCS. The vegetation density was measured in accordance with procedures detailed in Gadi et al. (2017) by collecting photographic images of vegetated surface with varying time and processing them with a freeware Image analysis program (Image-J) similar to methods followed by Shaikh et al. (2019b). The infiltration rate was attained through sequential measurements of 150 ml Mini disk infiltrometer (MDI, Meter Group Inc. (2019b)) at every location as mentioned

Figure 1 MLCS test setup during a rainfall simulation event

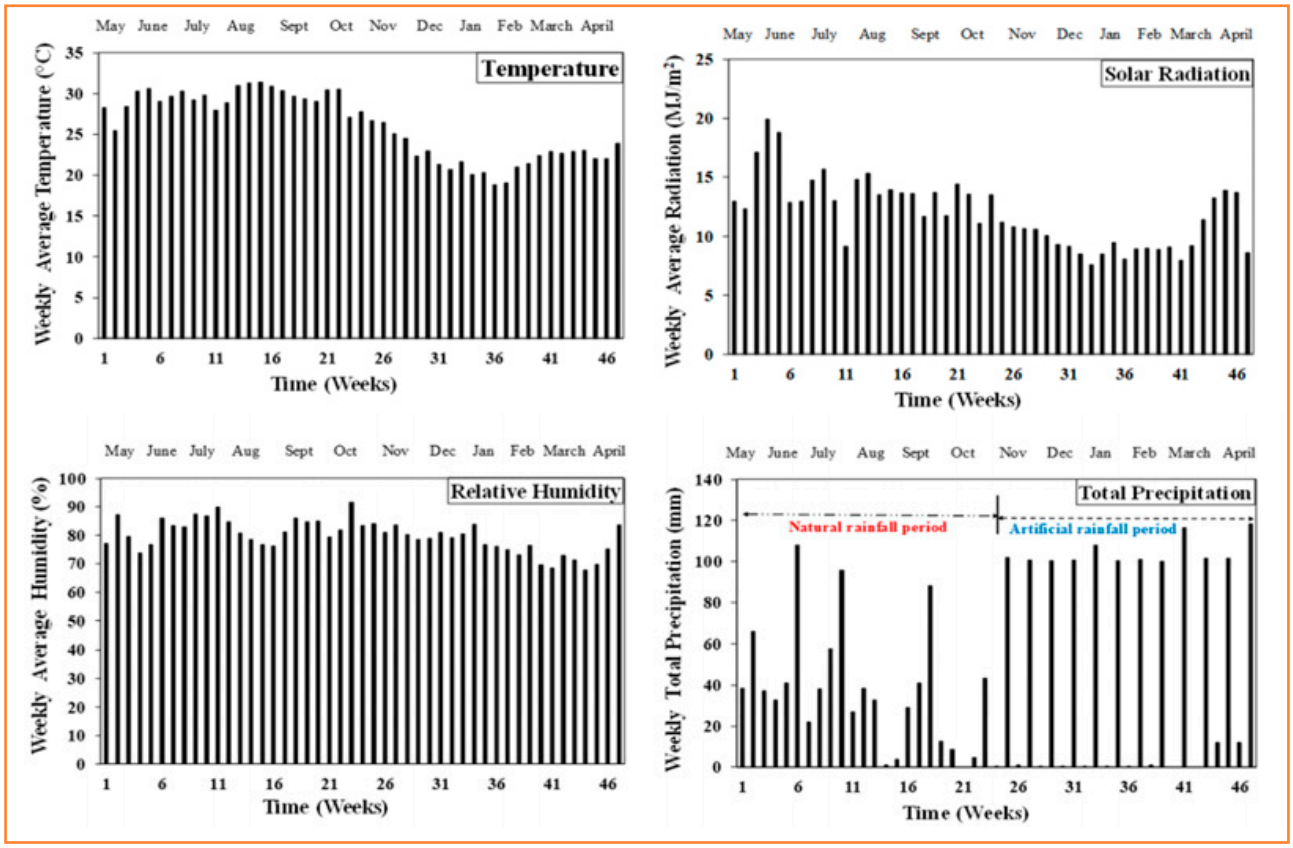

Figure 2 Weather monitoring during the test period monitored using ECRN 100

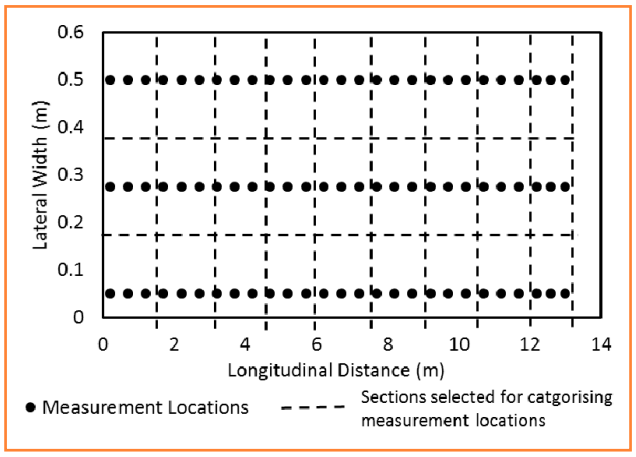

Figure 3 Schematic layout of measurement locations involved in evaluating surface layer

Figure 4 Repeated infiltration measurements around desiccation cracks on surface soil

in the grid. Measurements were repeated in locations with desiccation cracks and increased grass cover, to account for all real field conditions as depicted in Fig. 4. Further, the varying depth of surface is measured using Vernier calipers at different points, to attain a spatial soil loss profile on temporal basis throughout the study period.

3 Results and discussion

3.1 Temporal variation of infiltration, vegetation, and erosion

Fig. 5 depicts the contours describing the temporal variation of infiltration rate, vegetation density, and eroded depth of surface layer of the pilot MLCS under above-shown weather conditions. Though the study was conducted for one year and the data were evaluated

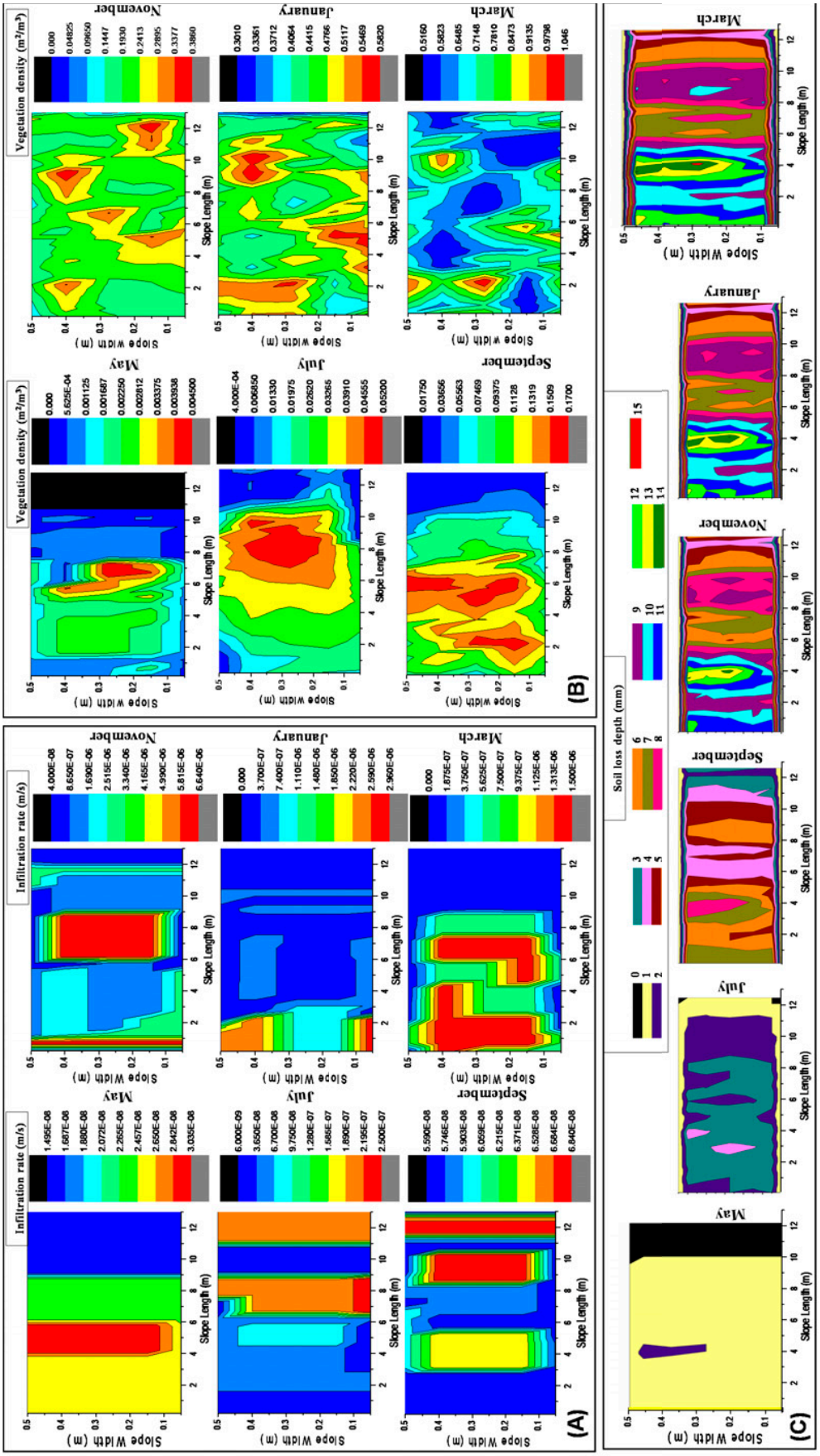

Figure 5 Temporal and spatial variation of infiltration, vegetation, and erosion

on weekly basis, every two-month average results were considered in describing the contours to reduce the number of figures and have a representative picture. From the depicted results it can be observed that within the initial days the amount of infiltration, vegetation density, and eroded depth are relatively low indicating the effect of newly compacted surface layer. Similar results are observed by Shrestha et al. (2005); Bhave and Sreeja (2013); Adams and Smith (2014); Yamsani et al. (2017). The infiltration was observed to vary 6E-09 to 1.5E-06 throughout the study period. The least infiltration was observed in months of July on the surface subjected to intense drying; such a behaviour is expected in general. The variation in infiltration rate for a particular period of time is about tenfold within the considered area of study. Greater degree of variation is observed with growing vegetation. Variation was also observed around the mild cracks generated during the dry spell. However, it was also noted that these mild cracks were found to be closed with high intensity rainfall simulations in the months of November and December. As a result, there is a decrease in corresponding infiltration rate for that particular time.

The eroded depth of soil was observed to vary from 0 to 15 mm within the considered study period accounting to about 5% of the surface soil thickness (300 mm as suggested in USEPA (1989)). Significant amount of erosion was noted during the rainfall simulation period nearly 12 mm, while during natural rainfall only about 6 mm of erosion was observed. The purpose of simulation experiments was to observe the worst possible behaviour of surface soil layer. Fig. 2 depicts only 3 weeks of about 100 mm cumulative precipitation during the natural monsoon, and there were only couple of cloud burst events accounting to about 70 mm rainfall during the natural cycle. Consecutive simulation of 12 cloud burst events has generated about 12 mm depth of soil loss. In this 12 mm of erosion depth, most of it was observed in the early months of July to November. Further, no significant variations in depth of erosion were noticed from months of November to March indicating nearly stable behaviour. Increased vegetation density and reduced climatic variations might be attributed for this stable behaviour which was similar to the observation made by Shaikh et al. (2019b).

3.2 Spatial variation of infiltration, vegetation, and erosion

Early results in Fig. 5, indicate that the infiltration increased with increasing the length of the slope. Infiltration in the toe regions was relatively high owing to the loose soil structure formed as a result of erosion from crest of the slope. In contrast, the vegetation density is relatively low towards the toe region. Thus, the interception (water retention on the plant leaves) was small. Hence, bigger proportion was distributed between infiltration and surface runoff. This significantly influences the variation in runoff as well as the settlement of eroded soil mass. The settled soil mass near the toe region even influenced the eroded depth to indicate a relatively lower value. However, all these variations are evident in initial stages of study, and in later stages, a uniform variation in observed parameters was noted. This could be likely due to the controlled rainfall condition in simulation experiments, relatively uniform weather conditions, and due to increased stability because of enhanced vegetation density in months of November to March. The all-time biggest soil loss depth was seen at the slope length of 4 m. This is likely due to lack of uniformity in compacting the soil of this region or the presence of some foreign loose matter in the soil of this region. The observed low soil loss towards the toe region is likely due to runoff sedimentation.

3.3 Influence of infiltration on erosion of vegetated soil

In general, the runoff and consecutive erosion are observed to be low when infiltration is high. However, the surface dryness was noted to increase infiltration and erosion in the months of July to November due to increased temperatures while the vegetation density was relatively low. And in the later stages of the study, as the vegetation density increased, the water holding capacity of surface soil was observed to increase. Hence, the average infiltration rate in both wet and dry weeks was observed to increase. Such findings were reported in Gadi et al. (2017) while studying hydraulic conductivity in green infrastructures. During this stage, the erosion rate is relatively low in comparison to early stages of study. In summary, this indicates the strong interplay between the infiltration and erosion behaviour of vegetated soil. For better understanding the relation between infiltration and erosion behaviour of vegetated soil, an integrated model that considers continuous changes of these parameters and resulting degradation needs to be developed. Such a study would bring a preliminary inference in developing effective soil loss models for surface soils used in MLCSs.

4 Conclusions

This article deals with the field evaluation of surface soil layer of a pilot MLCS in terms of its erosion and infiltration rate under the influence of natural and simulated rainfall for a period of a year. The study evidently presented the diverse reasons behind contrasting behaviour of erosion at higher rates of infiltration in vegetated and partially vegetated soil. Antecedent moisture contents have

greater influence on erosion and infiltration behaviour of surface soils. The rate of infiltration was observed to increase during days of no rainfall due to the formation of surface desiccation cracks and low in-situ water contents. Further, the infiltration was found to decrease with partial closure of desiccation cracks and increase in antecedent water contents owing to high intensity rainfall during simulated rainfall study. The high soil losses due to erosion during simulated rainfall events decreased significantly, as the vegetation increased. Vegetation was found to have significant effect on reducing the soil loss depth of surface soil layer of MLCSs. The study indicates the need of bioengineering for protecting the surface layer of MLCSs.

Acknowledgments

The authors would like to thankfully acknowledge the board of research in nuclear sciences (BRNS), Department of Atomic Energy (DAE), India for the financial support provided for the work reported in this paper vide project no. 2013/36/06-BRNS.

References

Adams, M. P., & Smith, P. L. (2014). A systematic approach to model the influence of the type and density of vegetation cover on urban heat using remote sensing. *Landscape and Urban Planning*, *132*, 47–54.

Anderson, C. E., & Stormont, J. C. (1997). *Prediction of long-term erosion from landfill covers in the southwest* (No. CONF-970208–PROC). USDOE, Washington, DC (United States). ASTM standard D2487 (2017). Standard practice for classification of soils for engineering purposes (unified soil classification system).

ASTM standard D422-63 (2007). Standard test method for particle-size analysis of soils.

ASTM standard D4318 (2017). Standard test methods for liquid limit, plastic limit, and plasticity index of soils.

ASTM standard D5084 (2014). Standard test methods for measurement of hydraulic conductivity of saturated porous materials using a flexible wall permeameter.

ASTM standard D854 (2014). Standard test method for specific gravity of soil solids by water pycnometer.

Barnswell, K. D., & Dwyer, D. F. (2012). Two-year performance by evapotranspiration covers for municipal solid waste landfills in northwest Ohio. *Waste Management*, *32*(12), 2336–2341.

Bhave, S., & Sreeja, P. (2013). Influence of initial soil condition on infiltration characteristics determined using a disk infiltrometer. *ISH Journal of Hydraulic Engineering*, *19*(3), 291–296.

Blight, G. (2009). Solar heating of the soil and evaporation from a soil surface. *Géotechnique*, *59*(4), 355–363.

Bonaparte, R., Daniel, D. E., & Koerner, R. M. (2002). *Assessment and Recommendations for Improving the Performance of Waste Containment Systems*. United States Environmental Protection Agency, Office of Research and Development, National Risk Management Research Laboratory.

Gadi, V. K., Tang, Y. R., Das, A., Monga, C., Garg, A., Berretta, C. & Sahoo, L. (2017). Spatial and temporal variation of hydraulic conductivity and vegetation growth in green infrastructures using infiltrometer and visual technique. *Catena*, *155*, 20–29.

Ghosh, B., Pekkat, S., & Yamsani, S. K. (2019). Evaluation of infiltrometers and permeameters for measuring hydraulic conductivity. *Advances in Civil Engineering Materials*, *8*(1).

Gray, D. H., & Sotir, R. B. (1996). *Biotechnical and Soil Bioengineering Slope Stabilization: A Practical Guide for Erosion Control*. New York: John Wiley & Sons.

Gross, B. A., Bonaparte, R., & Giroud, J. P. (2002). *Waste containment systems: problems and lessons learned* (Appendix F in Assessment and Recommendations for Optimal Performance of Waste Containment Systems). US Environmental Protection Agency, National Risk Management Research Laboratory.

Hoor, A., & Rowe, R. K. (2013). Potential for desiccation of geosynthetic clay liners used in barrier systems. *Journal of Geotechnical and Geoenvironmental Engineering*, *139*(10), 1648–1664.

Jarvis, A., Ramirez, J., Bonilla-Findji, O., & Zapata, E. (2011). Impacts of climate change on crop production in Latin America. *Crop adaptation to climate change* (pp. 44–56).

Khapre, A., Kumar, S., & Rajasekaran, C. (2017). Phytocapping: an alternate cover option for municipal solid waste landfills. *Environmental Technology, Taylor & Francis*, *6*, 1–8.

Koerner, R. M., & Daniel, D. E. (1997). *Final covers for solid waste landfills and abandoned dumps*. Thomas Telford, ASCE Press.

Landreth, R. E., Daniel, D. E., Koerner, R. M., Schroeder, P. R., & Richardson, G. N. (1991). *Design and construction of RCRA-CERCLA final covers*. Seminar Peblication.

Maqsoud, A., Bussière, B., Aubertin, M., Chouteau, M., & Mbonimpa, M. (2011). Field investigation of a suction break designed to control slope-induced desaturation in an oxygen barrier. *Canadian Geotechnical Journal*, *48*(1), 53–71.

Meter Group Inc. (2019a). *Microclimate monitoring system for measuring various weather parameters*. Operator's User Manual. Meter Group Inc., Pullman, WA. Retrieved December 30, 2020 from https://www.metergroup.com/environment/products/ecrn-100/

Meter Group Inc. (2019b). *Mini disk infiltrometer*. Operator's User Manual. Meter Group Inc., Pullman, WA 99163. Retrieved December 30, 2020 from https://www.metergroup.com/environment/products/mini-disk-infiltrometer/

Morris, C. E., & Stormont, J. C. (1998). Evaluation of numerical simulations of capillary barrier field tests. *Geotechnical and Geological Engineering*, *16*(3), 201–213.

Nyhan, J. W. (2005). A Seven-Year Water Balance Study of an Evapotranspiration Landfill Cover Varying in Slope for Semiarid Regions. *Vadose Zone Journal*, *4*(3), 466.

Nyhan, J. W., Hakonson, T. E., & Drennon, B. J. (1990). A water balance study of two landfill cover designs for semiarid regions. *Journal of Environmental Quality*, *19*(2), 281–288.

Øygarden, L., Kværner, J., & Jenssen, P. D. (1997). Soil erosion via preferential flow to drainage systems in clay soils. *Geoderma*, *76*(1–2), 65–86.

Schnabel, W. E., Munk, J., Lee, W. J., & Barnes, D. L. (2012). Four-year performance evaluation of a pilot-scale evapotranspiration

landfill cover in Southcentral Alaska. *Cold Regions Science and Technology*, *82*, 1–7.

Shaikh, J., Bordoloi, S., Yamsani, S. K., Sekharan, S., Rakesh, R. R., & Sarmah, A. K. (2019a). Long-term hydraulic performance of landfill cover system in extreme humid region: Field monitoring and numerical approach. *Science of the Total Environ.*, *688*, 409–423.

Shaikh, J., Yamsani, S. K., Bora, M. J., Sekharan, S., Rakesh, R. R., Mungale, A., & Bordoloi, S. (2019b). Impact assessment of vegetation growth on soil erosion of a landfill cover surface. *Acta Horticulturae et Regiotecturae*, *22*(2), 75–79.

Shaikh, J., Bordoloi, S., Leung, A. K., Yamsani, S. K., Sekharan, S., & Rakesh, R. R. (2021). Seepage characteristics of three-layered landfill cover system constituting fly-ash under extreme ponding condition. *Science of the Total Environ.*, *758*, 143683.

Sherard, J. L., Dunnigan, L. P., & Decker, R. S. (1976). Identification and Nature of Dispersive Soils. *Journal of the Geotechnical Engineering Division*, *102*(GT4), 287–301.

Shrestha, G., Stahl, P. D., & Ingram, L. (2005). Influence of reclamation management practices on soil bulk density and infiltration rates on surface coal mine lands in Wyoming. *National Meeting of the American Society of Mining and Reclamation* (pp. 1042–1056), Lexington, KY: ASMR.

Sinnathamby, G., Pasky, A., Phillips, D. H. H., & Sivakumar, V. (2014). Landfill cap models under simulated climate change precipitation: impacts of cracks and root growth. *Géotechnique*, *64*(2), 95–107.

Song, L., Li, J. H., Zhou, T., & Fredlund, D. G. (2017). Experimental study on unsaturated hydraulic properties of vegetated soil. *Ecological Engineering*, *103*, 207–216.

Swope, G. L. (1975). *Revegetation of Landfill Cover Sites.* Pennsylvania State University, State Park, PA.

USEPA. (1989). *Requirements for hazardous waste landfill design, construction, and closure* (pp. 1–127. Seminar publication, Report No. 625/4-89/022). United States Environmental Protection Agency.

Xue, Q., Chen, Y. J., & Liu, L. (2016). Erosion characteristics of ecological sludge evapotranspiration cover slopes for landfill closure. *Environmental Earth Sciences*, *75*(5), 419.

Yamsani, S. K., Kumar, S., Sekharan, S., & Ranjan, R. R. (2017). Determination of soil erosion index for surface soils of landfill covers. *Environmental Geotechnics*, *6*(6), 373–380.

Zhan, T. L., Ng, C. W., & Fredlund, D. G. (2007). Field study of rainfall infiltration into a grassed unsaturated expansive soil slope. *Canadian Geotechnical Journal*, *44*(4), 392–408.

Zhang, X., Yu, G. Q., Li, Z. B., & Li, P. (2014). Experimental study on slope runoff, erosion and sediment under different vegetation types. *Water resources management*, *28*(9), 2415–2433.

sciendo

DOI: 10.2478/ahr-2021-0019
Acta hort regiotec, 24, 2021(1): 9–13

Research Article

Effects of repeated passages of a wheeled tractor on some physical properties of clayey loam soil

Eugene Balashov[1]*, Sergio Pellegrini[2], Paolo Bazzoffi[2]
[1]*Agrophysical Research Institute, St. Petersburg, Russia*
[2]*CREA-AA Centro di Ricerca Agricoltura e Ambiente, Firenze, Italy*

Article Details: Received: 2021-01-14 | Accepted: 2021-03-08 | Available online: 2021-05-31

Licensed under a Creative Commons Attribution 4.0 International License

SCREENED BY iThenticate Professional Plagiarism Prevention

The objective of the study was to quantify the differences in soil physical indicators between inter-track (uncompacted) zone and track (compacted) zone created by four passages of a wheeled tractor (Landini Globus 70/DBKL Techno). Field studies were carried out on plots of the Vicarello experimental station, Tuscany (43° 27′ N, 11° 30′ E). A local average annual precipitation is 678 mm and average annual air temperature is 12.7 °C with absolute extreme values -10 °C and 40 °C. Bulk density, moisture content, water-stable aggregation, and penetration resistance were determined by conventional methods in the 0–0.40 m soil layers. The results showed that the 0.05–0.10 m soil layer, compared to the 0.20–0.25 m and 0.35–0.40 m soil layers, showed a higher degree of compaction by tractor wheels. In this soil layer, significant (at P <0.05 and <0.01) differences between the inter-track and track zone were observed for bulk density (1.18 ±0.10 g.cm^{-3} and 1.35 ±0.10 g.cm^{-3}) and moisture content (24.9 ±2.3% and 27.9 ±2.3% of volume). Passages of tractor even resulted in an insignificant increase of total amounts (from 66.2 ±4.7% to 68.6 ±2.7%) and mean weight-diameters (from 2.29 ±0.30 mm to 2.40 ±0.04 mm) of water-stable aggregates. There were no significant differences in average penetration resistance of the uppermost 0–0.10 m soil layers between the inter-track (0.77 ±0.26 MPa) and track zone (0.64 ±0.12 MPa). Average soil penetration resistance was significantly (P <0.001) higher in the 0–0.40 m layer of the track zone (1.07 ±0.23 MPa) than in that of the inter-track zone (0.76 ±0.11 MPa).

Keywords: tractor wheels, compaction, soil properties

1 Introduction

Soil compaction by tractor wheels is one of the unfavourable factors of soil degradation (Botta et al., 2010; Pagliai et al., 2003). Soil compaction reduces soil porosity and aeration, rates of water movement and nutrients, and root growth (Pott et al., 2020; Seehusen et al., 2019). Soil penetration resistance, bulk density, aggregate formation, and stability are important indicators of soil quality (Šimanský et al., 2018; Batey, 2009; Gregory et al., 2009). These indicators are also useful for evaluating physical resistance to compaction and recovery of compacted soils due to different soil processes (Bartzen et al., 2019). In order to understand better whether a field is subjected or not to soil compaction, it is necessary to reply to questions about intensity, extension, depth and time of compaction, which requires a site-specific investigation across the field (Carrara et al., 2007). Therefore, studies of effects of tractor passages on site-specific key quality indicators of soils can be useful tools for evaluating their resistance to repeated passages of wheeled tractors

The objective of the study was to quantify possible differences in four soil physical indicators between inter-track (uncompacted) zone and track (compacted) zone created by four passages of a wheeled tractor.

2 Material and methods

Field studies were carried out on arable plots of the Vicarello experimental station, Volterra, Tuscany (43° 27′ N, 11° 30′ E) of the former Experimental Institute for Soil Survey and Conservation (Florence, Italy). A local average annual precipitation is 678 mm and average annual air temperature is 12.7 °C with absolute extreme values -10 °C and 40 °C (Torri et al., 1999). The soil is classified as clayey loam Vertic Cambisol (WRB).

***Corresponding Author:** Eugene Balashov, Agrophysical Research Institute, Department of Soil Physics, Physical Chemistry and Biophysics, 14 Grazhdansky prospekt, St. Petersburg, 195220, Russia; e-mail: Eugene_Balashov@mail.ru

Properties of the Ap soil horizon were: sand – 15%, silt – 43%, clay – 42%, pH – 8.2, total $CaCO_3$ – 12.8%, total organic matter – 0.5% (Torri et al., 1999).

A size of the studied arable plot with winter wheat (*Triticum aestivum* L., cv. Pandas) was equal to 10 × 25 m. Disturbed field moist samples of clayey loam Vertic Cambisol were taken in the inter-track and track zone created after 4 passages of a wheeled tractor (Landini Globus 70/DBKL Techno) with engine power of 48 kW and mass of 25,595 kg. An average ground contact pressure and total contact area of front/rear tractor tyres on a soil surface were equal to: 60/50 kPa and 0.18/0.30 m^2 (Pagliai et al., 2003). These ground contact pressures are in the ranges of conventional pressures of wheeled tractors on soils (Holthusen et al., 2018).

The combined soil samples, consisting of four 1-kg soil subsamples, were taken from the depth of 0–0.25 m to analyse amounts of size fractions of water-stable aggregates (WSA). Two subsamples were taken from the inter-track zone and two subsamples were collected from the track zone. The soil samples were air-dried. Afterwards, 500 g of air-dried soil samples were sieved through a set of sieves with diameters of openings of 0.25, 0.5, 1.0, 2.8, 5.66 and 9.51 mm to quantify a distribution of amounts of each size fraction of dry stable aggregates. Then, 50 g of these aggregates were composed from the corresponding mean-weighted portions of each size fraction. The amounts of size fractions of WSA were measured in three replicates by a wet sieving method using a set of sieves with the above-mentioned diameters of openings. The 0.25–9.51 mm dry stable aggregates were capillary saturated by water for 10 min, placed on a top of a set of the sieves, immersed directly into water in an apparatus for vertical oscillation, and mechanically oscillated with a stroke of 40 mm and at the frequency of 30 cycles.min^{-1} for 10 min (Valboa et al., 2015). Afterwards, size fractions of WSA were collected from each sieve and subjected to drying at 40 °C in a thermostat. The weight of each size fraction, corrected for sand content, was expressed as a percentage of the total amount of WSA. Data on the amounts of size fractions of WSA were used for calculations of mean weight diameters of WSA (Šimanský et al., 2018).

In the inter-track and track zone, six soil samples were collected from each soil depth of 0.05–0.10 m, 0.20–0.25 and 0.35–0.40 m to determine moisture content and bulk density. The soil moisture content was measured by the gravimetric method (oven drying at 105 °C). The soil bulk density was determined by the method of sampling steel corers: volume – 0.0001 m^3, internal diameter – 0.05 m, length – 0.051 m, wall thickness – 0.0015 m. The samples were weighed and oven-dried (at 105 °C) up to achieving a constant weight. The soil penetration resistance was measured by an Eijkelkamp electronic penetrometer with conventional parameters: cone diameter of 0.016 m, cone angle of 60°, base area of 100 mm^2 and average penetration speed of 0.02 $m.s^{-1}$. In each studied zone, 20 penetrometer readings were done at 0.01 m intervals over the depth of 0–0.40 m (Pagliai et al., 2003).

One-way ANOVA analysis of variance was applied to evaluate the significance of differences between means of the studied data (at $P \leq 0.05$).

3 Results and discussion

The results of our studies showed that significant (at $P < 0.01$) differences in bulk density between the inter-track and track zone were observed only at the depth of 0.05–0.10 m (Fig. 1). As compared to the 0.20–0.25 m and 0.35–0.40 m soil layers, the 0.05–0.10 m soil layer showed a higher degree of compaction by tractor wheels. In this soil layer, significant (at $P < 0.05$ and < 0.01) differences between the inter-track and track zone were observed for bulk density: 1.18 ±0.10 $g.cm^{-3}$ and 1.35 ±0.10 $g.cm^{-3}$, respectively. According to Fulajtár (2006), threshold values of bulk density of clayey loam soil exceed 1.40 $g.cm^{-3}$. The soil bulk density increased with increasing soil depth in the inter-track and track zone. In the inter-track and track zone, soil bulk density demonstrated a high variability at all the studied soil layers, and often exceeded its critical values.

Significant (at $P < 0.05$) differences in soil bulk density were recorded only between the soil layers of 0.05–0.10 m (1.18 ±0.10 $g.cm^{-3}$) and 0.20–0.25 m (1.31 ±0.10 $g.cm^{-3}$) in the inter-track zone. Differences in soil bulk density between soil layers in the track zone were not significant although the soil bulk density of 0.35–0.40 m soil layer showed maximum values in this zone (Fig. 1).

The soil moisture content in the inter-track and track zone also increased with the depth (Fig. 2).

In the inter-track zone, significant differences in the soil moisture content were observed between the 0.05–0.10 and 0.20–0.25 m layers (at $P = 0.05$) and between the 0.05–0.10 m and 0.35–0.40 m layers (at $P < 0.01$). There were no significant inter-layer differences in the soil moisture content in the track zone.

Soil compaction by tractor wheels resulted in a significant (at $P = 0.05$) increase of moisture content only at the 0.05–0.10 m layer. A decrease in macroporosity, in general, and volumes of storage (0.5–50 μm) and transmission (elongated and continuous, 50–500 μm) of pores, could be a reason of the significant differences in the soil bulk density and moisture content in the 0.05–0.10 m soil layer in the track zone (Głąb & Kulig, 2008; Pagliai et al.,

© Slovak University of Agriculture in Nitra

2003). Elongated pores larger than 500 µm are important for drainage in fine-textured soils (Pagliai et al., 2003). These changes in the soil porous space could be responsible for an increase in water retention by meso- and micropores and for a decrease in hydraulic conductivity of compacted 0.05–0.10 m soil layer (Lipiec et al., 2006). The 0.20–0.25 m and 0.35–0.40 m soil layers probably had a similar distribution of macro-, meso- and micropores and, therefore, showed no significant differences in the soil moisture content between the inter-track and track zone. Threshold values of moisture content of clay loam and clayey soil are 20–24% (Fulajtár, 2006). Our results showed that if the soil moisture content exceeded 25%, then the compaction of the 0.05–0.10 m soil layer could lead to an unfavourable increase in its bulk density above the threshold values.

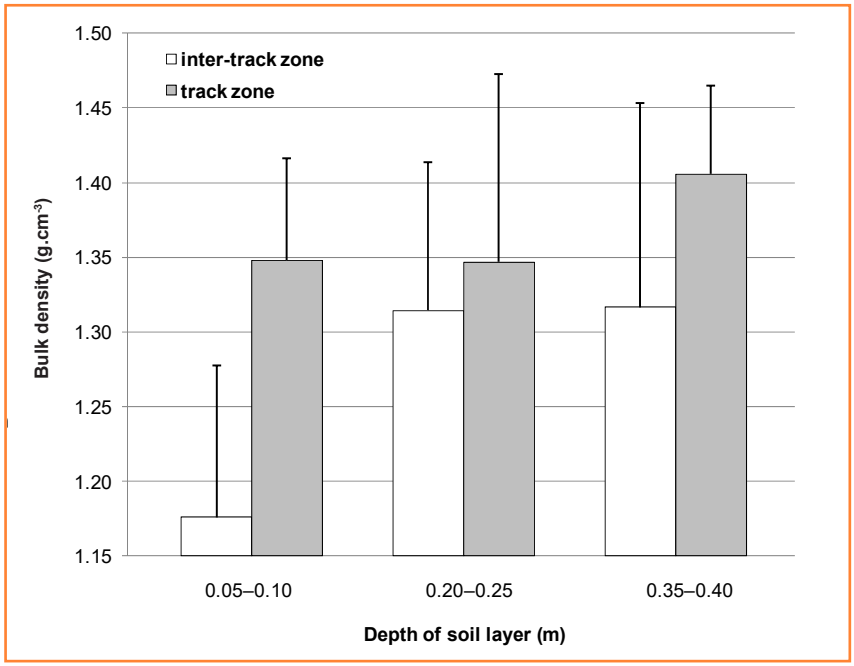

Figure 1 Distribution of bulk density at the layers of 0.05–0.10 m, 0.20–0.25 m and 0.35–0.40 m in the inter track and track zone of clayey loam soil (bars show standard deviations)

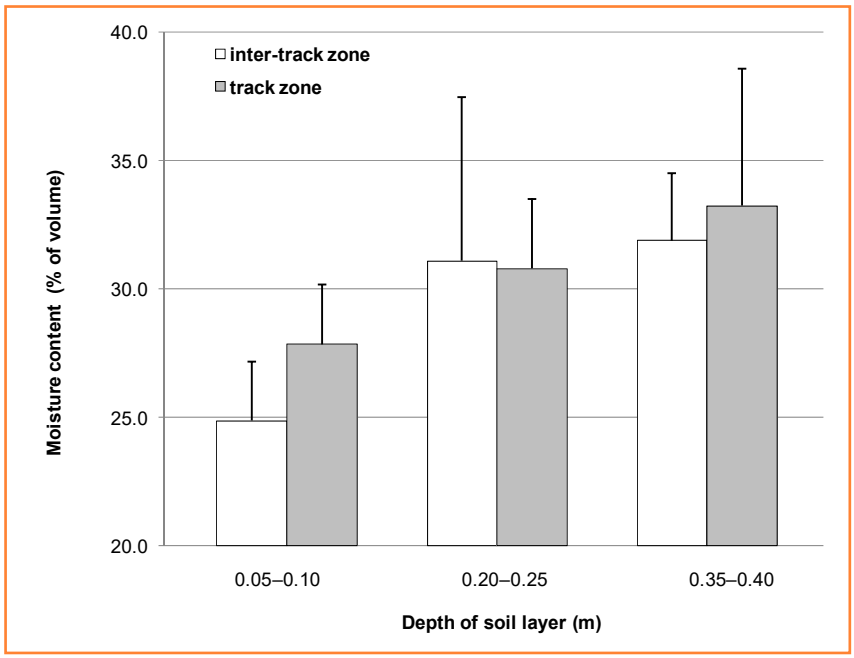

Figure 2 Distribution of moisture content at the layers of 0.05–0.10 m, 0.20–0.25 m and 0.35–0.40 m in the inter-track and track zone of clayey loam soil

The passages of wheeled tractor did not significantly affect the total amounts of size fractions of WSA at the surface 0–0.25 m soil layer despite the significant increase in the soil bulk density of the compacted 0.05–0.10 m soil layer. The total amounts of size fractions of WSA were equal to 66.2 ±4.7% in the inter-track zone and 68.6 ±2.4% in the track zone. Mean weight diameters of WSA also showed no significant differences in the inter-track (2.29 ±0.30 mm) and track zone (2.30 ±0.04 mm).

The distribution of size fractions of WSA is presented in Fig. 3.

Maximum amounts of WSA size fractions of 1.0–2.8 mm and 5.66–9.51 mm were observed in the inter-track zone and track zone, respectively. There was only a trend in increasing amounts of almost all size fractions of WSA in the track zone. The 1.0–2.8 mm size fraction of WSA was most sensitive to the compaction by a wheeled tractor. The size fractions of WSA of clayey loam soil showed a high resistance to ground contact pressures of a wheeled tractor because of clay particles having strong binding forces (de Andrade Bonetti et al., 2017).

The results of our studies demonstrated that the penetration resistance increased after soil compaction by the wheeled tractor (Fig. 4).

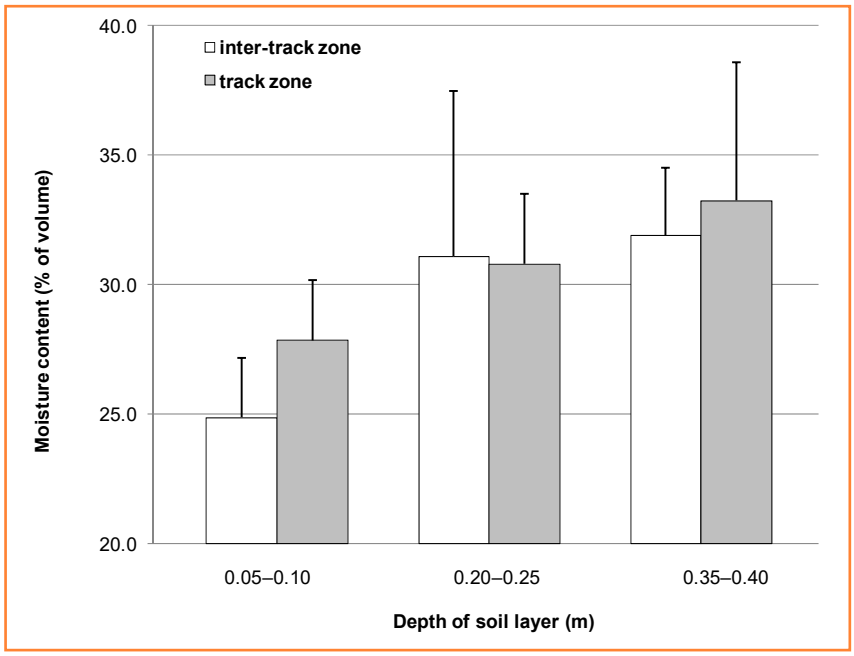

Figure 3 Distributions of amounts of size fractions of water-stable aggregates in the inter-track and track zone of clayey loam soil

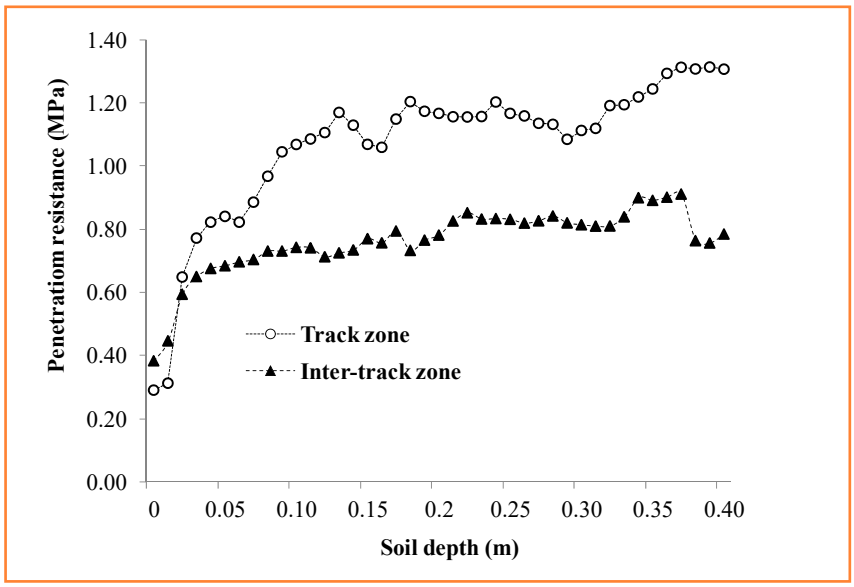

Figure 4 Depth distribution of penetration resistance of the 0–0.40 m layer in the inter-track and track zone of clayey loam soil

According to our results, mean values of penetration resistance of the 0–0.40 m layers were equal to 0.76 ±0.11 MPa in the inter-track zone and 1.07 ±0.23 MPa in the track zone. There were significant (at P <0.001) differences in penetration resistance of these soil layers in the inter-track and track zone. There were no significant differences in average penetration resistance of the uppermost 0–0.10 m soil layers between the inter-track (0.77 ±0.26 MPa) and track zone (0.64 ±0.12 MPa). Mean values of penetration resistance of clayey loam soil did not exceed its critical value of 2.5 MPa for plants (Carrara et al., 2007).

4 Conclusions

Repeated passages of a wheeled tractor on the clayey loam Vertic Cambisol contributed to the formation of track zones with significantly higher values of bulk density and moisture content only in the 0.05–0.10 m layers compared to the 0.20–0.25 m and 0.35–0.40 m layers. The size fractions of WSA of clayey loam soil in the 0–0.25 m layer showed a high resistance to loadings of a wheeled tractor because of clay particles having strong binding forces. Soil penetration resistance was significantly higher in the track zone than in the inter-track zone only in the 0–0.40 m layers but did not show significant differences in the 0–0.10 m soil layers. Recommendations are to:

1. avoid wheeling when the soil moisture content corresponds to threshold values,
2. reduce the number of passages of wheeled tractors.

Acknowledgement

Dr. E Balashov carried out these joint studies in the framework of the Outreach Fellowship Programme of the National Research Council (Italy) and partly in the framework of the

research plan of the Agrophysical Research Institute (St. Petersburg, Russia).

References

Bartzen, B. T., Hoelscher, G. L., Ribeiro, L. L. O., & Seidel, E. P. (2019). How the Soil Resistance to Penetration Affects the Development of Agricultural Crops? *Journal of Experimental Agriculture International*, *30*(5), 1–17. https://doi.org/10.9734/JEAI/2019/46589

Batey, T. (2009). Soil compaction and management – review. *Soil Use and Management*, *25*, 335–345. https://doi.org/10.1111/j.1475-2743.2009.00236.x

Botta, G. F., Tolon-Becerra, A., Lastra-Bravo, X., & Tourn, M. (2010). Tillage and traffic effects (planters and tractors) on soil compaction and soybean (*Glycine max* L.) yields in Argentinean pampas. *Soil and Tillage Research*, *1*(1), 167–174. https://doi.org/10.1016/j.still.2010.07.001

Carrara, M., Castrignanò, A., Comparetti, A., Febo, P., & Orlando, S. (2007). Mapping of penetrometer resistance in relation to tractor traffic using multivariate geostatistics. *Geoderma*, *142*(3–4), 294–307. https://doi.org/10.1016/j.geoderma.2007.08.020

de Andrade Bonetti, J., Anghinoni, I., Gubiani, P. I., Cecagno, D., & de Moraes, M. T. (2019). Impact of a long-term crop-livestock system on the physical and hydraulic properties of an Oxisol. *Soil and Tillage Research*, *186*, 280–291. https://doi.org/10.1016/j.still.2018.11.003

Fulajtár, E. (2006). *Physical parameters of soil* (142 p). VÚPOP (in Slovak).

Głąb, T., & Kulig, B. (2008). Effect of mulch and tillage system on soil porosity under wheat (*Triticum aestivum*). *Soil and Tillage Research*, *99*(2), 169–178. https://doi.org/10.1016/j.still.2008.02.004

Gregory, A. S., Watts, C. W., Griffiths, B. S., Hallett, P. D., Kuan, H. L., & Whitmore, A. P. (2009). The effect of long-term soil management on the physical and biological resilience of a range of arable and grassland soils in England. *Geoderma*, *153*(1–2), 172–185. https://doi.org/10.1016/j.geoderma.2009.08.002

Holthusen, D., Brandt, A. A., Reichert, J. M., Horn, R., Fleige, H., & Zink, A. (2018). Soil functions and in situ stress distribution in subtropical soils as affected by land use, vehicle type, tire inflation pressure and plant residue removal. *Soil and Tillage Research*, *184*, 78–92. https://doi.org/10.1016/j.still.2018.07.009

Lipiec, J., Kuś, J., Słowińska-Jurkiewicz, A., & Nosalewicz, A. (2006). Soil porosity and water infiltration as influenced by tillage methods. *Soil and Tillage Research*, *89*(2), 210–220. https://doi.org/10.1016/j.still.2005.07.012

Pagliai, M., Marsili, A., Servadio, P., Vignozzi, N., & Pellegrini, S. (2003). Changes in some physical properties of a clay soil in Central Italy following the passage of rubber tracked and wheeled tractors of medium power. *Soil and Tillage Research*, *73*(1–2), 119–129. https://doi.org/10.1016/S0167-1987(03)00105-3

Pott, L. P., Amado, T. J., Leal, O. A., & Ciampitti, I. A. (2020). Mitigation of soil compaction for boosting crop productivity at varying yield environments in southern Brazil. *European Journal of Soil Science*, *71*(6), 1157–1172. https://doi.org/10.1111/ejss.12880

Seehusen, T., Riggert, R., Fleige, H., Horn, R., & Riley, H. (2019). Soil compaction and stress propagation after different wheeling intensities on a silt soil in South-East Norway. *Acta Agriculturae Scandinavica, Section B – Soil & Plant Science, 69*(4), 343–355. https://doi.org/10.1080/09064710.2019.1576762

Šimanský, V., Igaz, D., Horák, J., Šurda, P., Kolenčík, M., Buchkina, N. P., Uzarovicz, Ł., Juriga, M., Šrank, D., & Pauková, Ž. (2018). Response of soil organic carbon and water-stable aggregates to different biochar treatments including nitrogen fertilization. *Journal of Hydrology and Hydromechanics*, *66*(4), 429–436. https://doi.org/10.2478/johh-2018-0033

Torri, D., Regüés, D., Pellegrini, S., & Bazzoffi, P. (1999). Within-storm soil surface dynamics and erosive effects of rainstorms. *Catena*, *38*(2), 131–150. https://doi.org/10.1016/S0341-8162(99)00059-4

Valboa, G., Lagomarsino, A., Brandi, G., Agnelli, A. E., Simoncini, S., Papini, R., Vignozzi, N., & Pellegrini, S. (2015). Long-term variations in soil organic matter under different tillage intensities. *Soil and Tillage Research*, *154*, 126–135. https://doi.org/10.1016/j.still.2015.06.017

sciendo
Acta hort regiotec, 24, 2021(1): 14–20
DOI: 10.2478/ahr-2021-0020

Research Article

Relationships between soil organic matter and crop yield after biochar substrates application and their combination with mineral fertilizers on sandy soil

Vladimír Šimanský*, Dušan Šrank
Slovak University of Agriculture in Nitra, Faculty of Agrobiology and Food Resources, Department of Soil Science, Slovakia

Article Details: Received: 2020-10-27 | Accepted: 2021-02-21 | Available online: 2021-05-31

Licensed under a Creative Commons Attribution 4.0 International License

SCREENED BY iThenticate® Professional Plagiarism Prevention

In this field study, under the soil conditions of southern Slovakia (Dolná Streda, sandy Haplic Arenosol), there were quantified the effects of biochar substrates (1. Effeco 50:50; 2. Effeco 33:33:33) in two rates (10 and 20 t.ha^{-1}) applied alone or in combination with mineral fertilization on soil organic matter (SOM) content and crop yields for period of 3 years (2018-2020) but also the linear relationships between SOM and crop yields depending on the application of biochar substrates and its combination with mineral fertilizers. The results showed that the content of soil organic carbon (SOC) increased from 8.5 g.kg^{-1} in unfertilized control to 13.8 g.kg^{-1} in Effeco 33:33:33 at 20 t ha^{-1}. However, SOC decreased from 13.6 g.kg^{-1} in fertilized control to 10.1 g.kg^{-1} in Effeco 50:50 at 10 t.ha^{-1}. Biochar substrates and their combination with mineral fertilizers did not have a significant effect on changes in labile carbon in the soil. The effect on the crop yields was diametrically different in the first year after the application of biochar substrates compared to the second and third year. In the second and third year, the same trend was observed in the reaction to substrates – including a more robust effect on the increase in crop yields in the third year after the application of biochar substrates and also biochar substrates with mineral fertilizers. The linear relationships between SOC and crop yields were found only in biochar substrates alone treatments.

Keywords: sunflower seeds, durum wheat, maize, soil organic carbon, labile carbon, Effeco, Arenosol

1 Introduction

Crops growth and productivity are strongly influenced by various biotic and abiotic stresses and soil quality (Thalmann & Santelia, 2017). These factors can be affected on a larger or a smaller scale by human activities. Plants require a number of soil nutrients such as N, P, and K for their growth, but soil nutrient levels may decrease over time after crop harvesting, as nutrients are not returned to the soil (Rawat et al., 2019) and therefore the use of fertilizers, ameliorants and amendments is justified. In modern agriculture, fertilization is considered to be an intensifying factor that can significantly increase the yield of cultivated crops, especially on sandy soils. In general, sandy soils are characterized by low sorption capacity, low organic carbon content (SOC) and especially low nutrient content (Behera & Shukla, 2015). SOC is a key parameter of soil quality, and its content in sandy soil is often below 1%. Sandy soil has typically higher levels of aeration and heat leading to higher levels of decomposition in soil organic matter (Osman, 2018).

Within the Slovak Republic, the soil fund is highly heterogeneous. Textural light soils (sandy, loamy-sandy) represent only about 9% of the agricultural land fund in Slovakia, but in some localities of the Záhorská Lowland or the Danubian Lowland they are among the dominant ones. In order for sandy soils to be suitable for agricultural production, farmers must pay considerable attention to them through various intensification practices, including fertilization. In recent years, in addition to conventional organic and mineral fertilizers, biochar has been applied to the soil, especially for its positive benefits for agronomic practice (Horák et al., 2020). As published, the biochar increases soil pH (Gondek et al., 2020), mainly in acid soils (Horák, 2015), improves soil sorption capacity (Cornelissen et al., 2018; Gondek et al., 2020) and a whole complex of soil physical properties such as: soil structure (Obia et al., 2016), soil water regime (Igaz et al., 2018), as well as soil biological properties (Mierzwa-Hersztek et al., 2018) resulting in an increase in plant productivity (Mierzwa-Hersztek et al., 2018).The

***Corresponding Author:** Vladimír Šimanský, Slovak University of Agriculture, Nitra, Slovakia;
e-mail: vladimir.simansky@uniag.sk ORCID: https://orcid.org/0000-0003-3271-6858

behaviour of biochar in the soil environment significantly depends on its properties, which are influenced by the feedstock for its production, methods and conditions during its production (Singh & Cowie, 2010), but also the soil-climatic conditions of sites.

In the soil-climatic conditions of the Slovak Republic, the application of biochar is associated with a lack of knowledge of its effects on soil properties, and on crop yields. However, the most important consideration for farmers is whether biochar, when applied to the soil, brings sufficient benefits through increased yields, and influence on soil properties leading to clear economic benefits.

There is a presumption that biochar will not be a balanced fertilizer in the soil environment due to its high stability, but its addition to the soil may play a key role in nutrient dynamics through the direct addition or indirect influence of soil properties that increase nutrient availability (e. g. by increasing the pH of acidic soils or by increasing the content of organic substances). Biochar producers must focus on achieving a product with the best possible properties during the production process or recommend biochar application with other fertilizers in various combinations. Subsequently, before the actual use of such products, it is necessary to verify them in production conditions, and their effects must be tested in different soil-climatic conditions, including the place of use, i.e. Slovakia.

Based on the above overview, the aim of this study was to quantify the effects of added biochar substrates and their combination with mineral fertilization on C content and crop yields during a period of 3 years from its application in sandy soil.

2 Material and methods

In autumn 2017, the field research with biochar substrates and their combinations with other mineral fertilizers were carried out on the cultivated soil of the Dolná Streda locality (Slovakia). Soil was classified as Haplic Arenosol (Arenic, Calcic) (WRB, 2015). The soil contained 819 $g.kg^{-1}$ of sand, 105 $g.kg^{-1}$ of silt and 76 $g.kg^{-1}$ of clay on average (classified as sandy in texture), 9.7 $g.kg^{-1}$ of soil organic carbon and the content of total nitrogen was 1.3 $g.kg^{-1}$, contents of available P and K were 175 and 165 $mg.kg^{-1}$, respectively, and the average soil pH in H_2O was 7.6. At the experiment site, a long-term average annual rainfall is in the range 520–600 mm and the average annual temperature ranging from 9–10 °C was recorded.

A long segments block design was applied, with plots measuring 7.5 × 12 m (90 m^2) with a protective belt of 1 m left between individual plots (the total of 10 plots). Experimental treatments are shown in Table 1. Biochar substrates were applied to each plot and incorporated to 0.15 m by disking. The control plots were also disked. In 2017 (before experiment establishment), durum wheat was grown as the preceding crop. During the experiment, sunflower, durum wheat, and maize were planted in 2018, 2019 and 2020, respectively. The disking performed up to the depth of 0.15–0.18 m was used. Before the sowing of sunflower in spring 2018, urea was applied into the soil. The dose of urea was 100 $kg.ha^{-1}$. In the spring 2019, both mineral fertilizer – urea and monoammonium phosphate (AMOFOS NP 12-52) at rates of 100 $kg.ha^{-1}$ and 100 $kg.ha^{-1}$ respectively were applied. In 2020, during the vegetation season for maize, urea and AMOFOS were applied at rates of 100 and 100 $kg.ha^{-1}$ – 50% before sowing and the other 50% on June 10.

Effeco 50:50 is the biochar (pyrolyzed hard wood) blended with dried sheep manure in the proportion 1 : 1 and it contains 43% of total organic carbon, 1.2% total N, 0.49% P, and 24.6% K, and its pH is 8.18. Effeco 33:33:33 is the biochar (pyrolyzed hard wood) blended with dried sheep manure and the residue from the biogas station (originally – cattle manure) in the proportion 1 : 1 : 1, and it contains 45.4% of total organic carbon, 1.3% of total N, 0.79% P, and 15.5% K, and its pH is 8.44. The content of heavy metals in both types of biochar does not exceed the limit rates, which are set by agriculture regulation 577/2005. Both types of biochar substrates are granulated into pellets and all substrates are trademarks of the company Zdroje Zeme ag.

Soil samples were collected in all treatments from the depth 0–0.2 m, twice a year (spring and autumn) during the 3-year period. For each sampled zone (included all treatments), three different locations were chosen

Table 1 The investigated treatments

Treatment	Rates ($t.ha^{-1}$)	Treatment	Rates ($t.ha^{-1}$)
Control – no fertilization	0	**Fertilized Control – mineral fertilization (MF)**	0
Effeco 50:50	10	**Effeco 50:50 + MF**	10
Effeco 50:50	20	**Effeco 50:50 + MF**	20
Effeco 33:33:33	10	**Effeco 33:33:33 + MF**	10
Effeco 33:33:33	20	**Effeco 33:33:33 + MF**	20

© Slovak University of Agriculture in Nitra
www.uniag.sk

randomly. At each location, soil samples were collected and mixed to create an average sample. Soil samples were dried at laboratory temperature and grinded. SOC content was measured using the wet combustion method-oxidation of SOM by a mixture of 0.07 mol. dm^{-3} H_2SO_4 and $K_2Cr_2O_7$ with titration using Mohr's salt, and labile carbon (C_L) content was determined using 0.005 mol.dm^{-3} $KMnO_4$ (Hrivňáková et al., 2011).

Plants of sunflower, durum wheat, and maize were sampled in triple repetition at the end of the vegetation season. The ears of maize and sunflowers capes were taken from one randomly selected 1.2 m row – (wide row crops), while the durum wheat was sampled from a randomly selected 1 × 1 m square – narrow row crop. Ears, capes, grains, and seeds from each plant were obtained under laboratory conditions.

All results were compared by the analysis of variance (ANOVA) procedure by using the Statgraphics Centurion XV.I (Statpoint Technologies, Inc., Warrenton, VA). Differences in means were determined by calculating the least significant difference (LSD) using the 5% level. To evaluate the trends between SOM and crop yields, the simple linear regression model was used.

3 Results and discussion

3. 1 Soil organic carbon

A higher content of SOC was determined at higher rate than lower rate of both tested biochar substrates applied alone, however, a statistically significant increase of SOC was observed in Effeco 33:33:33 at 20 $t.ha^{-1}$ compared to the control (Table 2). Biochar is a significant source of stable carbon and its stability is a result of the production process. During the production process, the carbon base of the biological materials used to produce biochar is rearranged and aliphatic carbon chains (chain structures whose chemical bonds are easily attacked by microbial enzymes) are converted to aromatic rings (usually six carbon – such as benzene or occasionally other atoms, such as nitrogen, linked in the ring structure by strong chemical bonds that are resistant to microbial decomposition). Further restructuring leads to the coupling of these aromatic groups into large complexes by the process known as condensation. This is achieved using well-pyrolyzed biochar made up of leaves of condensed aromatic rings of various sizes, along with ash and traces of smaller molecules. Aromaticity and the degree of condensation are associated with the stability of biochar (Shackley et al., 2016). In this study, the biochar substrates contained 43.0% (Effeco 50:50) and 45.4% (Effeco 33:33:33) of C and for this reason, the increase of SOC in sandy soil due to their applications is not surprising. Biochar substrates application into the soil can be linked with decreasing microbial activity, lower CO_2 production, and a fall in mineralization which results in an increase in SOC in the soil – a negative priming effect (Cheng et al., 2016). Interestingly, the increase in labile carbon content (C_L) in the soil was not statistically confirmed due to the large variance of values in the biochar substrate alone treatments. It was more at a lower than a higher application rate for both biochar substrates alone. Its more significant increase could be inhibited by the sorption of labile carbon by biochar alone in the substrate, which in turn promotes the formation of relatively stable organic matter in the soil (Jones et al., 2012).

Different effects on the content of SOC but also C_L were observed in the treatments of biochar substrates combined with mineral fertilization (Table 2). Mineral fertilizers are considered to be significant accelerators of some soil processes (Horák et al., 2017), which was

Table 2 Contents of soil organic carbon and labile carbon in the individual treatments (2018–2020 – average)

Treatment	Rate ($t.ha^{-1}$)	SOC (%)	C_L ($mg.kg^{-1}$)
Control – no fertilization	0	0.90a	828a
Effeco 50:50	10	1.06ab	1,047a
Effeco 50:50	20	1.17ab	1,025a
Effeco 33:33:33	10	1.23ab	1,110a
Effeco 33:33:33	20	1.38b	1,081a
Fertilized control – mineral fertilization (MF)	0	1.36bc	1,149a
Effeco 50:50 + MF	10	1.01a	936a
Effeco 50:50 + MF	20	1.47c	1,448a
Effeco 33:33:33 + MF	10	1.11ab	1,012a
Effeco 33:33:33 + MF	20	1.10ab	1,074a

Different letters (a, b, c) indicate that treatment means are significantly different at $p \leq 0.05$ according to the LSD multiple-range test

Table 3 The crops yield in the individual treatments

Treatment	Rate (t.ha^{-1})	Crops yield (t.ha^{-1})		
		sunflower 2018	wheat 2019	maize 2020
Control – no fertilization	0	1.86a	1.99a	1.85a
Effeco 50:50	10	2.23a	2.69b	2.13a
Effeco 50:50	20	3.39b	3.04b	3.95b
Effeco 33:33:33	10	2.16a	3.11b	4.33b
Effeco 33:33:33	20	2.27a	3.95c	5.78c
Fertilized Control – mineral fertilization (MF)	0	1.93a	2.04a	1.90a
Effeco 50:50 + MF	10	2.94a	2.99b	4.85b
Effeco 50:50 + MF	20	5.09b	5.06c	5.90b
Effeco 33:33:33 + MF	10	2.20a	2.58ab	2.18a
Effeco 33:33:33 + MF	20	2.54a	2.69ab	3.07a

Different letters (a, b, c) indicate that treatment means are significantly different at $p \leq 0.05$ according to the LSD multiple-range test

confirmed by our results. The SOC decreased significantly from 1.36% (MF-control) to 1.01% in Effeco 50:50 at 10 t.ha^{-1} + MF and in the Effeco 33:33:33 both rates + MF decreased and in the Effeco 50:50 at 20 t.ha^{-1} + MF even increased, but these results were not statistically significant. The C_L contents corresponded to the SOC in the individual treatments, which means that in addition to the Effeco 50:50 at 20 t.ha^{-1} + mineral fertilization treatment, the C_L values decreased compared to the MF-control, but statistically insignificant for large variability in the replicates (Table 2). Under certain conditions, the mineral fertilizers applied together with biochar substrates can contribute to the preferential use of these substrates by stimulating microbial activity, while soil microorganisms can preferentially utilize labile sources of added biochar substrate or soil organic matter (Singh & Cowie, 2014), which can cause the so-called positive priming effect with consequent reduction of SOC.

3.2 Crops yield

The crops yield during the first three years of biochar substrates application and their combinations with mineral fertilizers are summarized in Table 3. In our case, the average yield of sunflower seeds was 1.86 t.ha^{-1} (control) and only after application of the biochar substrate Effeco 50:50 at a rate of 20 t.ha^{-1} the yield increased statistically significantly. In the case of a lower rate but also both rates of the Effeco 33:33:33, we did not find a statistically significant increase in the yield of sunflower seeds. The effect of biochar substrates on crops yield was also assessed in comparison with conventional sunflower fertilization on this sandy soil, this means the second control was a treatment with additional urea fertilization at a rate of 100 kg.ha^{-1} (Mineral fertilization, MF-control). Compared to the MF-control (Urea at rate of 100 kg.ha^{-1} in 2018), we observed on average an increase in the yield of sunflower seeds in the treatments Effeco 33:33:33 in rates of 10 and 20 t.ha^{-1} + MF by 270 and 610 kg.ha^{-1} respectively, and in treatment Effeco 50:50 at a rate of 10 t.ha^{-1} + MF by an average of 1.01 t.ha^{-1}, but these findings were not statistically significant due to the large variance of values between replicates (total of 3 replicates). However, between the MF-control and the biochar substrate Effeco 50:50 at a rate of 20 t.ha^{-1} + MF, we noticed a statistically significant difference in the yield of sunflower seeds. It is clear from the above that a higher rate of biochar substrate Effeco 50:50 without additional fertilization, but also in combination with 100 kg of urea per hectare had the most significant effect on increasing the yield of sunflower seeds on sandy soil in 2018.

Interestingly, in the next two years the same trends in the crops yield after biochar substrate treatments were observed, being completely different compared to 2018. In 2019, the wheat grain yield increased statistically significantly in the treatments with both biochar substrates in both rates compared to the unfertilized control. Compared to the unfertilized control, the grain yield increased by 56, 98, 35 and 53% in the treatments Effeco 33:33:33 at 10 t.ha^{-1}, Effeco 33:33:33 at 20 t.ha^{-1}, Effeco 50:50 at 10 t.ha^{-1} and Effeco 50:50 at 20 t.ha^{-1} respectively. When compared to fertilized control (MF-control: Amofos + Urea of 2019), wheat grain yield increased statistically significantly only in the case of Effeco 50:50 substrate – significantly more after the higher than the lower application rate. As mentioned above, also in 2020, the trends in increasing the yield in individual biochar substrate treatments followed the year 2019.

The size of crops yield is dependent on various factors including soil-climatic conditions and soil management

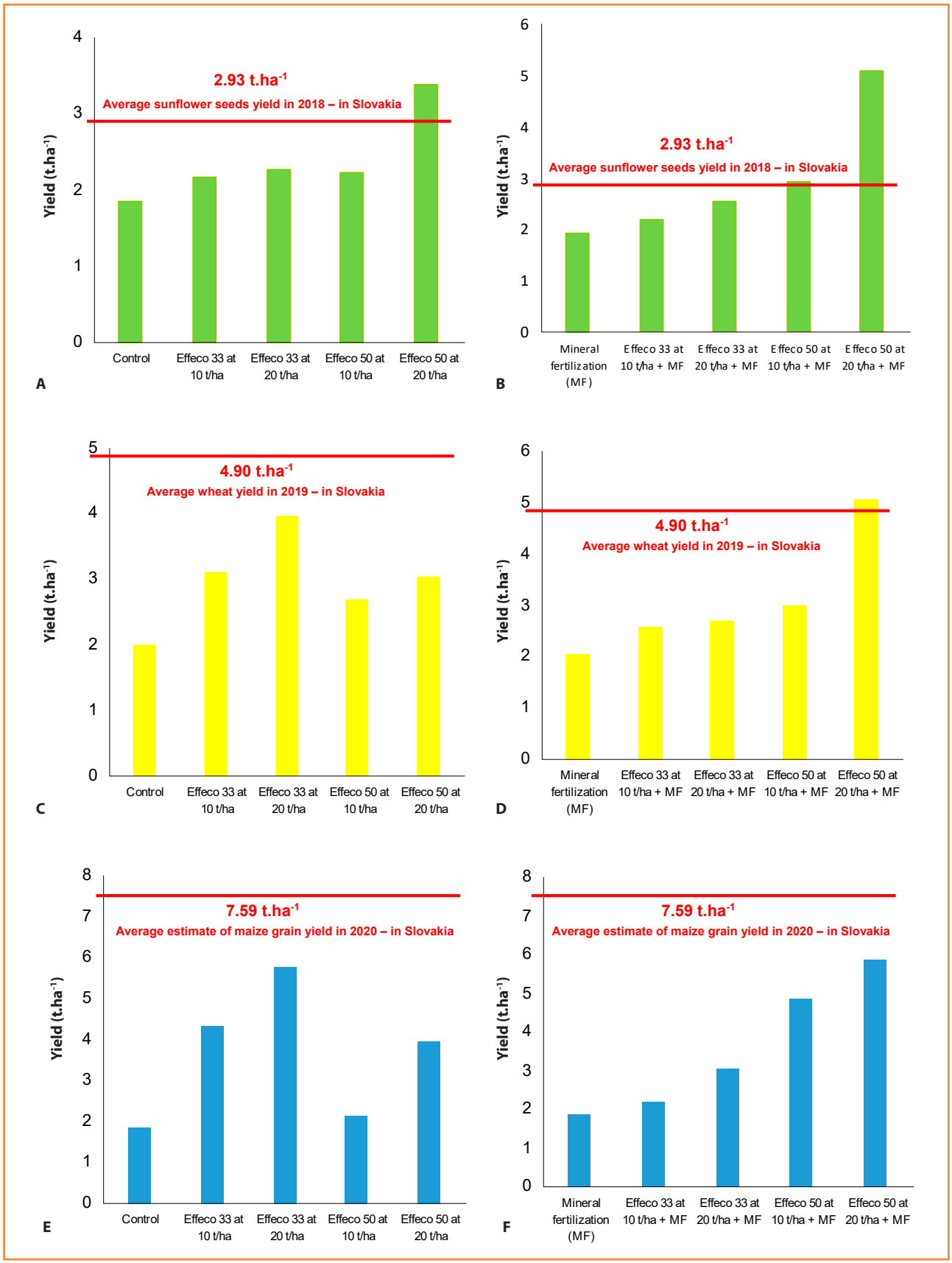

Figure 1 Effect of biochar substrates and combination of biochar substrates together with mineral fertilizers application A, B) on the seeds yield of sunflower in 2018, C, D) durum wheat in 2019, and E, F) grain yield of maize in 2020 in comparison to average crop yield (red line)

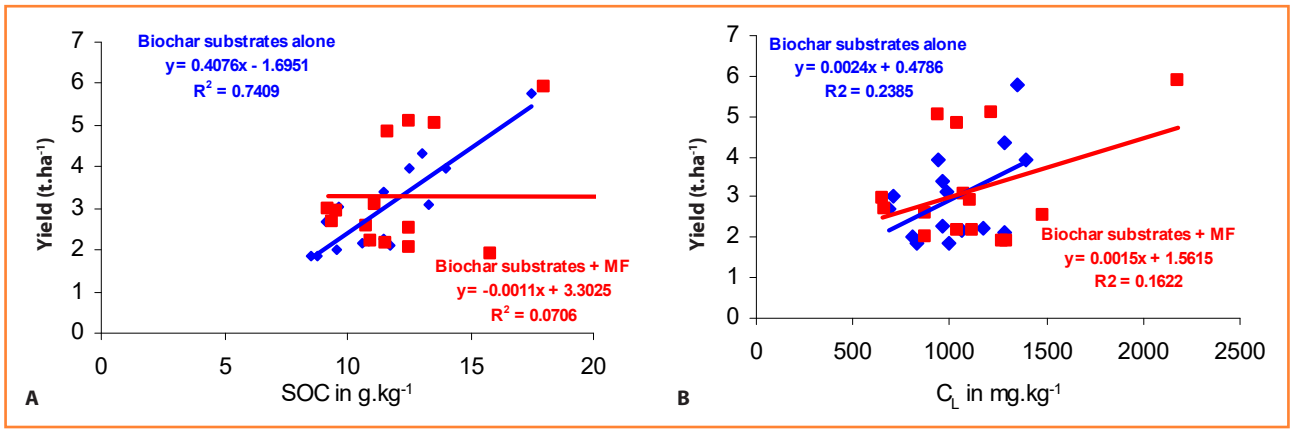

Figure 2 Linear relationships between A) soil organic carbon, B) labile carbon and crop yields

practices including fertilization. One of the most significant factors affecting crops yield is climate (Kováčik & Ryant, 2019; Aydin et al., 2020). Crops have different requirements on temperature and precipitation; however, their optimal distribution is crucial during the vegetation season of crops (Gantner et al., 2008). Observed sunflower seeds and wheat grain yield data in 2018 and 2019 respectively, were compared to the average crop yields obtained for specific crops during the studied seasons in Slovakia, and the maize grain yield in 2020 is an estimate of average yields (Fig. 1). The average gained yield of sunflower seeds in 2018 and wheat in 2019 in Slovakia was reported to be 2.93 t.ha^{-1} and 4.90 t.ha^{-1}, respectively. In 2020, the average estimate of corn grain yield was 7.59 t.ha^{-1} (STATdat, 2020). Considering the limitation of tillage operations on the site (only disking and reduced tillage) since the biochar substrates application in autumn 2017, the observed crop yields in the field experiment were compared to the lower values referring to the country's average. However, we must also remember that the soil at the experimental site was sandy. And so, for this reason, it is not surprising that the yields were below the average yields of individual crops in Slovakia. According to the results of Agegnehu et al. (2016) as well as Aydin et al. (2020), the application of biochar and its combination with other manure or mineral fertilizers significantly increased crop yields; however, this effect is more significant in low productive sandy soils than in high productive loam, silt loam, silty clay loam or clay soils (El-Naggara et al., 2019).

3.3 Relationships between soil organic carbon and crops yield

Since biochar is a source of carbon, we assumed that the application of biochar substrates to the soil would increase its content in the soil, which could result in an increase in crop yields. The linear relationships between total, labile carbon and crop yields are shown in Fig. 2. It is evident from the data that the higher content of SOC in the soil resulted in higher crop yields, but a statistically significant effect was found only in the case of biochar substrates alone treatments. In the case of biochar substrates combined with mineral fertilizers, we did not find a statistically significant linear relationship between SOC and crop yields, which could indicate that other factors may have influenced the formation of crops in those treatments – e.g. soil properties influenced through the application of supplied biochar substrates or mineral fertilization – improving soil pH, sorption capacity, nutrient regime or physical properties (Horák, 2015; Igaz et al., 2018; Juriga & Šimanský, 2019). Despite the fact that a positive correlation was found between the content of SOC and C_L (in treatments with biochar substrates alone $r = 0.738$, $P < 0.01$; also, in treatments biochar substrates with mineral fertilizers $r = 0.806$, $P < 0.001$) the content of C_L did not have a statistically significant effect on increasing the crop yields not even in biochar substrates alone treatments, nor in biochar substrates combined with mineral fertilizers.

4 Conclusions

The results showed that the effects of biochar substrates on change in SOM and crop yields is dependent on the rates and type of biochar substrates employed as well as their combination with other mineral fertilizers. Overall, our results showed a robust effect on crop yields due to applied biochar substrates in the second year after its incorporation to the sandy soil with the same trend in the third year especially in treatments using biochar substrates alone, compared to the first year after their application. Increase in crop yields is linked to higher SOC in the soil due to biochar substrates alone being applied, and in the case of treatments using biochar substrates together with mineral fertilizers, the increase of crop yields was affected by other factors – probably as a result of the improvement of other soil properties, nutrient supply etc. after the

incorporation of biochar substrates to the soil, but also additional mineral fertilization. Going forward, further research is important to identify those effects which are responsible for the increase in crop yields in biochar substrates with mineral fertilizers treatments.

Acknowledgments

The authors would like to thank very much Zdroje Zeme a.g. for the financial support.

References

Agegnehu, G., Bass, A. M., Nelson, P. N., & Bird, M. I. (2016). Benefits of biochar, compost and biochar-compost for soil quality, maize yield and greenhouse gas emissions in a tropical agricultural soil. *Science of The Total Environment*, *543*, 295–306. https://doi.org/10.1016/j.scitotenv.2015.11.054

Aydin, E., Šimanský, V. Horák, J., & Igaz, D. (2020). Potential of biochar to alternate soil properties and crop yields 3 and 4 years after the application. *Agronomy*, *10*, 889. https://doi.org/10.3390/agronomy10060889

Behera, S. K., & Shukla, A. K. (2015). Spatial distribution of surface soil acidity, electrical conductivity, soil organic carbon content and exchangeable potassium calcium and magnesium in some cropped acid soils of India. *Land Degradation and Development*, *26*, 71–79.

Cornelissen, G., Jubaedah, Nurida, N. L., Hale, S. E., Martinsen, V., Silvani, L., & Mulder, J. (2018). Fading positive effect of biochar on crop yield and soil acidity during five growth seasons in an Indonesian Ultisol. *Science of the Total Environm*ent, *634*, 561–568. https://doi.org/j.scietotenv.2018.03.380

El-Naggar, A., Lee, S., Rinklebe, J., Farooq, M., Song, H., Sarmah, A. K., Zimmerman, A. R., Ahmad, M., Shaheen, S. M., & Ok, S. Y. (2019). Biochar application to low fertility soils: A review of current status, and future prospects. *Geoderma*, *337*, 536–554. https://doi.org/10.1016/j.geoderma.2018.09.034

Gantner, R., Stjepanivić, M., & Gantner, V. (2008). Precipitation and temperature effects upon grain yield of field pea. *Cereal Research Communication*, *36*, 1503–1506.

Gondek, K., Mierzwa-Hersztek, M., Kopeć, M., Lošák, T., von Bennewitz, E., Spandel, A., & Kuc, K. (2020). The effectiveness of biochar in mitigating changes in the chemical properties of sandy soil treated with various chemicals. *Journal of Elementology*, *25*(3), 1045–1058. https://doi.org/10.5601/jelem.2019.24.4.1941

Horák, J. (2015). Testing biochar as a possible way to ameliorate slightly acidic soil at the research field located in the Danubian Lowland. *Acta Horticulturae et Regiotecturae*, *1*, 20–24. https://doi.org/10.1515/ahr-2015.0005

Horák, J., Aydin, E., Igaz, D., Šimanský, V., Felber, R., Lukac, M., Balashov, E. Buchkina, N., Rizhiya, E., & Jankowski, M. (2017). Biochar and biochar with N-fertilizer affect soil N_2O emission in Haplic Luvisol. *Biologia*, *72*(9), 995–1001. https://doi.org/10.1515/biolog-2017-0109

Horák, J., Šimanský, V., & Aydin, E. (2020). Benefits of biochar and its combination with nitrogen fertilization for soil quality and grain yields of barley, wheat and corn. *Journal of Elementology*, *25*, 443-458. https://doi.org/10.5601/jelem.2019.24.3.1887

Hrivňáková, K., Makovníková, J., Barančíková, G., Bezák, P., Bezáková, Z., Dodok, R., Grečo, V., Chlpík, J., Kobza, J., Lištjak, J., Mališ, J., Píš, V., Schlosserová, J., Slávik, O., Styk, J., & Širáň, M. (2011). *Uniform working procedures of soil analysis*. VÚPOP.

Cheng, H., Hill, P. W., Bastami, M., S., & Jones, D. L. (2016). Biochar stimulates the decomposition of simple organic matter and suppresses the decomposition of complex organic matter in a sandy loam soil. *GCB Bioenergy*, *9*(6), 1110–1121. https://doi.org/10.1111/gcbb.12402

Igaz, D., Šimanský, V., Horák, J., Aydin, E., Domanová, J., Rodný, M., & Buchkina, N. (2018). Can a single dose of biochar affected soil physical and chemical characteristics? *Journal of Hydrology and Hydromechanics*, *66*(2), 421–428. https://doi.org/10.2478/john-2018-0034

IUSS Working Group (WRB). (2015). *World Reference Base for Soil Resources 2014, update 2015*. *International soil classification system for naming soils and creating legends for soil maps* (World Soil Resources Reports No. 106). FAO.

Jones, D. L., Rousk, J., Edwards-Jones, G., DeLuca, T. H., & Murphy, D. V. (2012). Biocharmediated changes in soil quality and plant growth in a three year field trial. *Soil Biololgy and Biochemistry*, *45*, 113–124. https://doi.org/10.1016/j.soilbio.2011.10.012

Juriga, M., & Šimanský, V. (2019). Effect of biochar and its reapplication on soil pH and sorption properties of silt loam Haplic Luvisol. *Acta Horticulturae et Regiotecturae*, *22*(2), 65–70. https://doi.org/10.2478/ahr-2019-0012

Kováčik, P., & Ryant, P. (2019). *Agrochemistry* (principles and practice). SUA.

Mierzwa-Hersztek, M., Gondek, K., Klimkowicz-Pawlas, A., Kopeć, M., & Lošák, T. (2018). Effect of coapplication of poultry litter biochar and mineral fertilisers on soil quality and crop yield. *Zemdirbyste-Agriculture*, *105*(3), 203–210. https://doi.org/10.13080/z-a.2018.105.026

Obia, A., Mulder, J., Martinsen, V., & Cornelissen, G. (2016). In situ if bichar on aggregation, water retention and porosity in light-textured tropical soil. *Soil & Tillage Research*, *155*, 35–44. https://doi.org/10.1016/j.still.2015.08.002

Osman, K. T. (2018). *Management of soil problems*. Routledge.

Rawat, J., Saxena, J., & Sanwal, P. (2019). Biochar: a sustainable approach for improving plant growth and soil properties. In Abrol, V., & Sharma, P. (Eds.) *Biochar, an imperative amendment for soil and the environment* (pp. 3–19). IntechOpen.

Shackley, S., Ruysschaert, G., Zwart, K., & Glaser, B. (2016). *Biochar in European soils and agriculture*. Routledge.

Singh, B. P., & Cowie, A. L. (2014). Long-term influence of biochar on native organic carbon mineralisation in a low-carbon clayey soil. *Science Reports*, *4*, 1–9. https://doi.org/10.1038/srep03687

Singh, B., & Cowie, A. L. (2010). Characterisation and evaluation of biochars for their application as a soil amendment. *Australian Journal of Soil Research*, *48*, 516–525.

STATdat (2020). B*ranch Statistics* > *Agriculture, Forestry, Fisheries* > *Yields of Selected Agricultural Crops* > *Select Data* > *Hectare Yields* (Tons). http://statdat.statistics.sk

Thalmann, M., & Santelia, D. (2017). Strach as a determinant of plant fitness under abiotic stress. *The New Phytologist*, *214*(3), 943–951.

sciendo

DOI: 10.2478/ahr-2021-0021
Acta hort regiotec, 24, 2021(1): 21–27

Research Article

Long-term effect of crops and fertilization on soil eco-chemical state

Jerzy Jonczak
Warsaw University of Life Sciences, Warsaw, Poland

Article Details: Received: 2020-12-29 | Accepted: 2021-03-08 | Available online: 2021-05-31

Licensed under a Creative Commons Attribution 4.0 International License

SCREENED BY iThenticate Professional Plagiarism Prevention

The study on long-term effects of various crops and fertilization practices on soil eco-chemical state was performed in the complex of Planosols at the Warsaw University of Life Sciences – SGGW experimental station in Skierniewice. The study covered three experiments – Ex-1 (established in 1923; no organic fertilization, cereals as a crop), Ex-2 (established in 1992; farmyard manure application every 4 years, cereals as a crop) and Ex-3 (established in 1975; no organic fertilization, blueberries as a crop). Additionally, each experiment covered three mineral fertilization options, including no fertilization, NPK and CaNPK. Soil samples were taken from A-horizons in 2017 and analysed using standard procedures. The results demonstrate considerable influence of crops and fertilization practices on soil eco-chemical state. Both mineral and organic fertilizers positively affected sorptive capacity as compared to control and modified ionic composition of soil sorption complex. Lower exchangeable acidity and higher sum of exchangeable basis and base saturation were noted in fertilized soils and cereals as a crop as compared to controls. Under blueberries there was observed strong acidification of the soil, in particular in combination with NPK fertilizers, as evidenced by the highest exchangeable acidity, hydrolytic acidity, and the lowest base saturation. Liming partially neutralized acidifying effect of blueberries. Fertilization and crops also strongly influenced buffering capacity of the soils. Extremely low ability to neutralize acidic ions was noted in unfertilized soils, whereas the highest at plots fertilized with Ca. The highest ability to neutralize alkaline ions was typical for NPK fertilized soils under blueberries.

Keywords: soil pH, soil sorption, buffering capacity, fertilization, soil quality

1 Introduction

Tillage is one of most widespread form of human impact on soil cover being sometimes highly destructive. However, it is a complicated issue that covers various aspects of crop rotation, cultivation technologies and fertilization and their influence on soil chemistry, physical properties, soil organic matter quality and quantity, and many others. Although above-mentioned issues have been frequently studied, there is still not sufficient knowledge in some fields. First of all, there is relatively little data from long-term, fully controlled field experiments. Most of publications are based on single sampling of the soils under various uses (crops/fertilization/other factors) or short-term observations with no sufficient reconstruction of land-use history, crop rotation, and fertilization. Therefore, the obtained data cannot be precisely interpreted, and final conclusions are not certain. Considering increasing intensity of agricultural production due to growing human population and limited resistance of the soils to external factors, detailed studies on tillage (in general) impact on soil cover are highly recommended.

The purpose of this study was to evaluate long-term effects of two crops (cereals and blueberries) and several fertilization practices (various combinations of farmyard manure, NPK, and CaNPK fertilizers) on chosen indicators of soil eco-chemical state, including pH, sorptive properties and buffering capacity. The studied soil properties are of key importance for nutrients management in arable soils and may influence environmental quality of agroecosystems.

2 Material and methods

The studies were performed at the Warsaw University of Life Sciences – SGGW experimental station in Skierniewice (51° 57′ 54.3″ N, 20° 9′ 31.8″ E). Average annual temperatures for this region are around 8 °C, whereas

***Corresponding Author:** Jerzy Jonczak, Warsaw University of Life Sciences-SGGW, Department of Soil Science, Nowoursynowska Str. 159, 02-787 Warsaw, Poland, ☎ +48 0 22 59 326 17; e-mail: jerzy_jonczak@sggw.edu.pl

sum of precipitation varies around 530 mm. The station is located in a flat post-glacial landscape and Planosols developed form sandy substrates over loams are typical soils. Beginning from the year 1923, in the station there are conducted long-term experiments on the effects of various crops and fertilization practices on soil properties and plant yielding. This study was based on three major experiments and several fertilization options, according to Fig. 1. Experiment 1 (Ex-1, established in 1923) covers various options of mineral fertilization without organic fertilization and cereals as a crop. Experiment 2 (Ex-2, established in 1992) covers various options of mineral fertilization and farmyard manure application at rate of 25 t.ha^{-1} every 4 years and cereals as a crop. The last experiment (Ex-3, established in 1975) covers various options of mineral fertilization without organic fertilization and blueberry as a crop. The following options of mineral fertilization were chosen for this study: control (no mineral fertilization), NPK, and CaNPK. In all experiments nitrogen was applied as ammonium sulfate (30 kg.ha^{-1} of N from 1921 to 1976 and 90 kg.ha^{-1} of N from 1976), phosphorus as superphosphate (30 kg.ha^{-1} of P_2O_5 from 1921 to 1976 and 26 kg.ha^{-1} of P_2O_5 from 1976) and potassium as potassium chloride (30 kg.ha^{-1} of K_2O from 1921 to 1976 and 91 kg.ha^{-1} of K_2O from 1975). Calcium was applied every 4 years as 1.6 t.ha^{-1} of CaO. All fertilization options covered three replications. The size of a single plot was 4 × 9 m (36 m^2), and spacing between the plots was 2 m.

The soils were sampled in August 2017. Three cores from A-horizons were taken from each plot and mixed into one average sample. The samples were air-dried and sieved though a 2.0 mm sieve. Earth fraction (<2.0 mm) was used for the further analysis. Bulk samples were taken from central parts of A-horizon using the 100 cm^3 steel rings. The following laboratory analyses were done:

- Bulk density and total porosity using the gravimetric method (Bednarek et al., 2004).
- Particle-size distribution by mixed pipette and sieve methods. The Polish Soil Science Society classification (PTG, 2009) was applied to determine textural fractions and groups.
- pH by the potentiometric method in a suspension with water and 1 mol.dm^{-3} solution of KCl (Bednarek et al., 2004).
- The content of total organic carbon (TOC) and total nitrogen (N) by dry combustion (Vario MacroCube, Elementar).
- The contents of basic cations (Ca^{2+}, Mg^{2+}, Na^+ and K^+) by inductively-coupled plasma atomic emission spectrometry (ICP-OES, Avio 200, Perkin Elmer) after samples extraction in 1 mol.dm^{-3}, pH = 7.0 solution of ammonium acetate.
- Exchange acidity (H_w) by the Sokolov method (Bednarek et al., 2004).
- Hydrolytic acidity (H_h) by the Kappen method (Bednarek et al., 2004).
- Buffering properties according to the Arrhenius procedure (Bednarek et al., 2004).

Moreover, the following parameters were calculated based on the results obtained: sum of exchangeable basis (TEB) as a sum of exchangeable Ca^{2+}, Mg^{2+}, Na^+ and K^+; cation exchange capacity (CEC) as TEB + H_w; basic saturation of soil sorption complex (BS) as (TEB × 100)/CEC. Statistical analysis included measures of central tendencies and dispersal, Dunn's test, correlations, and cluster analysis.

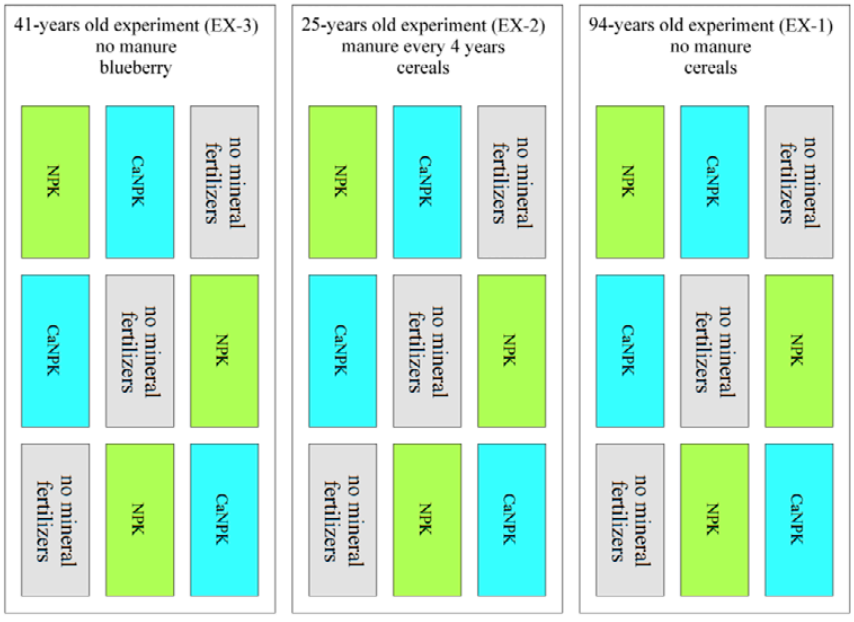

Figure 1 Design of the experiment

3 Results and discussion

3.1 Basic characteristics of the soils

Humic horizons of the studied Planosols were characterised by loamy sand texture at every plot, and contained 72.9–81.5% of sand (2.0–0.05 mm), 13.8–19.7% of silt (0.05–0.002 mm) and 4.0–7.7% of clay (<0.002 mm) fractions. Bulk density ranged from 1.45 to 1.66 g.cm^{-3}, whereas total porosity from 35.6 to 44.6% during the study period (Table 1). The soils contained

Table 1 Basic physical characteristics of the soils

Experiment options	Replicates	Textural group	Bulk density ($g.cm^{-3}$)	Total porosity (%)	TOC ($g.kg^{-1}$)	N ($g.kg^{-1}$)	TOC/N
Ex-1/Cont.	1	LS*	1.60	38.9	4.73	0.430	11.0
	2	LS	1.52	42.2	4.36	0.370	11.8
	3	LS	1.59	39.8	3.79	0.378	10.0
Ex-1/NPK	1	LS	1.66	36.5	5.80	0.544	10.7
	2	LS	1.58	40.9	5.42	0.466	11.6
	3	LS	1.59	39.3	5.50	0.476	11.6
Ex-1/CaNPK	1	LS	1.66	36.9	6.58	0.604	10.9
	2	LS	1.61	40.1	5.04	0.437	11.5
	3	LS	1.56	43.2	4.88	0.392	12.5
Ex-2/Cont.	1	LS	1.59	38.2	5.87	0.543	10.8
	2	LS	1.50	41.8	5.04	0.520	9.7
	3	LS	1.58	39.1	5.70	0.538	10.6
Ex-2/NPK	1	LS	1.64	37.1	7.11	0.671	10.6
	2	LS	1.47	42.2	8.39	0.833	10.1
	3	LS	1.48	42.7	6.98	0.603	11.6
Ex-2/CaNPK	1	LS	1.51	42.3	8.48	0.782	10.8
	2	LS	1.50	44.6	8.41	0.759	11.1
	3	LS	1.55	40.5	6.52	0.563	11.6
Ex-3/Cont.	1	LS	1.53	41.3	6.23	0.462	13.5
	2	LS	1.60	38.8	7.61	0.503	15.1
	3	LS	1.59	38.2	4.68	0.372	12.6
Ex-3/NPK	1	LS	1.45	43.1	11.23	0.913	12.3
	2	LS	1.49	42.5	7.29	0.562	13.0
	3	LS	1.52	40.4	11.79	0.783	15.1
Ex-3/CaNPK	1	LS	1.65	35.6	7.82	0.698	11.2
	2	LS	1.56	40.8	7.64	0.689	11.1
	3	LS	1.59	39.2	7.84	0.591	13.3

* LS – loamy sand

3.79–11.79 $g.kg^{-1}$ of TOC and 0.37–0.91 $g.kg^{-1}$ of N. Both TOC and N contents considerably varied between plots. TOC/N ratio ranged from 9.7 : 1 to 15.1 : 1.

3.2 Soil pH

Soil pH is an important factor influencing forms, mobility, bioavailability, and toxicity of chemical elements and various compounds. Therefore, it is a good indicator of living conditions of soil biota and biochemical processes (Kowalkowski, 2002; Błońska & Januszek, 2010). It is also one of key factors influencing crop production and quality (e.g. Limon-Ortega & Martinez-Cruz, 2014). Knowledge about pH and its feedbacks with other soil parameters is essential for the development of efficient nutrient management systems. Tillage and fertilization effects on soil pH have been frequently studied. The results of this study show importance of both crops and fertilization for this soil characteristics. Mean soil pH-H_2O varied from 5.03 to 6.53, whereas pH-KCl from 3.13 to 6.14 (Fig. 2). The lowest values were noted at plots Ex-3/NPK and Ex-3/CaNPK followed by slightly higher at Ex-1/NPK and Ex-1/Cont. The lowest pH at Ex-3/NPK and Ex-3/CaNPK plots can be explained by mixed effect of blueberries and NH_4^+ application as fertilizer. Ammonium form of nitrogen is preferred by blueberries, however, their uptake by roots is associated with secretion of H^+. Low pH at Ex-1/Cont. and Ex-1/NPK plots is probably an effect of leaching of basic cations and/or their removal with the crop. The process

of SOM decomposition as a source of H^+ (e.g. Hulugalle & Weaver, 2005) can also have some effect, however, the role of this factor is probably low and difficult for precise estimation. The highest pH noted at plots Ex-2/Cont., Ex-2/CaNPK and Ex-1/CaNPK confirm importance of manure and Ca fertilizers as agents neutralizing soil acidity.

3.3 Sorptive properties

Soil sorption capacity is a measure of soil solid phase potential to absorb ionic substances. Clay minerals and soil organic matter (SOM) play a key role in this area (Thompson et al., 1989; Okołowicz, 1996; Jaworska et al., 2008). Therefore, effects of various external factors on this property should be considered mainly from the perspective of changes in clay mineralogy and SOM. Crop rotation and fertilization effects on CEC were subjects of numerous studies (e.g. Rojas et al., 2013; Šimanský & Polláková, 2014). CEC in this study ranged from 3.06 to 6.76 $cmol_c.kg^{-1}$. The observed values are typical for loamy sand and sandy loam, poor-moderately abundant in SOM soils (Raczuk, 2011). The lowest mean value of CEC was noticed at Ex-1/Cont. and Ex-1/NPK plots, whereas the highest at plots fertilized with calcium, in particular in combination with farmyard manure (Ex-2/CaNPK) (Fig. 3). Previous studies of Šimanský et al. (2019) showed that soil of the studied plots fertilized with farmyard manure is characterized by better quality of SOM as evidenced by higher content of humic acids and lower of fulvic acids. The observed differences between experimental options in terms of CEC were statistically significant in many cases. There was not observed a significant correlation between CEC vs TOC content and positive correlation with clay content (r = 0.618). The lack of positive correlation with TOC content can be explained by heterogeneity of SOM quality as affected by various tillage practices. Importance of SOM quality as a factor influencing sorption of ionic substances by the soils was confirmed by the results of many studies (e.g. Vang & Huang, 2001; Kang et al., 2009).

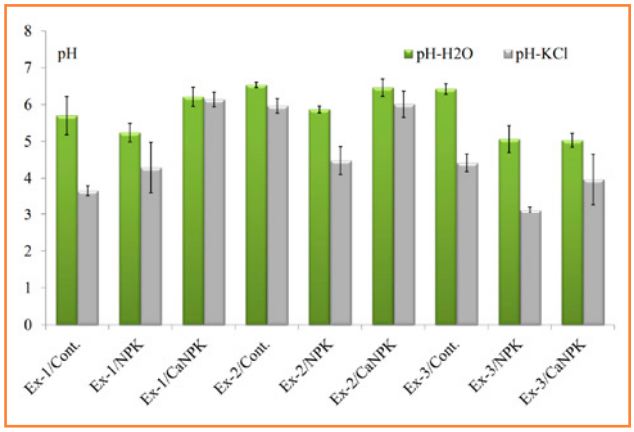

Figure 2 Soil pH under various crops and fertilization practices
mean values ±SD, n = 3

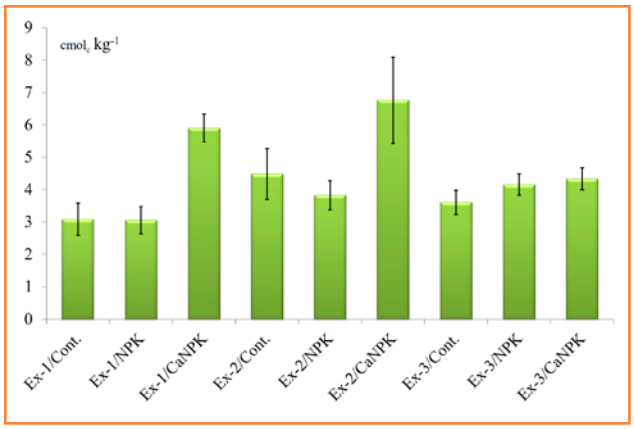

Figure 3 Cation exchange capacity under various crops and fertilization practices
mean values ±SD, n = 3

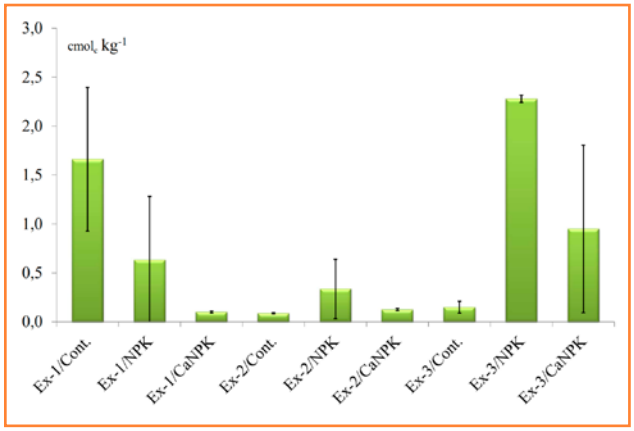

Figure 4 Exchangeable acidity in the soils under various crops and fertilization practices
mean values ±SD, n = 3

Exchange acidity strongly varied among the studied plots – from 0.09 to 2.28 $cmol_c.kg^{-1}$ (Fig. 4). It was the lowest at plots fertilized with Ca in experiments 1 and 2 and controls in experiment 2 and 3. The highest H_w was noted for Ex-3/NPK and Ex-1/Cont. The observed tendencies confirm acidifying effect of blueberries and neutralizing effects of lime and manure in relation to acidic ions.

Hydrolytic acidity is the content of exchangeable acidic ions and their easily hydrolysable forms. It ranged from 1.21 to 6.07 $cmol_c.kg^{-1}$, showing lower variability as compared to H_w. However, tendencies were also clear. The lowest values were generally observed at plots fertilized with Ca and/or farmyard manure, whereas the highest at Ex-3/NPK plots (Fig. 5). Positive correlation with TOC content (r = 0.592) confirm key role of SOM as a source of acidity.

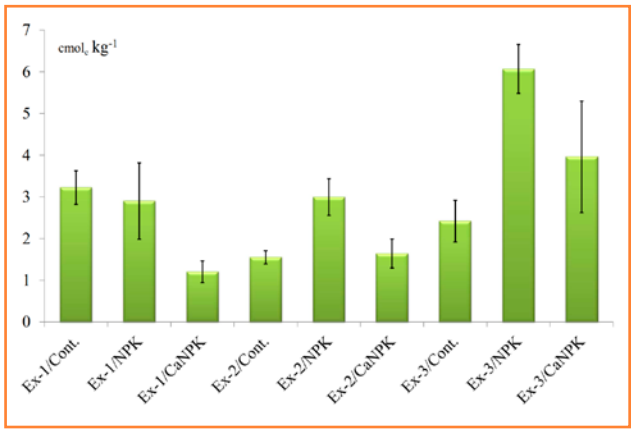

Figure 5 Hydrolytic acidity in the soils under various crops and fertilization practices
mean values ±SD, $n = 3$

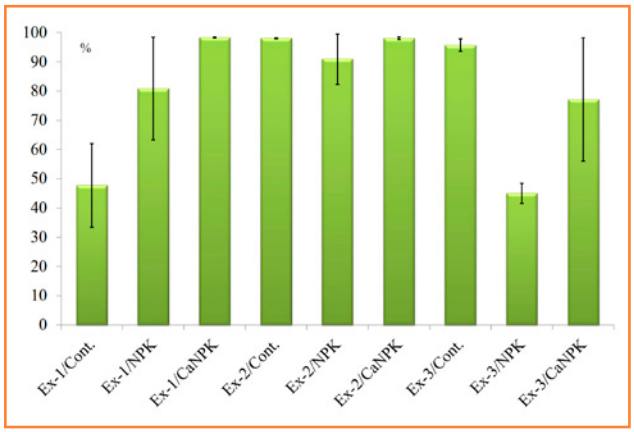

Figure 7 Base saturation in the soils under various crops and fertilization practices
mean values ±SD, $n = 3$

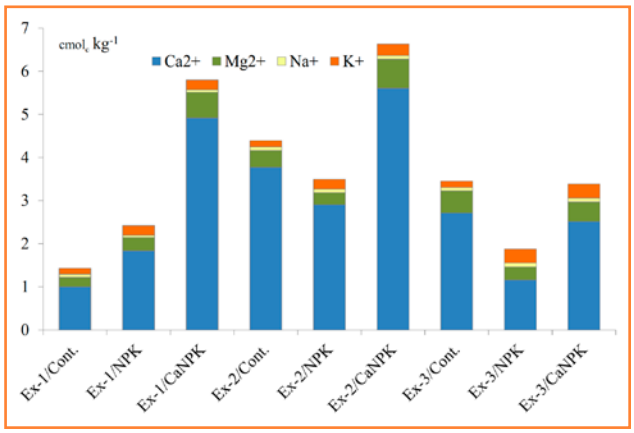

Figure 6 Average contents of basic cations in the soils under various crops and fertilization practices

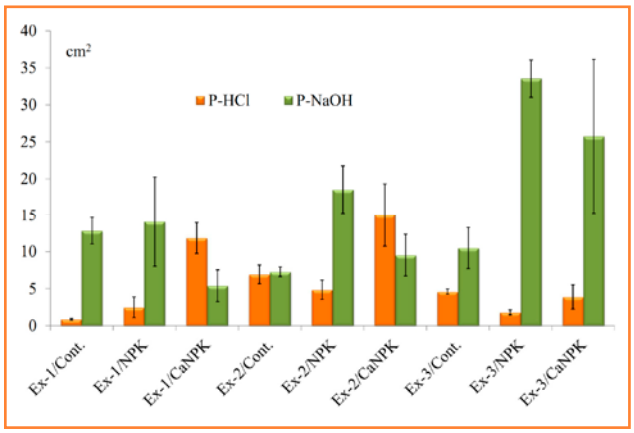

Figure 8 Buffering capacity (PHCl and PNaOH) in the soils under various crops and fertilization practices
mean values ±SD, $n = 3$

Basic cations occurred at amounts from 1.43 to 6.63 cmol$_c$.kg^{-1}. Their lowest contents were noted at Ex-1/Cont. plots followed by Ex-3/NPK. Most abundant were the plots fertilized with Ca in experiments 1 and 2 (Fig. 6). Generally, higher contents of exchangeable basis were recorded at plots with organic fertilization as compared to other plots. It highlights its important role as a source of basic cations. Calcium predominated among exchangeable basis in the studied soils, irrespective of crop and fertilization practices. It constituted 62.0–86.0% of basis on average. Exchangeable Mg constituted 7.9–15.8%, K 3.3–17.1% and Na 1.0–5.3% of basis (Fig. 7). The observed composition of soil sorption complex is typical for most soils of Poland (e.g. Orzechowski et al., 2005; Bartmiński & Klimowicz, 2008). Basis constituted 45.2–98.3% of exchangeable cations on average. The lowest BS was observed at Ex-1/Cont. and Ex-3/NPK plots, whereas the highest at plots of experiment 2, in general.

The ability to neutralize acidic and alkaline ionic substances (buffering properties) is controlled by a complex of soil physical, physicochemical and chemical properties. $CaCO_3$, clay minerals and SOM are the most important constituents in this area (Kowalkowski, 2002; Malczyk et al., 2008; Walenczak et al., 2009). Effects of some external factors on buffering capacity of the soils, including tillage and fertilization, are still poorly explored. Influence of some factors can be clearly explained; however, some have indirect effects. In the studied soils, buffering capacity of acids ranged from 0.86 to 15.03 cm^2, whereas alkali from 5.40 to 33.54 cm^2 (Fig. 8). The observed values are typical, considering characteristics of the soils (Raczuk, 2011). The lowest ability to neutralize acidic ions was noted at Ex-1/Cont. plots that were characterized by the lowest sorption capacity and content of basic cations. Only slightly higher values were observed for Ex-1/NPK and Ex-3/NPK experimental options. This observation demonstrates little relevance of NPK fertilization (in a form and doses like in the present study) as a factor increasing soil ability to neutralize acidic ions. The observation can be partially confirmed by Lieb et al. (2011), who

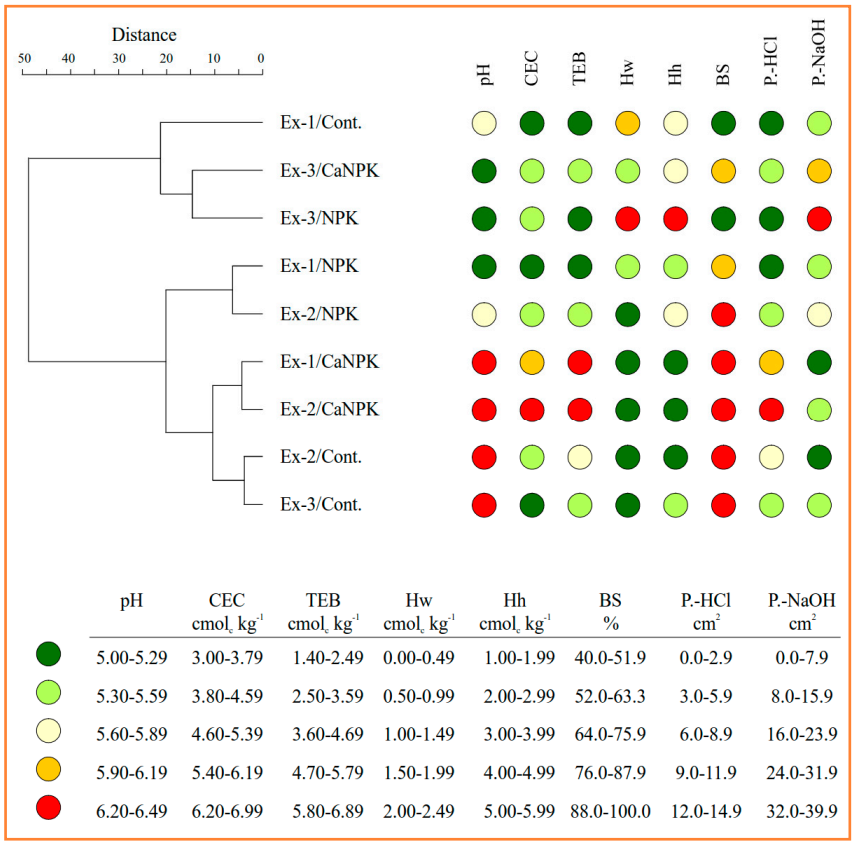

	pH	CEC cmol$_c$ kg^{-1}	TEB cmol$_c$ kg^{-1}	Hw cmol$_c$ kg^{-1}	Hh cmol$_c$ kg^{-1}	BS %	P.-HCl cm^2	P.-NaOH cm^2
	5.00-5.29	3.00-3.79	1.40-2.49	0.00-0.49	1.00-1.99	40.0-51.9	0.0-2.9	0.0-7.9
	5.30-5.59	3.80-4.59	2.50-3.59	0.50-0.99	2.00-2.99	52.0-63.3	3.0-5.9	8.0-15.9
	5.60-5.89	4.60-5.39	3.60-4.69	1.00-1.49	3.00-3.99	64.0-75.9	6.0-8.9	16.0-23.9
	5.90-6.19	5.40-6.19	4.70-5.79	1.50-1.99	4.00-4.99	76.0-87.9	9.0-11.9	24.0-31.9
	6.20-6.49	6.20-6.99	5.80-6.89	2.00-2.49	5.00-5.99	88.0-100.0	12.0-14.9	32.0-39.9

Figure 9 Cluster analysis of the studied soils based on pHH$_2$O, TEB, H_w, H_h, BS, CEC, PHCl and PNaOH (Ward method, Euclidean distance)

observed negative effect of nitrogen deposition on buffering capacity of alpine soils. Application of farmyard manure or CaO considerably increased the ability. Effect of Ca application in experiment 3 was partially neutralized by blueberries. Based on the Ulrich (1981) concept, silicate buffer system is active in most studied soils. This buffer system maintenance soil pH at level >5.0–≤6.3 and binding of acidic substances by weathering products of primary silicates is responsible mechanism. Higher ability to neutralize alkaline ions than acidic ones was noted in most studied soils. Particularly high P-NaOH values were observed at Ex-3/NPK and Ex-3/CaNPK plots (Fig. 8) that were characterized by the highest acidity. The obtained data clearly show strong impact of crops and fertilization on soil buffering capacity, as confirmed by statistically significant differences (Table 2).

Fig. 9 shows combined effects of the studied crops and fertilization practices on soil eco-chemical state indices based on cluster analysis. Two major groups of samples can be distinguished on the graph. The first group covers control plots of experiment 1 and NPK and CaNPK fertilization options in experiment 3. Such layout demonstrates strong impact of blueberries on soil eco-chemical state. The effect is accelerated by application of fertilizers containing ammonium form of nitrogen. Strong acidification, high acidity, low content of exchangeable basis and base saturation, as well as low ability to neutralize acidic ions are typical features of the soils in this group. The second group covers soil affected by manure and/or mineral fertilization under cereals as a crop. These are soils of higher pH and CEC, lower acidity, and larger ability to neutralize acidic substances.

Table 2 Comparison of chosen soil parameters at control plots (Ex-1/Cont.) vs other options of experiment based on *p*-values, Dunn Test

	Ex-1		Ex-2			Ex-3		
	NPK	CaNPK	Cont.	NPK	CaNPK	Cont.	NPK	CaNPK
pH-H$_2$O	0.471	0.355	0.060	0.837	0.095	0.136	0.258	0.280
pH-KCl	0.440	0.008	0.019	0.292	0.013	0.316	0.456	0.700
CEC	0.554	0.019	0.395	0.898	0.013	0.797	0.080	0.354
H_w	0.049	0.001	0.012	0.024	0.000	0.041	0.000	0.003
H_h	0.016	0.518	0.276	0.009	0.260	0.039	0.000	0.003
TEB	0.341	0.001	0.018	0.064	0.001	0.051	0.670	0.090
BS	0.292	0.002	0.006	0.181	0.006	0.090	0.837	0.328
P-HCl	0.092	0.000	0.001	0.007	0.000	0.008	0.154	0.016
P-NaOH	0.007	0.182	0.129	0.001	0.038	0.038	0.000	0.001

4 Conclusions

The results of this study clearly demonstrate the importance of crop and fertilization practices for soil eco-chemical state. Both mineral fertilizers and farmyard manure significantly contributed to higher sorptive capacity as compared to control. Lower exchangeable acidity and higher sum of exchangeable basis and base saturation were noted in fertilized soils and cereals as a crop. The studies confirmed strongly acidifying effect of blueberries, in particular in combination with NPK fertilizers, as evidenced by the highest exchangeable acidity, hydrolytic acidity and the lowest base saturation. Liming applied every 4 years partially neutralized the acidifying effect of blueberries. Fertilization and crops also strongly influenced buffering capacity of the studied soils. Extremely low ability to neutralize acidic ions was noted in unfertilized soils, whereas the highest in soils fertilized with Ca and cereals as a crop. The highest ability to neutralize alkaline ions was typical for fertilized soils under blueberries. In a broader context, this study confirmed huge role of long-term field experiments for understanding processes running in arable soils and their importance to sustain quality and productivity of agricultural soils.

Acknowledgements

This publication is the result of the project implementation "Scientific support of climate change adaptation in agriculture and mitigation of soil degradation" (ITMS2014+ 313011W580) supported by the Integrated Infrastructure Operational Programme funded by the ERDF.

References

Bartmiński, P., & Klimowicz, Z. (2008). Właściwości sorpcyjne czarnych ziem Kotliny Sandomierskiej wytworzonych z różnych skał macierzystych. *Roczniki Gleboznawcze*, *59*(3), 7–16.

Bednarek, R., Dziadowiec, H., Pokojska, U., & Prusinkiewicz, Z. (2004). *Badania ekologiczno-gleboznawcze*. PWN.

Błońska, E., & Januszek, K. (2010). Wpływ składu gatunkowego drzewostanów na aktywność enzymatyczną i właściwości fizykochemiczne gleb leśnych. *Roczniki Gleboznawcze*, *61*(2), 5–14.

Hulugalle, N. R., & Weaver, T. B. (2005). Short-term variations in chemical properties of Vertisols as affected by amounts, carbon/nitrogen ratio, and nutrient concentration of crop residues. *Communications in Soil Science and Plant Analysis*, *36*, 1449–1464. DOI https://doi.org/10.1081/CSS-200058489

Jaworska, H., Kobierski, M., & Dąbkowska-Naskręt, H. (2008). Kationowa pojemność wymienna i zawartość kationów wymiennych w glebach płowych o zróżnicowanym uziarnieniu. *Roczniki Gleboznawcze*, *59*(1), 84–89.

Kang, J., Hesterberg, D., & Osmond, D. L. (2009). Soil organic matter effects on phosphorus sorption: A path analysis. *Soil Science Society of America Journal*. *73*(2), 360–366. DOI https://doi.org/10.2136/sssaj2008.0113

Kowalkowski, A. (2002). Wskaźniki ekochemicznego stanu gleb leśnych zagrożonych przez zakwaszenie. *Regionalny Monitoring Środowiska Przyrodniczego*, *3*, 31–43.

Lieb, A. M., Darrouzet-Nardi, A., & Bowman, W. D. (2011). Nitrogen deposition decreases acid buffering capacity of alpine soils in the southern Rocky Mountains. *Geoderma*, *164*, 220–224. DOI https://doi.org/10.1016/j.geoderma.2011.06.013

Limon-Ortega, A., & Martinez-Cruz, E. (2014). Effects of soil pH on wheat grain yield and quality. *Communications in Soil Science and Plant Analysis*, *45*(5), 581–591. DOI https://doi.org/10.1080/00103624.2013.874018

Malczyk, P., Kobierski, M., Jaworska, H., & Dąbkowska-Naskręt, H. (2008). Zależność między wybranymi właściwościami gleb i pojemnością buforową w glebach uprawnych regionu Pomorza i Kujaw. *Roczniki Gleboznawcze*, *59*(1), 149–154.

Okołowicz, M. (1996). Właściwości sorpcyjne frakcji granulometrycznych wybranych gleb. *Roczniki Gleboznawcze*, *47*(1/2), 33–46.

Orzechowski, M., Smólczyński, S., & Sowiński, P. (2005). Właściwości sorpcyjne gleb aluwialnych Żuław Wiślanych. *Roczniki Gleboznawcze*, *56*(1/2), 119–127.

PTG. (2009). Klasyfikacja uziarnienia gleb i utworów mineralnych – PTG 2008. *Roczniki Gleboznawcze*, *60*(2), 5–17.

Raczuk, J. (2011). Acidity and buffering properties of soils of the Biała Podlaska Commune. *Ochrona Środowiska i Zasobów Naturalnych*, *49*, 186–192.

Rojas, R., Morillo, J., Usero, J., Delgado-Moreno, L., & Gan, J. (2013). Enhancing soil sorption capacity of an agricultural soil by addition of three different organic wastes. *Science of the Total Environm*ent (pp. 458–460, 614–623). DOI 10.1016/j.scitotenv.2013.04.032

Šimanský, V., Juriga, M., Jonczak, J., Uzarowicz, Ł., & Stępień, W. (2019). How relationships between soil organic matter parameters and soil structure characteristics are affected by the long-term fertilization of a sandy soil. *Geoderma*, *342*, 75–84. DOI https://doi.org/10.1016/j.geoderma.2019.02.020

Šimanský, V., & Polláková, N. (2014). Soil organic matter and sorption capacity under different soil management practices in a productive vineyard. *Archives of Agronomy and Soil Science*, *60*(8), 1145–1154.
DOI https://doi.org/10.1080/03650340.2013.865837

Thompson, M., L., Zhang, H., Kazemi, M., & Sandor, J. A. (1989). Contribution of organic matter to cation exchange capacity and specific surface area of fractionated soil materials. *Soil Science*, *148*, 250–257.

Ulrich, B. (1981). Ökologische Gruppierung von Böden nach ihrem chemischen Bodenzustand. *Zeitschrift für Pflanzenernährung und Bodenkunde*, *144*, 289–305.

Vang, F. L., & Huang, P. M. (2001). Effects of organic matter on the rate of potassium adsorption by soils. *Canadian Journal of Soil Science*, *81*(3), 325–330. DOI https://doi.org/10.4141/S00-069

Walenczak, K., Licznar, S. E., & Licznar, M. (2009). The role of organic matter and colloidal clay in forming of buffer properties of soils of the Szczytnicki Park. *Soil Science Annual*, *60*(2), 102–107.

WRB. (2015). *World Reference Base for Soil Resources 2014, update 2015. International soil classification system for naming soils and creating legends for soil maps*. FAO.

sciendo
Acta hort regiotec, 24, 2021(1): 28–48
DOI: 10.2478/ahr-2021-0022

Research Article

Numerical assessment of climate change impact on the hydrological regime of a small Mediterranean river, Lesvos Island, Greece

Eleni Ioanna Koutsovili[1]*, Ourania Tzoraki[1], Nicolaos Theodossiou[2], Petros Gaganis[3]
[1]*University of the Aegean, Department of Marine Sciences, Mytilene, Greece*
[2]*Aristotle University of Thessaloniki, Department of Civil Engineering, Thessaloniki, Greece*
[3]*University of the Aegean, Department of Environment, Mytilene, Greece*

Article Details: Received: 2021-02-22 | Accepted: 2021-03-31 | Available online: 2021-05-31

Licensed under a Creative Commons Attribution 4.0 International License

SCREENED BY iThenticate Professional Plagiarism Prevention

Frequency of flash floods and droughts in the Mediterranean climate zone is expected to rise in the coming years due to change of its climate. The assessment of the climate change impact at a basin scale is essential for developing mitigation and adaptation plans. This study analyses the variation of the hydrologic regime of a small Mediterranean river (the Kalloni river in Lesvos Island, Greece) by the examination of possible future climate change scenarios. The hydrologic response of the basin was simulated based on Hydrologic Modeling System developed by the Hydrologic Engineering Center (HEC-HMS). Weather Generator version 6 from the Long Ashton Research Station (LARS-WG 6.0) was utilized to forecast climate data from 2021 to 2080. These forecasted climate data were then assigned as weather inputs to HEC-HMS to downscale the climate predictions of five large-scale general circulation models (GCMs) for three possible emission scenarios (such as RCP 2.6, RCP 4.5, and RCP 8.5). The alteration of the Kalloni hydrologic regime is evaluated by comparing GCMs based estimates of future streamflow and evapotranspiration with business as usual (BaU) scenario. Variation was noted in seasonal and in annual scale forecasting of long-term average discharges, which show increasing trend in autumn and decreasing in summer and there is observed a general upward trend of actual evapotranspiration losses.

Keywords: climate change, hydrological regime, HEC-HMS model, GCMs, LARS-WG 6.0

1 Introduction

Water resources management and the design of flood prevention and adaptation strategies are becoming more challenging due to the uncertainties of climate change (Refsgaard et al., 2013). Global warming, variations in precipitation, and changes in the frequency of extreme events increase the probability of flood occurrences and change the total and seasonal water supply, among other impacts (Parry et al., 2007). Projections by the fifth iteration of the Intergovernmental Panel on Climate Change (IPCC) point towards a likely decrease in precipitation over the Mediterranean by 30–45%, especially if temperature rises by 1.4 °C (Cisneros, 2014; Zhai et al., 2018). Consequently, the frequency of flash floods and droughts in the region is expected to increase in the coming years, seriously altering the ecological and hydrological patterns of river basins (Tzoraki, 2020).

Addressing of climate change effects in the development of hazardous risk adaptation and mitigation plans has been on the agenda of many governments and institutions (Lavell et al., 2012). Hence, effective planning requires the examination of both current and projected climate change scenarios (Shrestha at al., 2017). According to IPCC, GCMs are advanced tools currently available for simulating the response of global climate system to increasing greenhouse gas concentrations. The use of GCMs has been the most crucial method for studying the implications of climate change (Wu et al., 2015). In a global scale, several studies have quantified potential changes in hydrological dynamics of river basins by climate change projections on the basis of GCMs (i.e., Sharafati et al., 2020; Ismail et al., 2020; Ebrahim et al., 2012; Hajian et al., 2016; QIN & LU, 2014; Emam et al., 2016; Yilmaz & Imteaz, 2011). The findings of these studies indicate that hydrological processes are highly sensitive to precipitation and temperature. Therefore, climate change can have a significant effect on hydrological regime of a river basin (Sharafati et al., 2020).

***Corresponding Author:** Eleni Ioanna Koutsovili. University of the Aegean, Environment School, Department of Marine Sciences, 81100 Mytilene, Greece; e-mail: mard18001@marine.aegean.gr

Although GCMs are very important tools for studying the implications of climate change, these contain biases when compared to observed data due to their parameterization systems and large grid size (Sharma et al., 2007). Outputs from the GCMs are typically defined at 250–600 km grids which are quite coarse relative to the scale of exposure units in most regional impact assessments. In fact, hydrological studies dealing with climate change impacts on small basins are particularly challenging, as they may require rainfall and temperature data at spatial resolution of 1 km^2 (Shrestha et al., 2017). In order to overcome this problem, many different downscaling methods have been developed over the last few decades (Ebrahim et al., 2012). These methods aim to provide sufficient hydrological variables by downscaling large-scale GCMs forecasts to a local scale (Ebrahim et al., 2012). Subsequently, the generated variables can be used as inputs to basin-scale hydrological models to predict climate-induced changes in flow patterns. There is a range of different downscaling techniques, which are mainly dynamical downscaling, statistical downscaling, regression based downscaling, weather typing procedure and the stochastic weather generator (Semenov & Barrow, 1997; Wilby et al., 2002; Sunyer et al., 2012; Shrestha et al., 2017). The most commonly applied are dynamic and statistical downscaling methods (Shrestha et al., 2017). Dynamic downscaling is based on high-resolution regional climate models combined with observations and output from lower-resolution larger-scale climate models, while statistical downscaling is based on the development and application of statistical relationships between local weather variables and large-scale predictors (Wilby et al., 2002; Hewer & Gough, 2018; Nourani et al., 2018; Sharafati et al., 2020). Additional, weather generators have been used successfully for downscaling the output of the GCMs over different regions (Sharafati et al., 2020). Weather Generator developed by the Long Ashton Research Station (LARS-WG) has been widely used to assess possible effects of climate change on hydrological processes (Sharafati et al., 2020). However, uncertainties associated with simulating various response mechanisms in GCMs are responsible for the fact that GCMs may simulate quite different responses to the same forcing (Randall et al., 2007). These differences are unlikely to be consistent with the uncertainty range of regional projections. Despite considerable improvements in computational power in recent years, climate models do not guarantee a representative range at finer scales of drainage systems (Shrestha et al., 2017).

Future greenhouse gas emission scenarios are appropriate tools for analyzing the influence on future emission outcomes due to various driving forces and assessing related uncertainties (IPCC, 2000). The IPCC defined a series of Representative Concentration Pathway (RCP) emission scenarios for future climate projections based on the Coupled Model Intercom Paring Project phase 5 (CMIP5). These scenarios are based on different 21st century pathways of greenhouse gas (GHG) emissions, population, and socio-economic conditions (IPCC, 2014). The RCPs include a stringent mitigation scenario (RCP2.6), two intermediate scenarios (RCP4.5 and RCP6.0), and one scenario with very high GHG emissions (RCP8.5) (IPCC, 2014). These various climate change scenarios can be used to define the climate change impact on hydrological processes, by downscaling the large-scale GCMs predictions to local scale with the LARS-WG (Sharafati et al., 2020).

The main objective of the current study is the numerical evaluation of climate change impact (2021–2080) on the hydrological regime of a smal Mediterranean river, the Kalloni river, which flows over Lesvos Island of Greece. The river basin is of significant importance due to high biodiversity richness of its NATURA 2000 areas. The developed approach based on the integration of spatial downscaling of GCMs and hydrological simulation has been adopted in the study.

2 Material and methods

A methodological framework summarized in Fig. 1 was developed in the study to assess climate change effects on the hydrology of the Kalloni river basin. Climate change impacts on the basin hydrology were evaluated by comparing GCMs based estimates of future streamflow and evapotranspiration with business as usual (BaU) or baseline scenario.

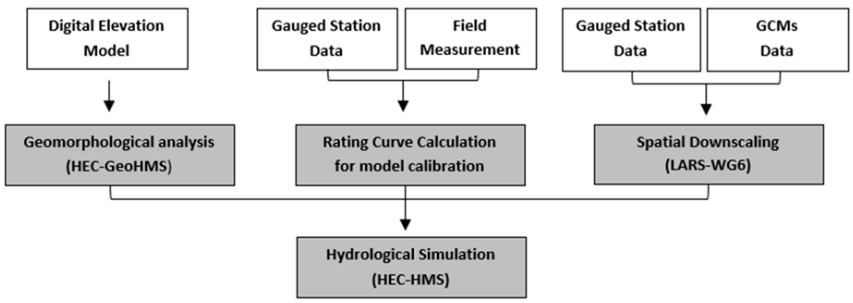

Figure 1 Flow diagram of methodological framework

Figure 2 Kalloni river basin in Lesvos Island, Greece

2.1 Study area

The Kalloni river basin illustrated in Fig. 2, which occupies the area of 40.28 km^2 was considered for the current study. The basin drains the wider area of the Kalloni settlement which is the second largest commercial centre of Lesvos Island. Its hydrographic network, with the total length of 34.92 km, is characterized as a dendritic type with many ephemeral streams. The basin area varies from lowland to mountainous in nature (Fig. 3a). North-western and western parts are mountainous areas with altitude reaching 690.3 m. North-eastern and central parts are intermediate hilly, of an average altitude of 300 m. The southern part is a large plain with an altitude almost equal to mean sea level. Main economic activities in the area are agriculture, livestock, and small local businesses. Fig. 3b shows that the watershed is primarily covered by agriculture (olive groves and cultivation patterns). Moreover, there are some small pine and oak forests at the northern tip of the basin, brushland habitats at the east and some artificial surfaces. Finally, in the southern part of the basin at the mouth of the torrent, wetlands and swampy areas develop. Land use data are provided by the Decentralized Administration of the North Aegean.

The study area has a Mediterranean climate with warm, dry summers and cool, mild, rainy winters (HMSO, 1962). More specifically, the average annual temperature is approximately 17 °C, with an average minimum temperature of 12.2 °C and an average maximum temperature of 21.4 °C. The mean annual rainfall depth over the Kalloni river basin is 514 mm, ranging from a daily minimum of 2.1 mm in summer (July) to a maximum of 98.5 mm in winter (January). Historical weather data from 2003 to 2020 in terms of daily precipitation, maximum and minimum temperature, solar radiation, relative humidity, and wind speed were collected from the Agia Paraskevi Meteorological Station. Water level data was obtained from automatic hydrometric station operating in Kalloni bridge. The river velocity and level were measured by field work to construct the rating curve.

In recent years, extended periods of drought are followed by sudden rainfalls of high intensity and short duration. This results in large volumes of water, which are not properly absorbed by the soil, ending up in the urban fabric. At the same time, the reduced cross-section of the riverbed at this point leads to overflow of the river with hazardous consequences for the infrastructures and the inhabitants. As a result, Kalloni experienced significant floods in 1986, 2005, 2011, 2016 (Matrai & Tzoraki, 2018).

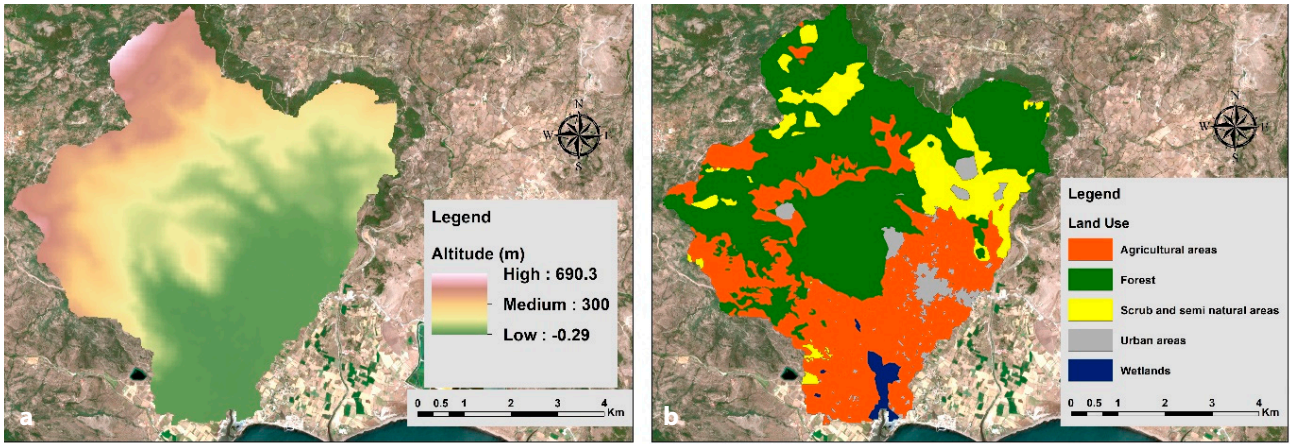

Figure 3 (a) Altitude and (b) Land uses of basin area

2.2 Geomorphological analysis

Analyses of geomorphological and hydrological characteristics of the study area were performed through HEC-GeoHMS extension of ArcMap and ArcHydro toolbox. HEC-GeoHMS extension was developed as a geospatial hydrology toolkit for engineers and hydrologists. The program allows users to visualize spatial information, document watershed characteristics, delineate subbasins and streams, and expediently create hydrologic inputs for Hydrologic Modeling System version 4.3 developed by the Hydrologic Engineering Center (HEC-HMS) (USACE, 2013). More specifically, HEC-GeoHMS produces a background map file and a basin model file as inputs to HEC-HMS. The map file visualizes basin's subbasins and watercourses of the study area, and the basin model file contains hydrological and geomorphological elements of the basin.

A digital elevation model (DEM) with 25 m grid from the European Environmental Agency was used as an input in HEC-GeoHMS to derive eight additional datasets that collectively describe drainage pattern of the watershed. The first step is to fill the sinks from the raw DEM and then use it as an input to delineate the Kalloni stream network and the watershed boundary. The produced datasets consist of five grid layers that represent the flow direction, flow accumulation, stream definition, stream segmentation, and watershed delineation, and two vector layers of the watershed and streams. Various stages of watershed generation in HEC-GeoHMS are shown in Figs 4, 5 and 6. Therefore, twenty-three subbasins and corresponding reaches are identified within the Kalloni basin area.

2.3 Rating curve calculation with field measurements

River monitoring is a critical issue for hydrological modeling that relies strongly on the use of flow rating curves (Manfreda, 2018). Rating curves define stage-discharge relationship and are usually developed by making frequent direct discharge measurements at stream gauging stations. Moreover, rating curves depend on the hydraulic characteristics of the stream channel and floodplain. Hence, they may vary over time in alluvial rivers, as river-bed characteristics change over time (Westerberg et al., 2011). This implies the need for frequent and time-consuming field survey.

In this study, field work measurements were carried out at characteristic cross sections of the streams aiming at calculating rating curves. The equipment consisted of a small flow meter device with a propeller, which is a portable flow measurement system in rivers, open canals or even in open water pipes. The rating curve

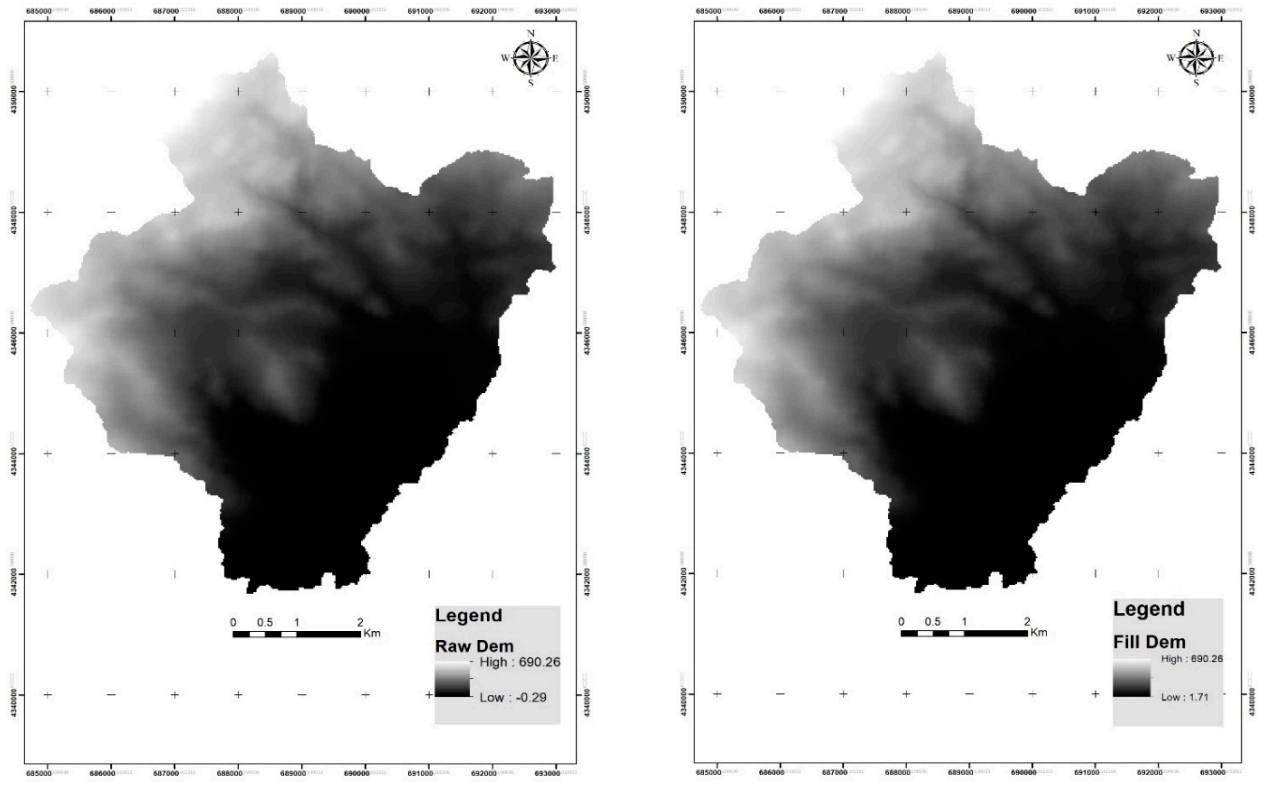

Figure 4 Kalloni raw DEM and fill DEM produced in HEC-GeoHMS

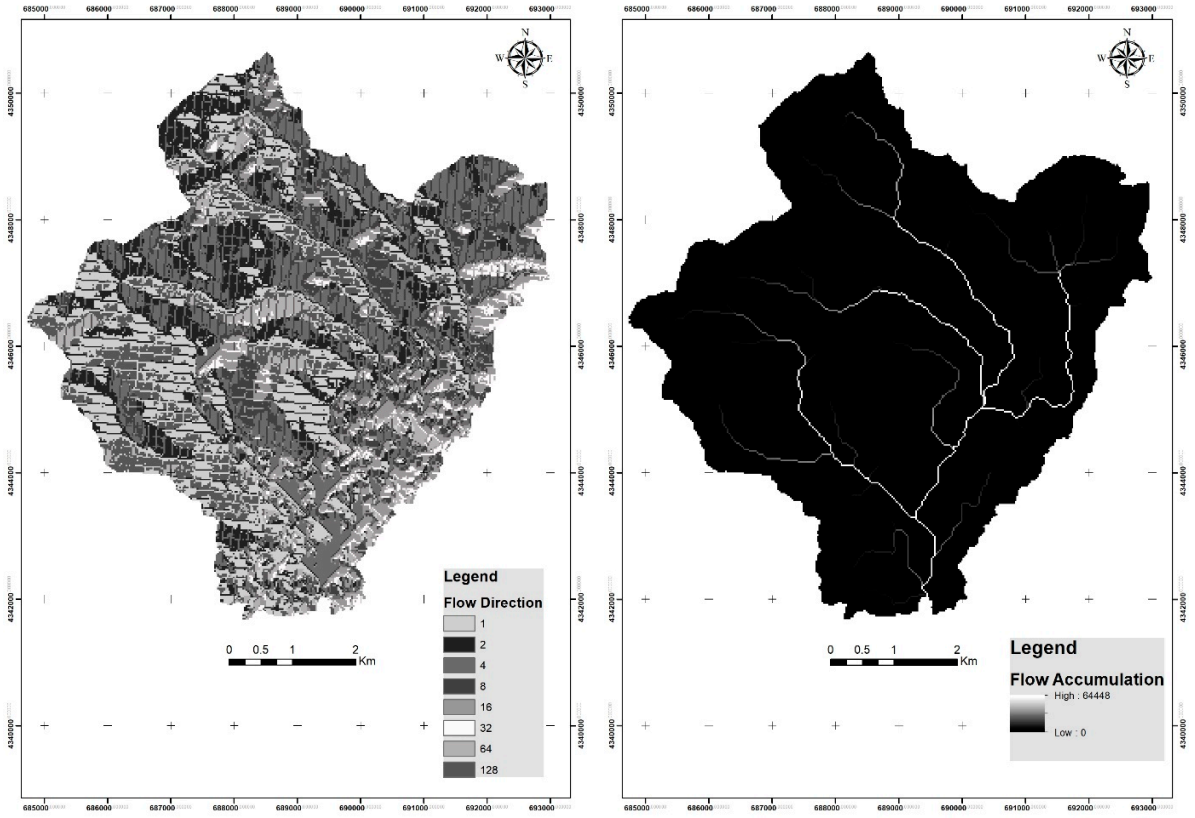

Figure 5 Flow direction and flow accumulation maps generated in HEC-GeoHMS

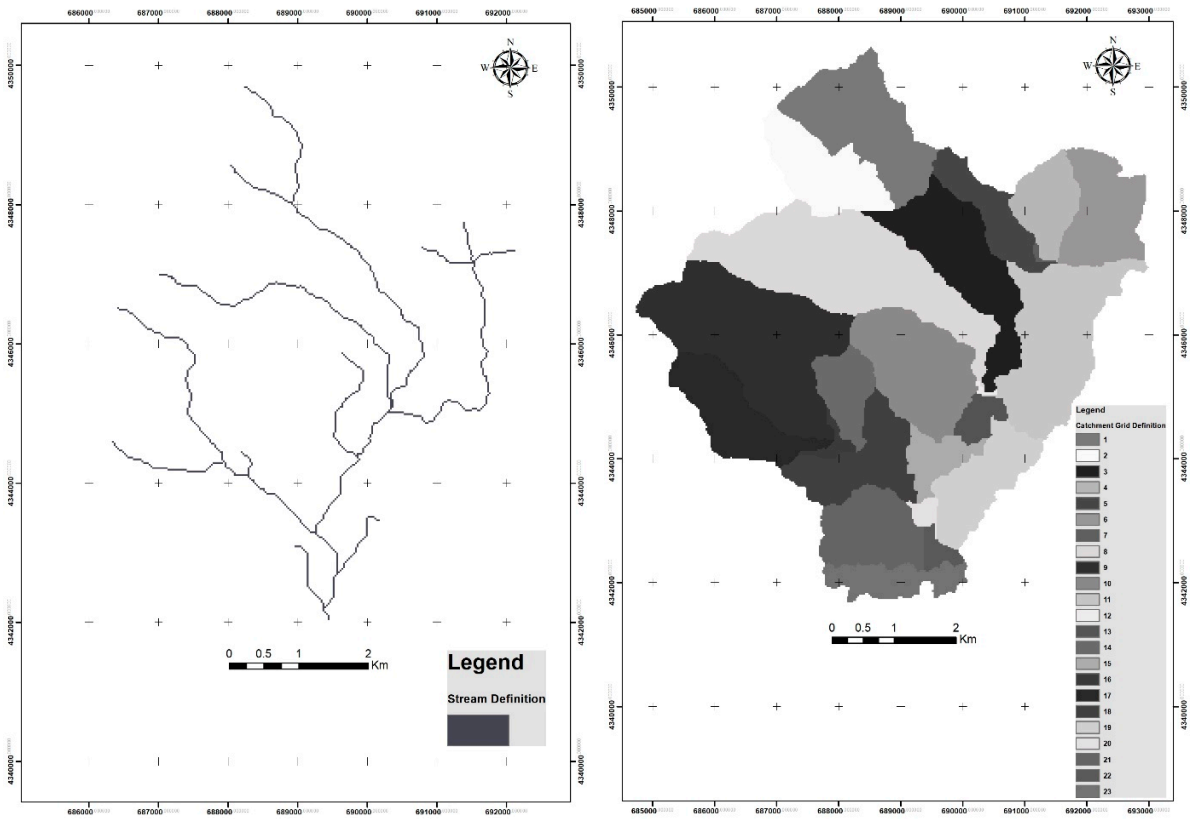

Figure 6 Stream network and watershed generation in HEC-GeoHMS

equation for discharge (Q) and stage (H) was calculated as follows:

$$Q = 2.7837 \times H^{1.1608} \quad (2.1)$$

Subsequently, the observed flow time series generated by the rating curve are used to calibrate the hydrological model HEC-HMS for time period 2018–2019. Each observed value of daily discharge was estimated from the rating curve equation using observed daily stage measured in real time by a telemetric station operating in Kalloni since 2018.

2.4 Spatial downscaling of large-scale climate predictions

Weather Generator version 6.0 from the Long Ashton Research Station (LARS-WG 6.0) is a single site numerical model for generating daily time-series of climate variables, namely, precipitation (mm), maximum and minimum temperature (°C), and solar radiation ($MJm^{-2}.day^{-1}$). LARS-WG 6.0 is suitable for downscaling coarse resolution climate model simulations in local spatial scale for different climate change scenarios (Sharafati et al., 2020). The model, after calibrating site parameters with observed weather data for the baseline period, is capable of simulating synthetic daily time series of weather data that are statistically similar to the observed weather (Wilks & Wilby, 1999). LARS-WG 6.0 uses a semi-empirical distribution to calculate the length of wet and dry days (Racsko et al., 1991). Moreover, it considers each weather variable as a stochastic variable, and simulates seasonal cycles through Fourier series (Sharafati et al., 2020).

Methodology for spatial downscaling using LARS-WG to generate future climate data can be divided into three major steps: model calibration (Site Analysis), model validation (QTest), and generation of synthetic weather data (Generator). Parameter files derived during the model calibration step are used to generate synthetic weather data having the same statistical characteristics as the original observed data but differing on a daily basis. In order to ensure that the simulated data probability distributions are close to the true long-term observed distributions, a model validation process must be performed. The QTest validation option of LARS-WG carries out a statistical comparison of generated and observed weather data using the Kolmogorov-Smirnov (K-S) test, the *T*-test, and the *F*-test. Once LARS-WG has been calibrated and the performance of the weather generator has been verified, synthetic weather data may be simulated using the Generator option. This option may be used to generate synthetic data which have the same statistical characteristics as the observed weather data (baseline scenario), or to generate synthetic weather data corresponding to a climate change scenario from GCMs (Semenov & Barrow, 2002).

The current version LARS-WG 6.0 generates high resolution climate change scenarios over a region using direct outputs from General Circulation Models (GCMs). LARS-WG 6.0 incorporates projections from five GCMs with the different climate scenarios RCP2.6, RCP4.5, and RCP8.5 used in the IPCC. Table 1 summarizes the different GCMs and RCPs that are taken into consideration in this study to forecast futuristic climate data for a period of 60 years from 2021 to 2080. Calibration of site parameters is performed for baseline period of 18 years from 2003 to 2020.

2.5 Hydrological simulation and calibration

Hydrologic Engineering Centre's Hydrologic Modeling System (HEC-HMS) was designed by the United States Army Corps of Engineers (USACE) as a software tool for simulating complete hydrological cycle in the context of solving engineering problems (Scharffenberg et al., 2010). HEC-HMS is a deterministic, semi-distributed, conceptual model which is designed to simulate precipitation-runoff processes of dendritic drainage basins. It is applicable to a wide range of geographic areas for solving the widest possible range of problems (USACE, 2013). The software has been applied in a wide variety of geographical regions, such as large river basins, and small municipal and natural watersheds. In addition, depending on objectives of the study, it can be applied

Table 1 Summary of the five GCMs and corresponding emission scenarios (RCPs)

GCM	Institution	Grid Resolution	RCP
EC-EARTH	European community Earth-System Model	1.125° × 1.125°	RCP4.5, RCP8.5
GFDL-CM3	NOAA Geophysical Fluid Dynamics Laboratory	2° × 2.5°	RCP4.5, RCP8.5
HadGEM2-ES	Met Office Hadley Center, United Kingdom	1.25° × 1.875o	RCP2.6, RCP4.5, RCP8.5
MIROC5	Atmosphere and Ocean Research Institute (The University of Tokyo), National Institute for Environment Studies and Japan Agency for Marine-Earth Science and Technology, Japan	1.40° × 1.41°	RCP4.5, RCP8.5
MPI-ESM-MR	Max Planck Institute for Meteorology, Germany	1.85° × 1.875°	RCP4.5, RCP8.5

for simulation of either individual events or continuous large-scale events.

HEC-HMS has been widely used all over the world in a number of studies, including flood forecasting (Verma et al., 2010), land use change impacts (Ali et al., 2011), and also assessing the impact of climate change. Nyaupane et al. (2018) used HEC-HMS for prediction of future peak flow condition in the Irwin Creek watershed located in Charlotte, North Carolina. The study highlighted the significance of consideration of climate change as a factor likely to result in increased peak discharge in the existing urban watersheds. The hydrologic impacts of climate change in the Tungabhadra river basin in India was also assessed by Meenu et al. (2012). They utilized the HEC-HMS to model hydrologic processes and the Statistical Down Scaling Model (SDSM) to downscale daily precipitation, and maximum and minimum temperature. Moreover, Bai et al. (2019) proposed a framework combining HEC-HMS and the Coupled Model Intercomparison Project Phase 5 (CMIP5) GCMs to assess the impact of climate change on flood events in the Nippersink Creek watershed located in Northeastern Illinois. They found that the increase in greenhouse gas concentration under RCP 8.5 scenario can increase future precipitation. It may induce a greater impact on flood events by 110% increase from historically-observed 100 year return period flood.

Each model run incorporates a basin model describing basin's connectivity and physical characteristics, a meteorological model storing the precipitation and evapotranspiration data, and a control specification with run options to attain outcomes (Verma et al., 2010). In HEC-HMS, a basin model is constructed by dividing the hydrological cycle (evaporation, surface runoff, infiltration, and groundwater recharge) into individual parts with possibility of processing each one separately. Therefore, each component of the hydrological cycle is represented by a mathematical model. HEC-HMS also provides supplemental analysis tools for model optimization, forecasting streamflow, depth-area reduction, assessing model uncertainty, erosion and sediment transport, and water quality (Wang et al., 2016). Furthermore, spatial data sets can be organized in GIS platforms using HEC-GeoHMS, and then directly imported into HEC-HMS (Ali et al., 2011).

In the present study, hydrological simulation is performed in the examined basin with a daily time step. For infiltration loss calculation of the watershed, the "deficit and constant" method is implemented. The deficit and constant loss model uses a single soil layer to account for continuous changes in moisture content (US Army Corps of Engineers, 2008). In addition, the "Clark unit hydrograph" method is used to transform the flows and calculate the direct runoff from excess precipitation. The runoff is considered to be through a linear reservoir. Furthermore, the "linear reservoir" method is used to account the baseflow. The central idea of the method is to take into account an underground reservoir charged during the infiltration phase of rainwater and then discharged, contributing to the surface flow after the end of the rainfall. Finally, the "Lag" method is selected as the channel routing model. Table 2 summarizes the calculation methods for all the components of the HEC-HMS model applied in the present study.

Table 2 Calculation methods for components of the basin and meteorological models

Component	Calculation method
Canopy	simple canopy
Loss	deficit and constant
Transform	clark unit hydrograph
Baseflow	linear reservoir
Routing	lag
Evapotranspiration	constant monthly

The inclusion of the evapotranspiration process in the HEC-HMS model is significant for long-term simulations, and it is also necessary when using the deficit and constant loss method. In the case of the Kalloni, the method of constant monthly evapotranspiration is selected, which requires a potential monthly evaporation rate (mm. month^{-1}) and a crop coefficient from all subbasins. The modified Blaney-Criddle method is applied to calculate the mean daily potential evapotranspiration for each month (Doorenbos & Pruitt, 1977):

$$ETd = a + b \times p \times (0.46 \times T + 8.16) \qquad (2.2)$$

where:
ETd – the daily potential evapotranspiration (mm.d^{-1}); T – the average monthly temperature (°C); p – the mean daily percentage of annual daytime hours (%), and a, b are the adjustment coefficients of the original Blaney-Criddle equation depending on the air humidity, the hours of actual sunshine and the wind speed. In this case, the values -2.15, 1.38 are chosen for the coefficients a, b, respectively. These values are selected for moderate relative humidity conditions during the day (20–50%), for average wind speed conditions, and for theoretical to actual sunshine ratio between 0.6 and 0.8 (Ponce, 989). The mean daily percentage of annual daytime hours (p) expresses the percentage (%) of daylight hours each

month in relation to the total daylight hours of the year. This percentage is calculated from the following equation (Blaney & Criddle, 1950):

$$p = \frac{N \times \mu}{365 \times 12} \times 100 \quad (2.3)$$

where:
N – the average astronomical daylight duration related to the latitude of the study area (h); m – the number of days in the month under consideration (d). Finally, the daily ETd is converted to monthly using the formula:

$$ETm = ETd \times \mu \quad (2.4)$$

where:
ETm – the monthly potential evapotranspiration (mm. month^{-1}); μ – the total number of days in the respective month

The HEC-HMS model is calibrated using observed data (e.g., river discharge) to improve the predictability and reliability of the model. The model accuracy is typically based on specific statistics and ratings developed to evaluate various performance criteria, such as accuracy of predicting peak flows, total hydrograph volume, peak flow, time to peak etc., depending on project goals (World Bank Group, 2015). In this research, a set of model parameters is estimated empirically and manually using the HMS model's tool "Calibration Aids". The accuracy and performance of the calibrated model is evaluated by three goodness-of-fit measures, the Nash–Sutcliffe efficiency (NSE) coefficient, the percentage bias error (PBIAS), and the Root Mean Squared Error standard deviation ratio (RMSE Std. Dev.) of observations.

1. Nash-Sutcliffe efficiency (NSE) coefficient (Nash & Sutcliffe, 1970):

$$NSE = 1 - \frac{\sum_{i=1}^{n}\left(Q_i^{sim} - Q_i^{obs}\right)^2}{\sum_{i=1}^{n}\left(Q_i^{obs} - \overline{Q^{obs}}\right)^2} \quad (2.5)$$

where:
Q_i^{obs} and Q_i^{sim} – the observed and simulated discharge value at the i^{th} step, respectively; $\overline{Q^{obs}}$ is the average of the observed discharge values; n – the number of observed/simulated values. The NSE coefficient determines the relative magnitude of the error variance compared to the observed data variance. NSE takes values in range between negative infinity (-∞) and 1; value of 1 indicates a perfect agreement, while negative values indicate very poor agreement. Generally, model calibration can be considered satisfactory if the NSE coefficient is greater than 0.50, while NSE coefficient values greater than 0.75 indicate a very good calibration of the model (Moriasi et al., 2007).

2. Percentage bias error (PBIAS), defined as:

$$PBIAS = \frac{\left|\overline{Q^{sim}} - \overline{Q^{obs}}\right|}{\overline{Q^{sim}}} \times 100 \quad (\%) \quad (2.6)$$

where:
$\overline{Q^{sim}}$ and $\overline{Q^{obs}}$ – the simulated and observed mean discharge, respectively. This measure reflects the model's capability to maintain water balance by reproducing total runoff volume. The lower PBIAS, the better is the model's performance.

3. Root Mean Squared Error standard deviation (RMSE Std. Dev.), given by:

$$\text{RMSE Std. Dev.} = \frac{\sqrt{\sum_{i=1}^{n}\left(Q_i^{obs} - Q_i^{sim}\right)^2}}{\sqrt{\sum_{i=1}^{n}\left(Q_i^{obs} - \overline{Q^{obs}}\right)^2}} \quad (2.7)$$

where:
Q_i^{obs} and Q_i^{sim} – the observed and simulated discharge value at the i^{th} step, respectively; $\overline{Q^{obs}}$ – the average of the observed discharge values, and n is the number of observed/simulated values. RMSE Std. Dev. incorporates the benefits of error index statistics and includes a normalization factor, so that the resulting statistic and reported values can apply to various constituents. RMSE Std. Dev. varies from the optimal value of 0 to a large positive value. Lower values of RMSE Std. Dev. nominate a lower root mean square error normalized by the standard deviation of the observations, which indicates the adequacy of the model simulation (Moriasi et al., 2007).

Table 3 General performance ratings for examining statistics

Performance rating	NSE	PBIAS	RMSE Std. Dev.
Very Good	0.75< NSE ≤1.00	PBIAS <±10%	0.00≤ RMSE Std. Dev. ≤0.50
Good	0.65< NSE ≤0.75	±10%≤ PBIAS <±15%	0.50< RMSE Std. Dev ≤0.60
Satisfactory	0.50< NSE ≤0.65	±15%≤ PBIAS <±25%	0.60< RMSE Std. Dev ≤0.70
Unsatisfactory	NSE ≤0.50	PBIAS ≥±25%	RMSE Std. Dev >0.70

Source: Moriasi et al., 2007

The performance ratings for the three goodness-f-fit measures given by Moriasi et al. (2007) are based on the evaluations and corresponding values reported from individual studies. The ratings are summarized in table 3.

3 Results and discussion

3.1 Calibration of the HEC-HMS model

Calibration of the HEC-HMS model are conducted manually using model's tool "Calibration Aids". Fig. 7 shows comparison of observed and simulated monthly discharge for the calibration period and Table 4 summarizes calibration performance metrics. As observed, the HEC-HMS model calibration succeeded, while it accurately estimates peak discharge and volume. The model performance for river discharge is very good according to NSE and RMSE Std. Dev. and good according to PBIAS measure.

3.2 Calibration and validation of the LARS-WG 6.0 model

Daily precipitation, temperature, and solar radiation data for the period 2003–2020 are used for the LARS-WG 6.0 model calibration. Generated time series from calibrated site is generated from random seeds, and performance of LARS-WG 6.0 is evaluated using the QTest validation option. The QTest compares probability distributions, means, and standard deviations for observed and generated data from LARS-WG 6.0. All statistical tests carried out in Qtest calculate a *p*-value. A very low *p*-value means that the simulated climate is unlikely to be the same as the 'true' climate. The level of *p*-value that is considered significant is subjective and depends on the importance of a very close fit for each application (Semenov & Barrow, 2002).

Evaluation of the LARS-WG 6.0 performance in simulating daily precipitation and temperature data for the Kalloni is presented in Tables 5 and 6. The K-S test was used to compare observed and generated data histograms. Table 5 showcased that simulation of both minimum and maximum temperature was perfect. It can also be noted that the model performed very well fitting for mean precipitation in winter and autumn seasons, while on the other hand, very poor performance was observed for summer period (Jun – Aug). The reason for the poor performance may be attributed to the lack of precipitation recorded in summer and small available database time series for baseline scenario. Semenov and Barrow (2002) have reported that sample size affects the likelihood of a significant *p*-value and the tests are more likely to give a significant result with more data. A small sample size with little observed precipitation data in summer gives little information, as to approach 'true' distribution. Chisanga et al. (2017) also reported a poor performance in precipitation due to the lack of observed data during summer. Furthermore, significant differences between simulated and observed data might be due to LARS-WG smoothing of observed data in order to eliminate random noise (Semenov &

Table 4 Calibration performance measures

	Peak discharge ($m^3.s^{-1}$)	Volume (mm)	Date of peak	NSE	PBIAS	RMSE Std. Dev.
Simulated	1.52	143.27	24/01/2019	0.784	-0.10%	0.46
Observed	1.52	143.27	24/01/2019			

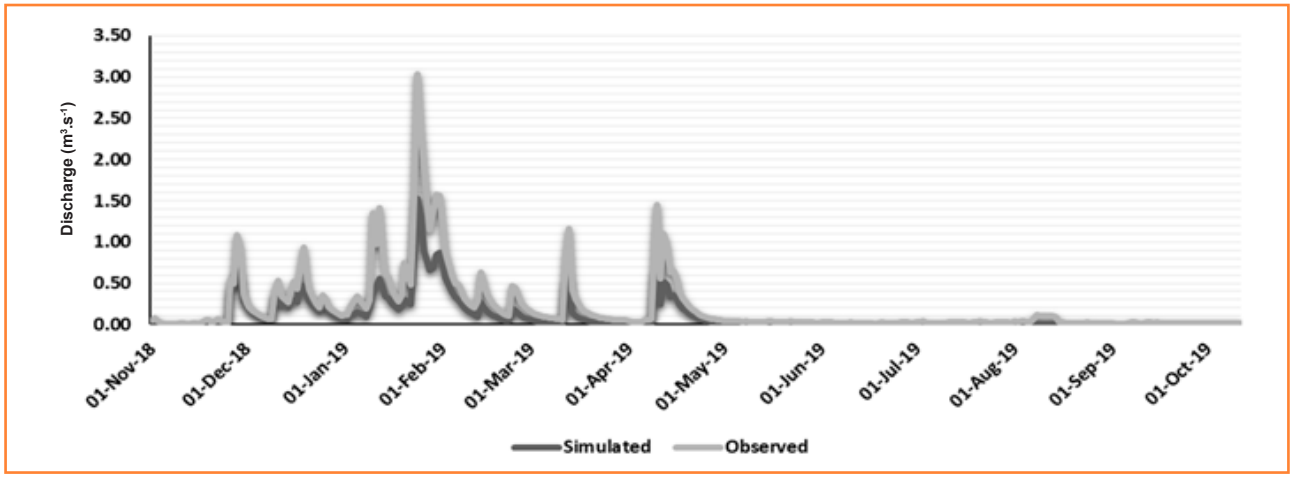

Figure 7 HEC-HMS calibration results for river discharge ($m^3 \cdot s^{-1}$)

Table 5 K-S test for daily precipitation, minimum and maximum temperature distributions

Month	Mean precipitation			Min temperature			Max temperature		
	K-S	*p*-value	assessment	K-S	*p*-value	assessment	K-S	*p*-value	assessment
Jan	0.14	0.97	perfect	0.05	1.00	perfect	0.11	1.00	perfect
Feb	0.05	1.00	perfect	0.11	1.00	perfect	0.05	1.00	perfect
Mar	0.09	1.00	perfect	0.05	1.00	perfect	0.05	1.00	perfect
Apr	0.06	1.00	perfect	0.09	1.00	perfect	0.05	1.00	perfect
May	0.07	1.00	perfect	0.05	1.00	perfect	0.05	1.00	perfect
Jun	0.24	0.49	good	0.05	1.00	perfect	0.05	1.00	perfect
Jul	0.54	0.00	very poor	0.11	1.00	perfect	0.05	1.00	perfect
Aug	0.64	0.00	very poor	0.05	1.00	perfect	0.05	1.00	perfect
Sep	0.15	0.95	perfect	0.05	1.00	perfect	0.05	1.00	perfect
Oct	0.05	1.00	perfect	0.05	1.00	perfect	0.05	1.00	perfect
Nov	0.04	1.00	perfect	0.05	1.00	perfect	0.05	1.00	perfect
Dec	0.03	1.00	perfect	0.11	1.00	perfect	0.05	1.00	perfect

Table 6 Performance results of LARS-WG 6.0 in fitting monthly precipitation and temperature statistics

	R^2	NSE	PBIAS
Mean monthly precipitation	0.983	0.977	5.370
Min monthly temperature	0.997	0.992	2.640
Max monthly temperature	0.997	0.996	0.900

Barrow, 2002). Ebrahim et al. (2012) have also stated that significant difference during winter season is likely due to LARS-WG smoothing for observed data.

Performance of LARS-WG 6.0 is also checked by using coefficient of determinant (R^2), the Nash–Sutcliffe efficiency (NSE) coefficient, and percentage bias error (PBIAS). Table 6 summarized results of analyses of statistical characteristics of observed and generated monthly weather data. R^2 value of 0.99 demonstrates excellent performance of LARS-WG 6.0 in simulating weather variables. Ratings of the Nash-Sutcliffe efficiency coefficient and percentage bias error also showed a very good performance of LARS-WG 6.0 in fitting monthly statistics. Performance of LARS-WG 6.0 in simulating climate variables is demonstrated in Fig. 8 which compares observed and generated average monthly precipitation, and minimum and maximum temperature.

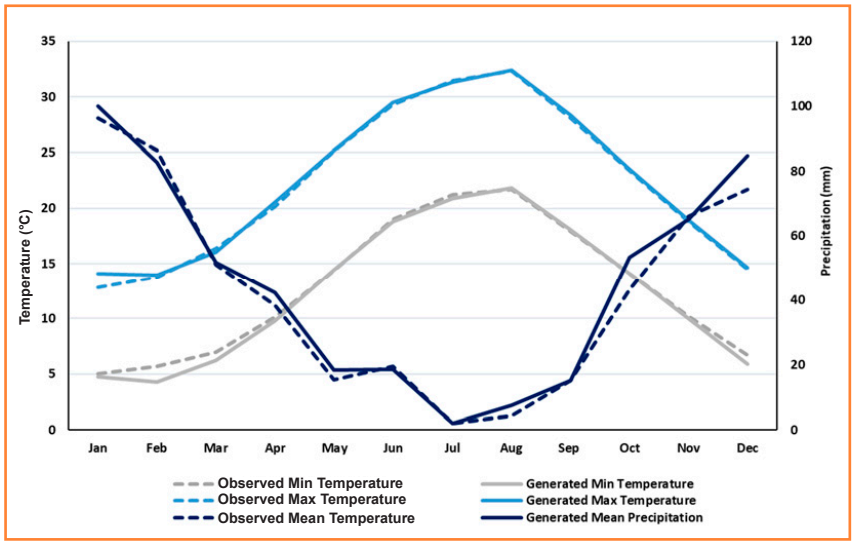

Figure 8 Comparison of LARS-WG 6.0 generated and observed baseline data of mean monthly precipitation, minimum and maximum monthly temperature

3.3 Analysis of precipitation and temperature variables

The first step in analysing effects of climate change on river basin hydrology is to quantify changes in weather variables. Table 7 summarized downscaling results for mean annual precipitation and temperature for various GCMs-RCP

Table 7 Annual changes in precipitation and temperature for all examined GCM-RCP scenarios

Scenario		Annual precipitation (mm)		Temperature (°C)	
GCM	**RCP**	**mean value**	**percent change (%)**	**mean value**	**percent change (%)**
HadGEM2-ES	2.6	529.49	5.36%	18.82	7.59%
EC-EARTH	4.5	537.59	6.97%	18.24	4.23%
GFDL-CM3	4.5	504.90	0.47%	19.25	10.01%
HadGEM2-ES	4.5	543.42	8.13%	19.00	8.63%
MIROC5	4.5	546.65	8.77%	18.83	7.63%
MPI-ESM-MR	4.5	548.50	9.14%	18.29	4.54%
EC-EARTH	8.5	525.75	4.61%	18.83	7.62%
GFDL-CM3	8.5	473.44	-5.79%	20.12	15.03%
HadGEM2-ES	8.5	517.97	3.07%	19.51	11.51%
MIROC5	8.5	537.67	6.99%	19.28	10.18%
MPI-ESM-MR	8.5	536.96	6.84%	18.66	6.63%
Baseline BaU		502.56	0.00%	17.50	0.00%

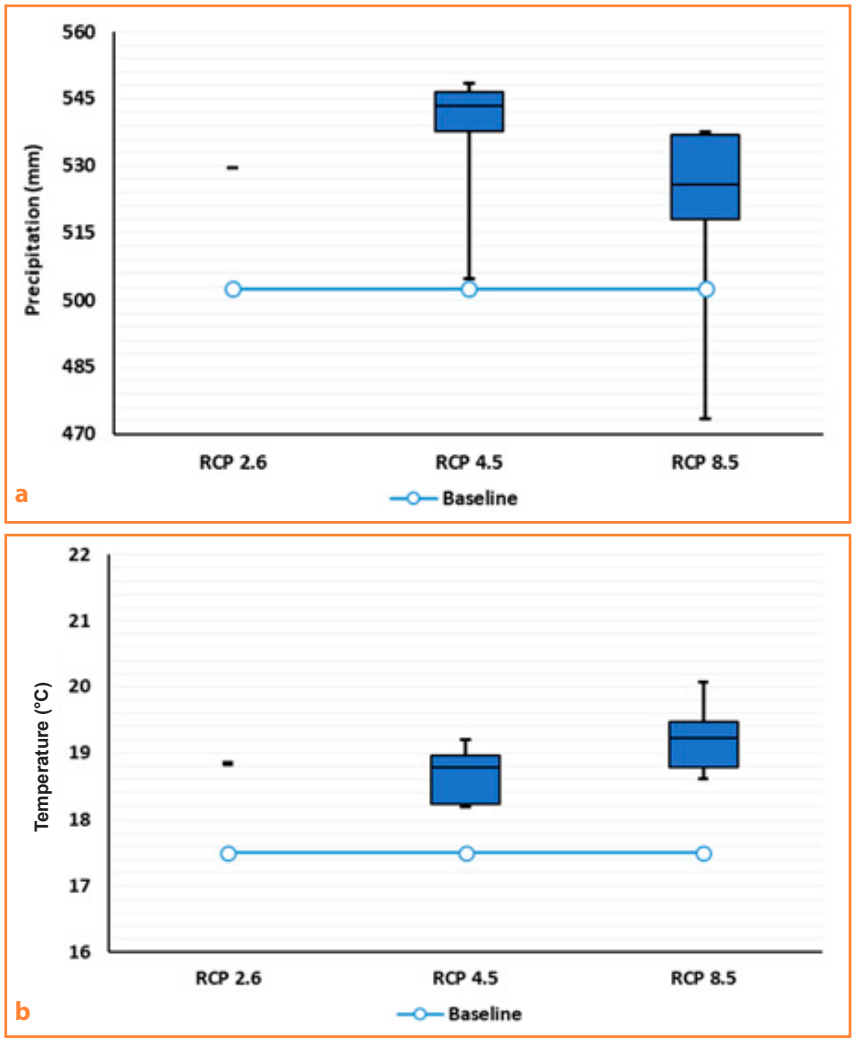

Figure 9 Variations in future (a) mean annual precipitation and (b) mean annual temperature forecasts compared to baseline scenario under the influence of each emissions scenario

scenarios as well as percentage changes of these parameters compared to baseline scenario. The results show a consistently increasing trend both in precipitation and temperature values for all climate models except GFDL-CM3 which shows a reduction of future rainfall by 5.79%. Table 7 also shows a large divergence in changes of annual rainfall totals which range from -5.79% (GFDL-CM3) to +6.99% (MIROC5) for RCP 8.5 and from +0.47% (GFDL-CM3) to +9.14% (MPI-ESM-MR) for RCP 4.5. The annual rate of changes of mean temperature at the Kalloni river basin also range from +6.63% (MPI-ESM-MR) to +15.03% (GFDL-CM3) for RCP 8.5 and +4.23% (EC-EARTH) to +10.01% (GFDL-CM3) for RCP 4.5.

Variations in GCMs outputs concerning predicted annual rainfall totals and average temperatures for future simulation period 2021–2080 are shown as boxplots in Figs 9a and 9b, respectively. The boxplots represent 25th, 50th (median) and 75th percentiles, and horizontal lines show mean annual values for Baseline Business as Usual (BaU) scenario. The generated data from Baseline BaU scenario for the period

2021–2080 match site statistics based on historical records without taking into account climate change. Variations in GCMs result indicate the range of uncertainty in GCM predictions and they arise mainly from wide rainfall patterns generated by different climate models (Hajian et al., 2016; Bates et al., 2008). Therefore, studies investigating the potential effects of climate change on water resources using outflows from a single GCM greatly reduce the validity and usefulness of the findings (Hajian et al., 2016).

Subsequently, it is important to examine the response of these parameters to climate change in a shorter time scale, as they show significant seasonal fluctuations. Tables 8 and 9 show average seasonal changes in total rainfall and average temperature. Table 8 shows that rainfall varies significantly between different GCMs, whereas Table 9 shows more uniform results for temperature. These variations, as well as the final values of the rainfall and temperature parameters on a monthly basis, are visualized in Figs 10a, b, c and 11a, b, c, respectively. As observed, the average cumulative rainfall shows a downward trend in spring and summer and

Table 8 Seasonal changes in mean precipitation for all simulated GCM-RCP scenarios

Scenario		Seasonal Precipitation (mm)				Seasonal percent change (%)			
GCM	RCP	winter	spring	summer	autumn	winter	spring	summer	autumn
HadGEM2-ES	2.6	267.63	93.15	32.43	137.47	1.12%	5.10%	7.10%	14.37%
EC-EARTH	4.5	274.33	81.09	27.61	155.94	3.65%	-8.51%	-8.82%	29.73%
GFDL-CM3	4.5	266.84	94.61	30.37	86.82	0.82%	6.75%	0.30%	-27.77%
HadGEM2-ES	4.5	275.80	87.46	33.05	148.44	4.21%	-1.32%	9.15%	23.49%
MIROC5	4.5	288.08	88.86	28.56	142.60	8.85%	0.26%	-5.68%	18.64%
MPI-ESM-MR	4.5	279.92	88.85	27.15	153.99	5.77%	0.25%	-10.34%	28.11%
EC-EARTH	8.5	262.57	83.54	28.23	152.74	-0.79%	-5.74%	-6.77%	27.07%
GFDL-CM3	8.5	234.61	91.97	32.50	82.70	-11.35%	3.77%	7.33%	-31.20%
HadGEM2-ES	8.5	267.23	87.66	31.59	132.66	0.97%	-1.09%	4.33%	10.37%
MIROC5	8.5	285.50	87.65	27.93	138.04	7.87%	-1.11%	-7.76%	14.84%
MPI-ESM-MR	8.5	276.69	88.60	25.37	147.62	4.55%	-0.03%	-16.22%	22.81%
Baseline BaU		264.66	88.63	30.28	120.20	0.00%	0.00%	0.00%	0.00%

Table 9 Seasonal changes in mean temperature for all simulated GCM-RCP scenarios

Scenario		Mean seasonal temperature (oC)				Seasonal percent change (%)			
GCM	RCP	winter	spring	summer	autumn	winter	spring	summer	autumn
HadGEM2-ES	2.6	10.89	17.00	27.19	20.04	12.53%	9.14%	5.18%	7.11%
EC-EARTH	4.5	10.35	16.32	26.63	19.47	6.89%	4.73%	3.04%	4.10%
GFDL-CM3	4.5	10.78	17.14	28.25	20.60	11.40%	10.01%	9.30%	10.10%
HadGEM2-ES	4.5	10.94	17.14	27.46	20.30	12.98%	10.03%	6.25%	8.50%
MIROC5	4.5	10.78	16.81	27.38	20.18	11.33%	7.87%	5.92%	7.86%
MPI-ESM-MR	4.5	10.35	16.47	26.81	19.35	6.96%	5.72%	3.71%	3.45%
EC-EARTH	8.5	10.97	16.93	27.18	20.06	13.36%	8.66%	5.15%	7.22%
GFDL-CM3	8.5	11.67	17.92	29.21	21.50	20.59%	15.00%	13.00%	14.93%
HadGEM2-ES	8.5	11.34	17.56	28.08	20.88	17.18%	12.71%	8.63%	11.60%
MIROC5	8.5	11.10	17.16	27.96	20.70	14.63%	10.16%	8.18%	10.67%
MPI-ESM-MR	8.5	10.48	16.72	27.35	19.89	8.23%	7.33%	5.83%	6.32%
Baseline BaU		9.68	15.58	25.85	18.71	0.00%	0.00%	0.00%	0.00%

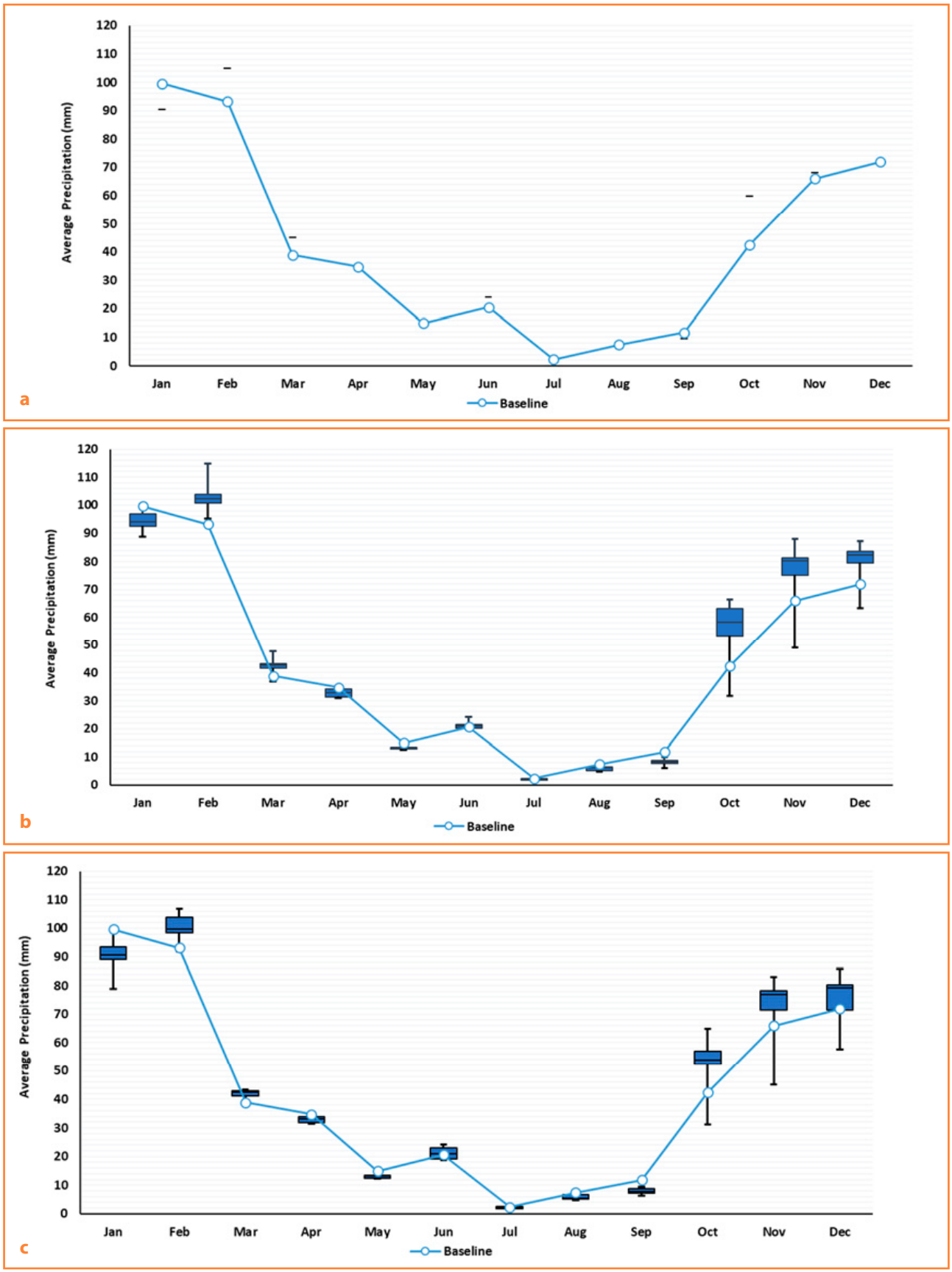

Figure 10 Variations in monthly precipitation forecasts compared to baseline BaU scenario under the influence of each emissions scenario (a) RCP 2.6, (b) RCP 4.5, and (c) RCP 8.5

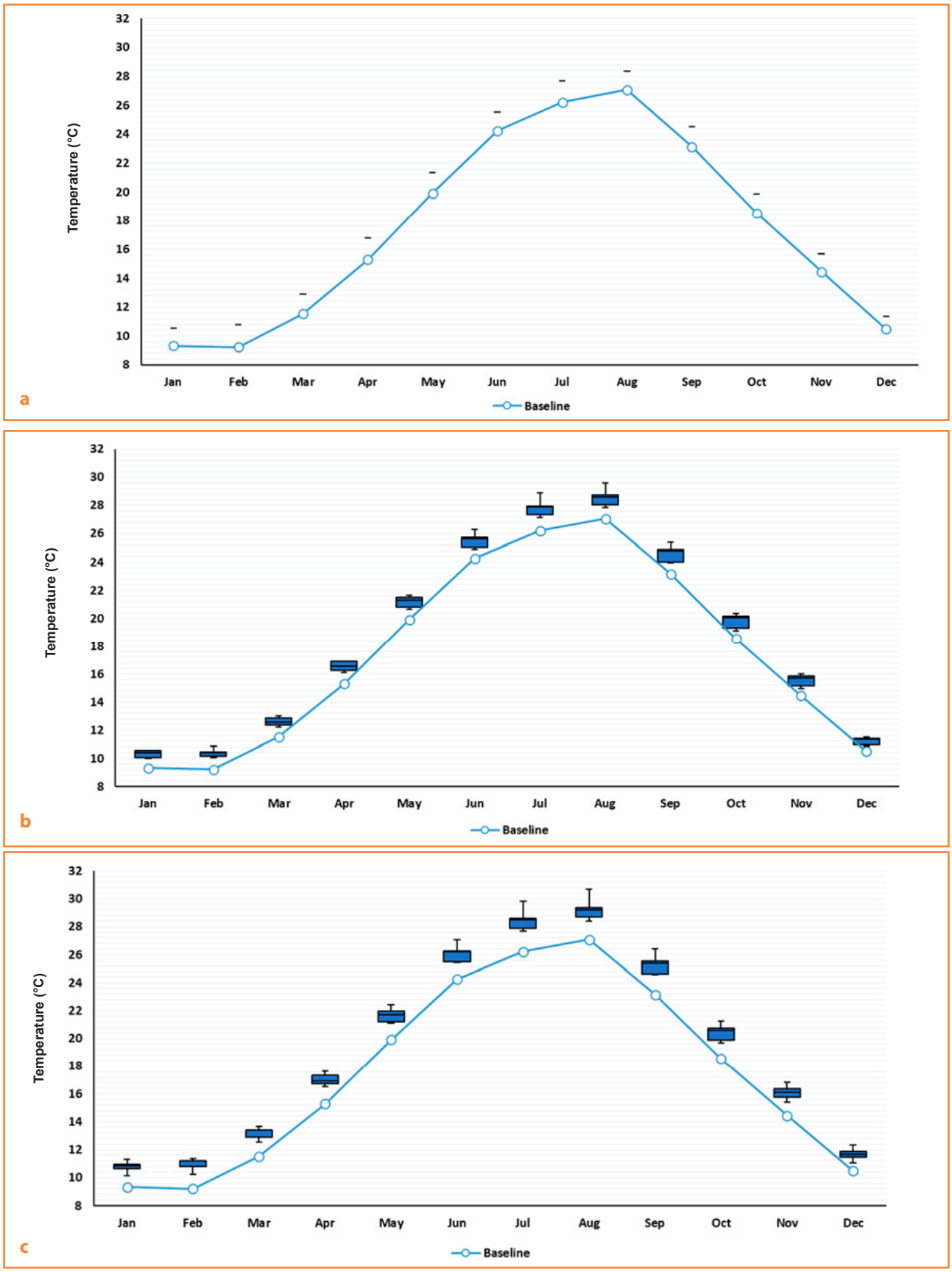

Figure 11 Variations in monthly temperature forecasts compared to baseline BaU scenario under the influence of each emissions scenario (a) RCP 2.6, (b) RCP 4.5, and (c) RCP 8.5

a particularly upward trend in winter and especially autumn. Moreover, there is a shift of peak rainfall from January to February, while January shows a drop in cumulative rainfall. Finally, in terms of temperature, there is a general increase in average temperature throughout the year, while the largest changes occur during the winter months.

3.4 Climate change impact on evapotranspiration

Monthly potential evapotranspiration is computed using the modified Blaney-Criddle method (Blaney & Criddle, 1950) with projected temperature data for 2021–2080 period. Evapotranspiration under various GSMs-RCP scenarios is compared to corresponding baseline Business as Usual (BaU) scenario and percentage changes are summarized in Table 10. Overall results indicate an increase in seasonal evapotranspiration in the region, with significant changes for instance of 7.42%, 7.07%, 7.77% and 7.78% for winter, spring, summer and autumn, respectively, occurring in GFDL-CM3 model for RCP 8.5 emission scenario. Variations in monthly evapotranspiration for all scenarios are represented in Figs 12a, 12b and 12c.

3.5 Climate change impact on streamflow

Annual peak and average monthly river discharges are computed using the calibrated HEC-HMS model based on projected weather data for 2021–2080 period. Figs 13a, b, c and 14a, b, c show annual peak and seasonal discharge variations respectively, under all examined GCM models for three RCP scenarios. Although the results from different scenarios vary considerably, a general increasing trend of flow peaks is observed, especially during the long-term period 2040–2080. In terms of monthly variations, January presents highest peaks in all scenarios as well

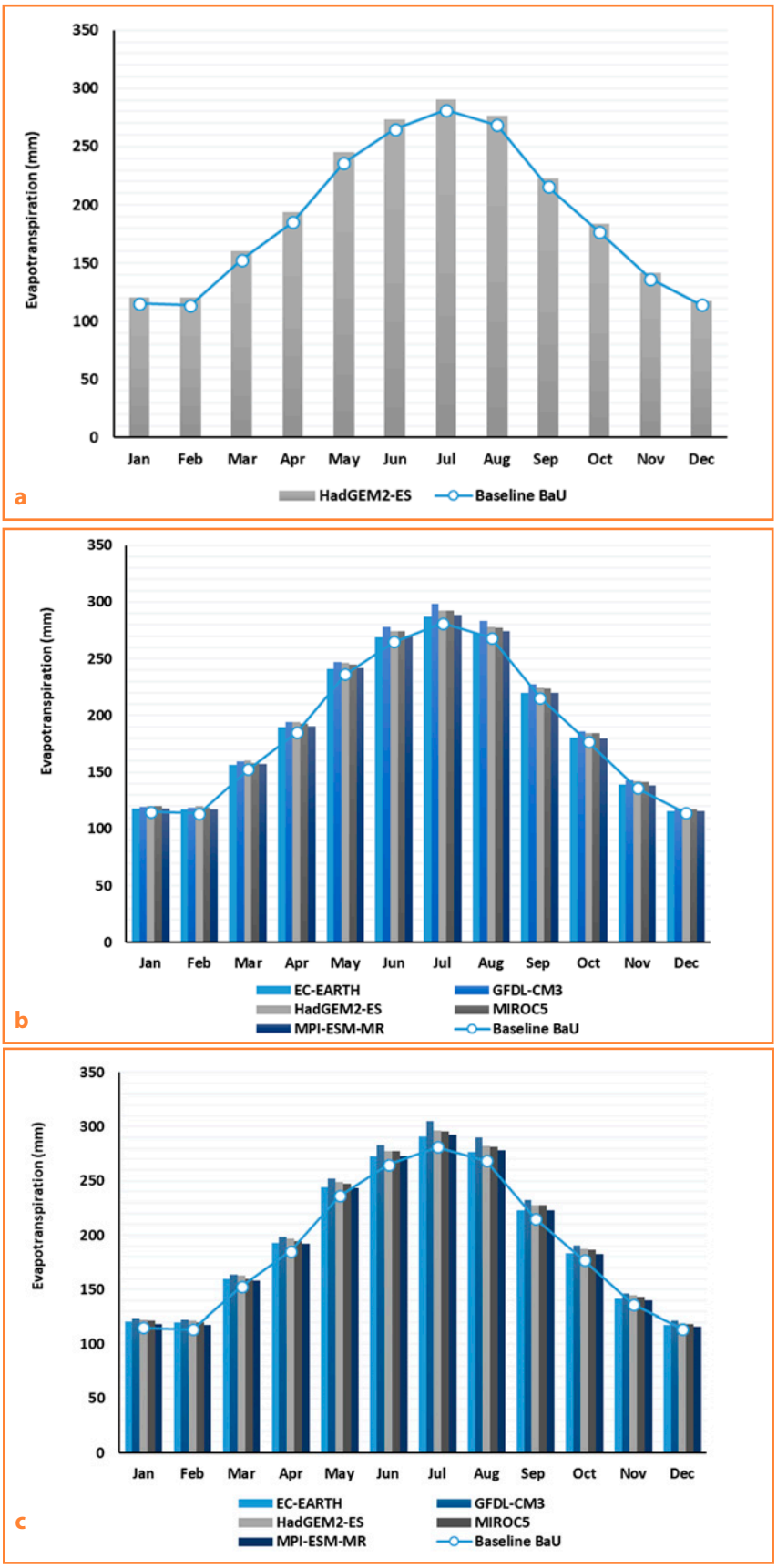

Figure 12 Monthly evapotranspiration variations under all examined GCM models for (a) RCP2.6, (b) RCP4.5, and (c) RCP8.5 scenarios

Table 10 Seasonal changes in evapotranspiration for all examined GCM-RCP scenarios

Scenario		Seasonal Evapotranspiration (mm)				Seasonal percent change (%)			
GCM	**RCP**	**winter**	**spring**	**summer**	**autumn**	**winter**	**spring**	**summer**	**autumn**
HadGEM2-ES	2.6	119.35	199.50	279.98	182.56	4.53%	4.29%	3.10%	3.68%
EC-EARTH	4.5	117.03	195.55	276.50	179.82	2.49%	2.22%	1.82%	2.12%
GFDL-CM3	4.5	118.87	200.36	286.64	185.36	4.11%	4.73%	5.56%	5.27%
HadGEM2-ES	4.5	119.54	200.32	281.71	183.86	4.69%	4.71%	3.74%	4.41%
MIROC5	4.5	118.85	198.42	281.17	183.28	4.09%	3.72%	3.54%	4.09%
MPI-ESM-MR	4.5	117.06	196.44	277.58	179.27	2.52%	2.69%	2.22%	1.81%
EC-EARTH	8.5	119.69	199.05	279.91	182.65	4.82%	4.05%	3.08%	3.73%
GFDL-CM3	8.5	122.65	204.82	292.64	189.78	7.42%	7.07%	7.77%	7.78%
HadGEM2-ES	8.5	121.26	202.73	285.56	186.68	6.20%	5.98%	5.16%	6.02%
MIROC5	8.5	120.21	200.50	284.83	185.87	5.28%	4.81%	4.89%	5.56%
MPI-ESM-MR	8.5	117.58	197.91	281.02	181.91	2.97%	3.45%	3.48%	3.31%
Baseline BaU		114.18	191.30	271.55	176.08	0.00%	0.00%	0.00%	0.00%

Table 11 Annual changes in river discharge for all examined GCM-RCP scenarios

Scenario		Annual discharge ($m^3.s^{-1}$)		Annual percent change (%)	
GCM	**RCP**	**peak**	**average**	**peak**	**average**
HadGEM2-ES	2.6	4.24	1.34	-5.57%	16.86%
EC-EARTH	4.5	4.79	1.56	6.68%	36.50%
GFDL-CM3	4.5	4.70	1.37	4.68%	19.49%
HadGEM2-ES	4.5	4.70	1.48	4.68%	29.26%
MIROC5	4.5	5.02	1.58	11.80%	38.23%
MPI-ESM-MR	4.5	4.76	1.60	6.01%	39.60%
EC-EARTH	8.5	4.70	1.44	4.68%	25.84%
GFDL-CM3	8.5	4.70	1.34	4.68%	16.74%
HadGEM2-ES	8.5	4.55	1.26	1.34%	10.13%
MIROC5	8.5	4.92	1.51	9.58%	32.22%
MPI-ESM-MR	8.5	4.53	1.53	0.89%	33.69%
Baseline BaU		4.49	1.14	0.00%	0.00%

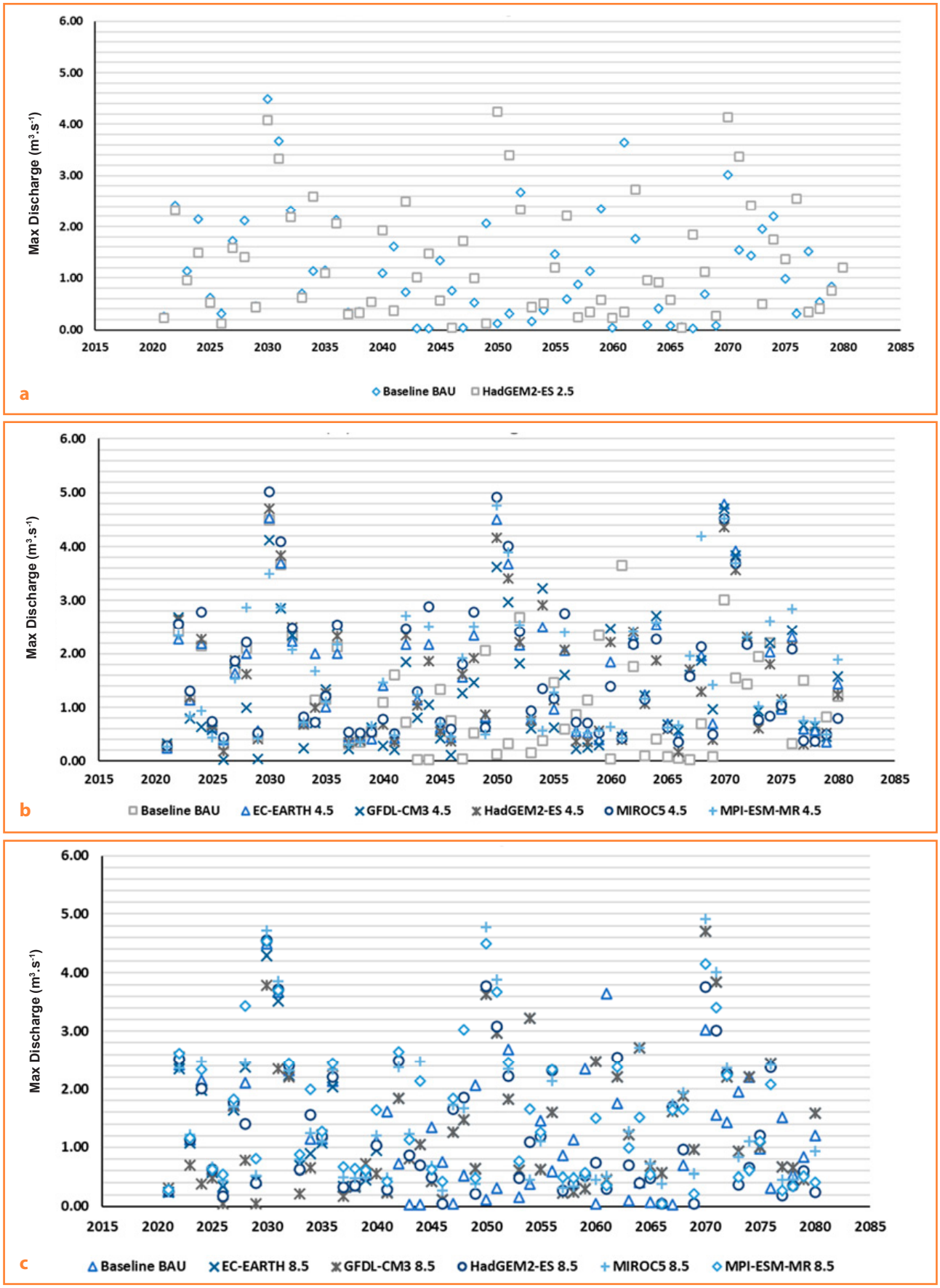

Figure 13 Annual peak discharge variations under all examined GCM models for (a) RCP2.6, (b) RCP4.5, and (c) RCP8.5 scenarios

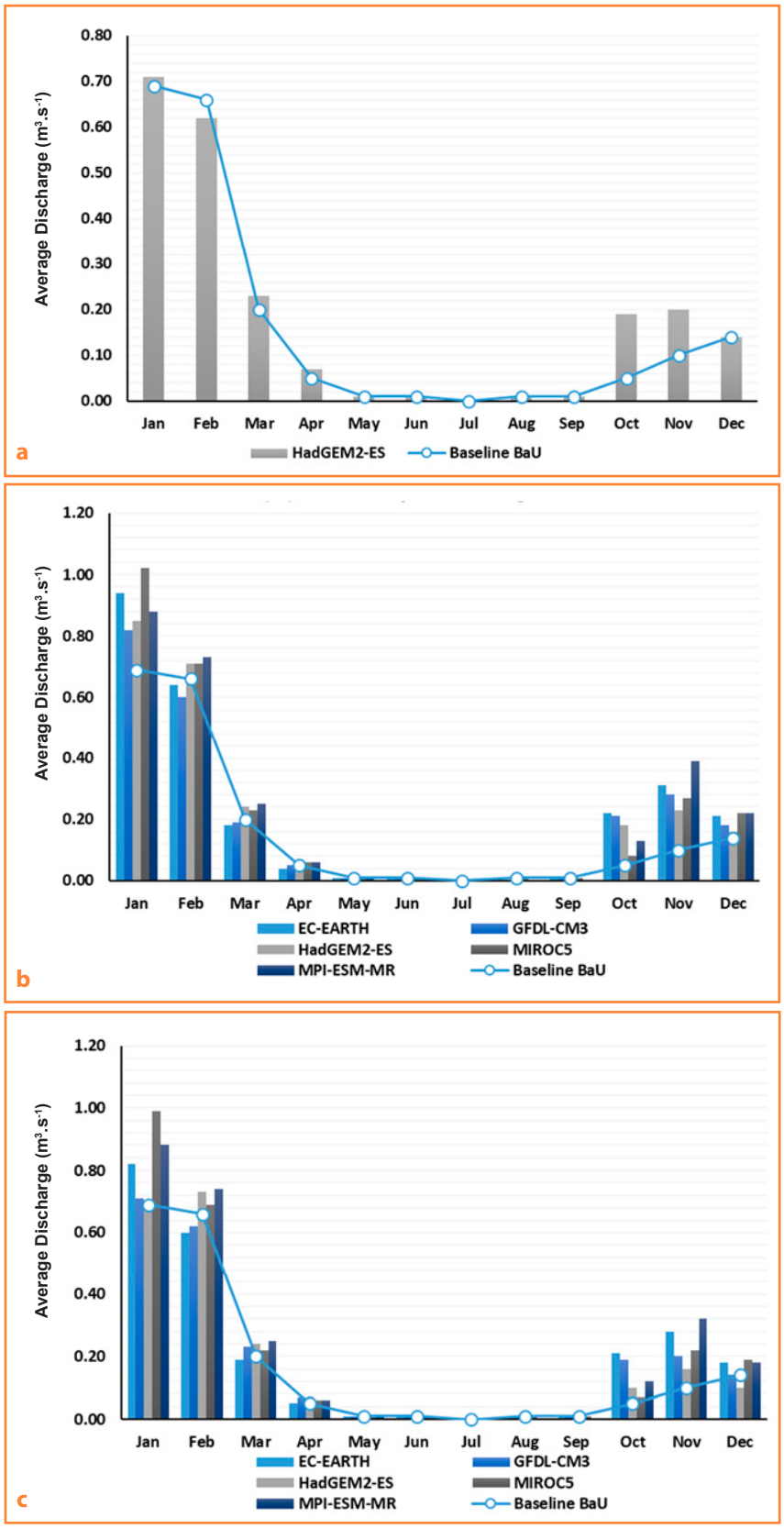

Figure 14 Monthly discharge variations under all examined GCM models for (a) RCP2.6, (b) RCP4.5, and (c) RCP8.5 scenarios

as in baseline scenario. However, the most critical months are October and November, which show more than double discharge compared to the baseline scenario. Also, in future, dry months August and September are expected to have even lower discharges. This sudden surge of streamflow from summer to autumn months is of particular concern as it increases the risk of flash floods occurrence.

Table 11 summarizes percent difference in annual average and peak discharge between baseline BaU scenario and each of future scenarios considered. It is observed that average discharge is increasing rapidly in future, with the most "optimistic" scenario being for HadGEM2-ES model and RCP8.5 (+10.13% increase) and the most "pessimistic" scenario being for MPI-ESM-MR model and RCP4.5 (+39.60% increase). On the other hand, annual peak discharge showed smaller changes, which vary from -5.75% decrease for HadGEM2-ES model and RCP8.5 to +11.80% increase for MIROC5 model and RCP4.5. Moreover, Table 12 summarizes seasonal changes in discharge as percentages of the mean values. Autumn shows the most significant expected increase in discharge as noted above, whereas summer and spring are the seasons with the largest number of discharge reductions. Finally, although winter is the season with the highest discharge amounts, it presents the smallest future percentage changes under climate change scenarios.

Table 12 Seasonal changes in river discharge for all examined GCM-RCP scenarios

Scenario		Seasonal discharge ($m^3.s^{-1}$)				Seasonal percent change (%)			
GCM	RCP	**winter**	**spring**	**summer**	**autumn**	**winter**	**spring**	**summer**	**autumn**
HadGEM2-ES	2.6	0.49	0.10	0.01	0.13	-1.34%	19.23%	0.00%	150.00%
EC-EARTH	4.5	0.60	0.08	0.00	0.18	20.13%	-11.54%	-50.00%	237.50%
GFDL-CM3	4.5	0.53	0.08	0.00	0.17	7.38%	-3.85%	-50.00%	212.50%
HadGEM2-ES	4.5	0.57	0.10	0.01	0.14	15.44%	15.38%	0.00%	162.50%
MIROC5	4.5	0.65	0.10	0.01	0.12	30.87%	15.38%	0.00%	125.00%
MPI-ESM-MR	4.5	0.61	0.11	0.00	0.17	22.82%	23.08%	-50.00%	225.00%
EC-EARTH	8.5	0.53	0.08	0.00	0.17	7.38%	-3.85%	-50.00%	212.50%
GFDL-CM3	8.5	0.49	0.10	0.01	0.13	-1.34%	19.23%	0.00%	150.00%
HadGEM2-ES	8.5	0.50	0.10	0.01	0.09	1.34%	15.38%	0.00%	62.50%
MIROC5	8.5	0.62	0.10	0.01	0.10	25.50%	11.54%	0.00%	87.50%
MPI-ESM-MR	8.5	0.60	0.11	0.00	0.15	20.81%	23.08%	-50.00%	175.00%
Baseline BaU		0.50	0.09	0.01	0.05	0.00%	0.00%	0.00%	0.00%

4 Conclusions

The present study investigates the climate change impact on hydrologic regime of the Kalloni river basin with intermittent flow in response to different climatic models and conditions. The LARS-WG version 6.0 was used along with five GCM models and three emission scenarios to generate climatic variables. In total, eleven sets of GCM-RCP scenarios were considered when predicting future rainfall, temperatures, and radiation patterns, covering a wide range of uncertainties. Hydrological model simulations were conducted for the baseline climate and each of the climate scenarios in the environment of HEC-HMS version 4.3. The results obtained demonstrate that the approach combining hydrological model HEC-HMS and LARS-WG weather generator is efficient for assessing the effects of climate change on the patterns of the river hydrology.

Annual and seasonal predictions of weather variables, evapotranspiration, and discharge for the Kalloni river basin were obtained based on various GCMs and RCPs scenarios for assessing climate change impact on hydrologic regime of the basin. Overall findings indicate an increase in mean annual rainfall and temperature for the region. In seasonal patterns, a significant increase in precipitation is expected in autumn. Slight increase or even decrease can be anticipated in summer and spring rainfall totals. A general increasing trend of mean temperature and a consequent change in evapotranspiration was observed throughout the year, with the most significant change occurring in winter. The projected decrease in summer precipitation and higher evapotranspiration are expected to cause a reduction in soil water and groundwater recharge in the basin area. This reduction in summer combined with the tremendous increase in autumn discharge leads to a high risk of flooding, particularly in the form of flash floods. Such findings indicate the need for integrated water management and flood mitigation strategies in the area of the Kalloni river basin.

This paper provides a quantitative framework for policymakers in small, intermittent flow, river basins in the Mediterranean, such as the Kalloni, to plan and manage the expected future challenges of river discharge and flood occurrence.

Acknowledgments

This research equipment's installation and operational cost was funded partly by the National Strategic Reference Framework (NSRF) 2014–2020, through the project "Observatory of Coastal Environment – AEGIS" and the ERMIS-flood Interreg project. Thanks are due to M. Champas, A. Gkerekos and G. Exintaris for their help in fieldwork and instrument installation and conservation at the Kalloni River and Professor K. Kalabokidis for the AEGIS-fire laboratory data provision.

References

Ali, M., Khan, S. J., Aslam, I., & Khan, Z. (2011). Simulation of the impacts of land-use change on surface runoff of Lai Nullah Basin in Islamabad, Pakistan. *Landsc. Urban Plan.*, *102*(4), 271–279.

Bai, Y., Zhang, Z., & Zhao, W. (2019). Assessing the Impact of Climate Change on Flood EventsUsing HEC-HMS and CMIP5. *Water Air Soil Pollution*. *230*(119).
https://doi.org/10.1007/s11270-019-4159-0

Bates, B.C. et al. (2008). *Climate change and water.* Technical paper of the Intergovernmental Panel on Climate Change. IPCC Secretariat.

Blaney, H. F., & Criddle, W. D. (1950). *Determining water requirements in irrigated areas from climatological and irrigated data.* SCS, TP-96, USDA.

Chisanga, C. B., Phiri, E., & Chinene, V. R. N. (2017). Statistical Downscaling of Precipitation and Temperature Using Long Ashton Research Station Weather Generator in Zambia: A Case of Mount Makulu Agriculture Research Station. *American Journal of Climate Change*, *6*, 487–512. DOI: 10.4236/ajcc.2017.63025. http://www.scirp.org/journal/ajcc

Cisneros, J. B.E. (2014). Part A: Global and Sectoral Aspects. Contribution of Working Group II to the Fifth Assessment Report of the Intergovernmental Panel on Climate Change. In V.R. Barros, C.B. Field, D.J. Dokken, M.D. Mastrandrea, K.J. Mach, T.E. Bilir, M. Chatterjee, K.L. Ebi, Y.O. Estrada, O.C. Genova, et al. Eds., *Climate Change 2014: Impacts, Adaptation, and Vulnerability* (pp. 229–269). Cambridge University Press.

Doorenbos, J., & Pruitt, W.O. (1977). *Crop water requirements* (Irrigation and Drainage Paper No. 24, 144 p.). FAO, United Nations.

Ebrahim, G. Y., Jonoski, A., van Griensven, A., & Di Baldassarre, G. (2012). Downscaling technique uncertainty in assessing hydrological impact of climate change in the Upper Beles River Basin, Ethiopia. *Hydrology Research, 44*(2)*, 377–398.* doi: 10.2166/nh.2012.037.

Emam, A. R., Mishra, B. K., Kumar, P., Masago, Y., & Fukushi, K. (2016). Impact Assessment of Climate and Land-Use Changes on Flooding Behavior in the Upper Ciliwung River, Jakarta, Indonesia. *Water*, *8*, 559. doi:10.3390/w8120559.

European Environmental Agency.
https://www.eea.europa.eu/data-and-maps/data/eu-dem

Hajian, F., Dykes, A. P., Zahabiyoun, B., & Ibsen, M. (2016). Prediction of climate change effects on the runoff regime of a forested basin in northern Iran. *Hydrological Sciences Journal*, *61*(15), 2729–2739. DOI: 10.1080/02626667.2016.1171870.

Hewer, M. J. & Gough, W.A. (2018). Thirty years of assessing the impacts of climate change on outdoor recreation and tourism in Canada. *Tour Manag Perspect, 26*,179–192. https://doi.org/10.1016/j.tmp.2017.07.003

HMSO. (1962). *Weather in the Mediterranean I: general meteorology* (2nd ed.). Her Majesty's Stationery Office.

Intergovernmental Panel on Climate Change (IPCC). (2000). *IPCC Special Report Emissions Scenarios*. Intergovernmental Panel on Climate Change, Working Group III. IPCC.

Intergovernmental Panel on Climate Change (IPCC). (2014). In R.K. Pachauri, L.A. Meyer (Eds.), *Climate Change 2014: Synthesis Report*. Core Writing Team, Contribution of Working Groups I, II and III to the Fifth Assessment Report of the Intergovernmental Panel on Climate Change. IPCC.

Ismail, H., Kamal, Md. R., Abdullah, A. F. B., Jada, D. T., & Hin, L. S. (2020). Modeling Future Streamflow for Adaptive Water Allocation under Climate Change for the Tanjung Karang Rice Irrigation Scheme Malaysia. *Applied Sciences*, *10*(14), 4885. doi:10.3390/app10144885.

Lavell, A., M. Oppenheimer, C. Diop, J. Hess, R. Lempert, J. Li, R. Muir-Wood, & Myeong, S. (2012). Climate change: new dimensions in disaster risk, exposure, vulnerability, and resilience. In C.B. Field, V. Barros, T.F. Stocker, D. Qin, D.J. Dokken, K.L. Ebi, M.D. Mastrandrea, K.J. Mach, G.-K. Plattner, S.K. Allen, M. Tignor, & P.M. Midgley (eds.), *Managing the Risks of Extreme Events and Disasters to Advance Climate Change Adaptation* (pp. 25–64). A Special Report of Working Groups I and II of the Intergovernmental Panel on Climate Change (IPCC). Cambridge University Press.

Manfreda, S. (2018). On the derivation of flow rating curves in data-scarce environments. *Journal of Hydrology, 562,* 151–154. DOI: 10.1016/j.jhydrol.2018.04.058.
https://doi.org/10.1016/j.jhydrol.2018.04.058

Matrai, I., & Tzoraki, O. (2018). Assessing stakeholder perceptions regarding floods in Kalloni and Agia Paraskevi, Lesvos Greece. *HYDROMEDIT Conference*, 818–820.

Meenu, R., Rehana, S., & Mujumdar, P. P. (2012). Assessment of hydrologic impacts of climate change in Tunga – Bhadra river basin, India with HEC-HMS and SDSM. *Hydrological prosesses*. DOI: 10.1002/hyp.9220.

Moriasi, D.N., Arnold, J.G., Van Liew, M.W., Bingner, R.L., Harmel, R.D. & Veith, T.L. (2007). Model evaluation guidelines for systematic quantification of accuracy in watershed simulations, *Trans. Am. Soc. Agric. and Biol. Eng*., *50*(3), 885−900.

Nash, J. E., & Sutcliffe, J. V. (1970). River flow forecasting through conceptual models part I: A discussion of principles. *Journal of Hydrology*, *10*(3), 282–290.

Nourani, V, Baghanam, A.H., & Gokcekus, H. (2018). Data-driven ensemble model to statistically downscale rainfall using nonlinear predictor screening approach. *J Hydrol, 565*,538–551. https://doi.org/10.1016/j.jhydrol.2018.08.049

Nyaupane, N., Mote, S. R., Bhandari, B., & Kalra, A. (2018). Rainfall-Runoff Simulation Using Climate Change Based Precipitation Prediction in HEC-HMS Model for Irwin Creek, Charlotte, North Carolina. *World Environmental and Water Resources Congress*.

Parry, M.L., Canziani, O.F., Palutikof, J.P., van der Linden, P.J., & Hanson, C.E. (Eds.) (2007). *Climate Change 2007: Impacts, Adaptation and Vulnerability.* Contribution of Working Group II to the Fourth Assessment Report of the Intergovernmental Panel on Climate Change, Cambridge University Press.

Ponce, V. M. (1989). *Engineering Hydrology, Principles and Practices*.

Qin, X. S., & Lu, Y. (2014). Study of Climate Change Impact on Flood Frequencies: A Combined Weather Generator and Hydrological Modeling Approach. *Journal of hydrometeorology*, *15*(3), 1205–1219. DOI: 10.1175/JHM-D-13-0126.1

Racsko, P., Szeidl, L., & Semenov, M. (1991). A serial approach to local stochastic weather models. *Ecol Model, 57*, 27–41. https://doi.org/10.1016/0304-3800(91)90053-4

Randall, D.A., Wood, R.A., Bony, S., Colman, R., Fichefet, T., Fyfe, J., Kattsov, V., Pitman, A., Shukla, J., Srinivasan, J., Stouffer, R.J., Sumi, A., & Taylor, K.E. (2007). Cilmate Models and Their Evaluation. In S. Solomon, D. Qin, M. Manning, Z. Chen, M. Marquis, K.B. Averyt, M.Tignor, H.L. Miller (Eds.), *Climate Change 2007: The Physical Science Basis*. Contribution of Working Group I to the Fourth Assessment Report of the Intergovernmental Panel on Climate Change. Cambridge University Press.

Refsgaard, J.C., Arnbjerg-Nielsen, K., & Drews, M., et al. (2013). The role of uncertainty in climate change adaptation

strategies – A Danish water management example. *Mitig Adapt Strateg Glob Change, 18*, 337–359. https://doi.org/10.1007/s11027-012-9366-6

Sharma, D., Gupta, A.D., & Babel, M.S. (2007). Spatial disaggregation of bias-corrected GCM precipitation for improved hydrologic simulation: Ping River Basin, Thailand. *Hydrology and Earth System Sciences*, *11*, 1373–1390. www.hydrol-earth-syst-sci.net/11/1373/2007/

Scharffenberg, W., Ely, P., Daly, S., Fleming, M., & Pak, J. (2010). Hydrologic Modeling System (HEC-HMS): Physically-Based Simulation Components. *2nd Joint Federal Interagency Conference,* Las Vegas, NV.

Semenov, M. A., & Barrow, E. M. (2002). LARS-WG – *A Stochastic Weather Generator for Use in Climate Impact Studies*. User Manual, Version 3.0

Semenov, M.A., & Barrow, E.M. (1997). Use of a stochastic weather generator in the development of climate change scenarios. *Clim. Chang., 35*, 397–414.

Sharafati, A., Pezeshki, E., Shahid, S., & Motta, D. (2020). Quantification and uncertainty of the impact of climate change on river discharge and sediment yield in the Dehbar river basin in Iran. *Journal of Soils and Sediments*, *20*, 2977–2996. https://doi.org/10.1007/s11368-020-02632-0

Shrestha, A., Babel, M. S., Weesakul, S., & Vojinovic, Z. (2017). Developing Intensity – Duration – Frequency (IDF) Curves under Climate Change Uncertainty: The Case of Bangkok, Thailand. *Water, 9*(145). doi:10.3390/w9020145

Sunyer, M.A., Madsen, H., & Ang, P.H. (2012). A comparison of different regional climate models and statistical downscaling methods for extreme rainfall estimation under climate change. *Atmos. Res., 103*, 119–128.

Tzoraki, O. (2020). Operating Small Hydropower Plants in Greece under Intermittent Flow Uncertainty: The Case of Tsiknias River (Lesvos). *Challenges*, *11*(17), doi:10.3390/challe11020017.

U.S. Army Corps of Engineers (USACE). (2013). *HEC-GeoHMS Geospatial Hydrologic Modeling Extension*. Hydrologic Engineering Center, User's Manual, Version 10.1.

U.S. Army Corps of Engineers (USACE). (2018). *Hydrologic Modeling System, HEC-HMS*. Hydrologic Engineering Center, User's Manual, Version 4.3.

Verma, A. K., Jha, M. K., & Mahana, R. K. (2010). Evaluation of HEC-HMS and WEPP for simulating watershed runoff using remote sensing and geographical information system. *Paddy Water Environ.*, *8*(2), 131–144.

Wang, M., Zhang, L., & Baddoo, T. D. (2016). Hydrological Modeling in A Semi-Arid Region Using HEC-HMS. *Journal of Water Resource and Hydraulic Engineering*. DOI: 10.5963/JWRHE0503004.

Westerberg, I., Guerrero, J.-L., Seibert, J., Beven, K.J., & Halldin, S. (2011). Stage-discharge uncertainty derived with a non-stationary rating curve in the Choluteca River. *Hydrol. Process*, *25*, 603–613. 10.1002/hyp.7848.

Wilby, R., Dawson, C., & Barrow, E. (2002). SDSM – A decision support tool for the assessment of regional climate change impacts. *Environ. Model. Softw., 17*, 145–157.

Wilks, D.S., & Wilby, R.L. (1999). The weather generation game: A review of stochastic weather models. *Prog. Phys. Geogr., 23*, 329–357.

World Bank Group. (2015). *Water and Climate Adaptation Plan for the Sava River Basin*. ANNEX 1 – Development of the Hydrologic Model for the Sava River Basin.

Wu, C.H., Huang, G.R., & Yu, H.J. (2015). Prediction of extreme floods based on CMIP5 climate models: a case study in the Beijiang River basin, South China. *Hydrology and Earth System Sciences*, *19*(3), 1385–1399.

Yilmaz, A. G. & Imteaz, M. A. (2011). Impact of climate change on runoff in the upper part of the Euphrates basin. *Hydrological Sciences Journal – Journal des Sciences Hydrologiques*, *56*(7), 1265–1279. DOI:10.1080/02626667.2011.609173.

Zhai, P., Pörtner, H.O., & Roberts, D. (2018) Summary for policymakers. In *Global Warming of 1.5 C. An IPCC Special Report on the Impacts of Global Warming of 1.5 C above Pre-Industrial Levels and Related Global Greenhouse Gas Emission Pathways*, p. 32. IPCC.

sciendo

DOI: 10.2478/ahr-2021-0023
Acta hort regiotec, 24, 2021(1): 49–55

Research Article

Comparison of laser diffraction method and hydrometer method for soil particle size distribution analysis

Kateřina Sedláčková*, Lenka Ševelová
Mendel University in Brno, Brno Czech Republic

Article Details: Received: 2021-01-28 | Accepted: 2021-03-17 | Available online: 2021-05-31

Licensed under a Creative Commons Attribution 4.0 International License

SCREENED BY iThenticate® Professional Plagiarism Prevention

The article aims to present a comparative study of two methods used to determine the particle size distribution of fine and medium coarse soils. These methods are used to determine the grain size distribution curve in practice; however, for different purposes. The classical sedimentation method, based on the Stoke's sedimentation law (hydrometer, areometric, the Casagrande's method), standardized for a geotechnical classification of soils was compared with the laser diffraction method on the Mastersizer 3,000 analyser used for soil science purposes. The first comparison on nine samples showed significant differences, especially for larger fractions above 0.01 mm. All measured values of falls from laser diffraction analysis (LDA) showed higher values of all analysed fractions. It was also interesting to follow the trend between the tests for the preparation of conversion factors. The analysis also outlined the direction for further comparison. For the geotechnical use of the LDA, it will be necessary to take into account the sample preparation and processing before analysis.

Keywords: aerometer test, densitometer test, geotechnical analyses, laser diffraction, pipette method, sedimentation method

1 Introduction

Soil texture is an elemental parameter for soil classification. Soil type determined according to soil particle size distribution is the key parameter for mechanical properties determination in geotechnical analyses (Ševelová et al., 2020) and soil nutrification conditions in the pedologic analysis (Wlodarczyk et al., 2008). Soil texture indicates the content of the individual grain size fractions in the soil. The representation of the individual grain size fractions is graphically represented in the grain size distribution curve (Rejšek & Vácha, 2018).

Particle size distribution (PSD) is an important method in soil science and also in geotechnics. Each of the fields uses different classification systems of grain size fractions in the soils and performs PSD analysis for a different purpose. In soil science, PSD is determined as it affects the soil properties such as porosity, gas exchange and water retention (Walczak et al., 2004; Witkowska-Walczak et al., 2002), soil conductivity (Sławiński et al., 2006), sorption properties (Usowicz et al., 2008), etc. In geotechnics, PSD is needed to determine the soil type and the related design strength parameters for the building structure reliable design. PSD analysis procedure is defined for each of these fields by its standard methods, based on different sedimentation methods. Although these methods are validated and other methods are based on them, they are also time-consuming and burdened with human error in manual sample processing.

The grain size distribution curve for geotechnical analyses is created by a combination of sieve analysis (particles between 125 mm and 0.063 mm) and hydrometer (densitometer) test (particles less than 0.063 mm). Hydrometer (areometer, densitometer, the Casagrande's test) is based on free and continuous sedimentation of the suspension (the Stoke's law). During sedimentation, the density of the solution is read in seven defined time intervals – 2', 5', 15', 30', 60', 120', 240' and 24 hours. Subsequently, fictitious sieves are formed from these density readings and converted to grain size fractions. The data obtained by the sieving and hydrometer method were merged and plotted in the form of the grain size distribution curve (Hanák, 2001).

***Corresponding Author:** Kateřina Sedláčková, Mendel University in Brno, Faculty of Forestry and Wood Technology, Czech Republic; e-mail: katerin.sedlackova@gmail.com

Most comparisons between the LDA and the sedimentation method were made for the pipette method (Igaz et al., 2017; Taubner et al., 2009; Beuselinck et al., 1998; Yang et al., 2019). The pipette method determines the mass percentage concentration of the settling suspension. The hydrometer determines its density (Bieganowski et al., 2018). For the pipette method, sample preparation, measurement method, measurement times, and the maximum grain size of the fraction that enters the sedimentation analysis (particles below 0.25 mm) differ. The principle is based on pipetting from predetermined depths and at predetermined time intervals. The samples are then dried, weighed, and the percentage of the individual fractions is calculated accordingly (Igaz et al., 2017).

The laser diffraction analysis (LDA) is a modern method that can be used, besides other purposes, to determine soil texture. LDA is used to measure the particle size distribution in the soil sample. The principle of laser diffraction consists of irradiating the sample particles with a laser beam. Sample particles bend light (diffraction). The angle of light refraction is inversely proportional to the measured particles size – large particles scatter light at a small angle but with low intensity, and vice versa. The light amount that is determined in different directions is used to calculate the particle size and the calculation depends on the sample refractive index and the medium in which it is dispersed. The majority of the LDA devices currently available enable measurements of fractions under 2 mm (Šulcová & Beneš, 2008); however, the measuring range is expanding up to 0.01–3,000 µm (Igaz et al., 2020). LDA is therefore used for also for PSD analysis of smaller soil particles as well as another method, the pipette method (Taubner et al., 2009).

The PSD determination of bulk materials using LDA is used mainly for homogenous materials with the expected narrow range of grain size fractions. By this analysis, materials with one-grain size fraction are most often analysed with high reliability – such as powder, gunpowder, or cocoa. For soil science purposes, many studies have been performed, which in some cases confirm the concordance of PSD performed using LDA and some sedimentation method, most often the pipette method (Ryżak & Bieganowski, 2010).

The purpose of the presented work was to verify the possibility of using LDA also for geotechnical purposes and to replace this analysis with the hydrometer used for grain size analysis according to ČSN EN ISO 17892-4 (2017). Therefore, the results on two methods of the PSD determination were compared – the hydrometer method (sedimentation, the Casagrande's method) and the laser diffraction analysis (LDA). The comparative analysis aimed to streamline the methods that lead to grain size distribution curve preparation.

2 Material and methods

2.1 The samples

Nine samples of 0–4 mm fraction were used for comparative analysis. The samples were sandy loam mixtures, and their texture was classified according to the Unified Soil Classification System (USCS) (ČSN EN ISO 14688-2, 2005). Then, they were classified according to Table 1 (ČSN EN ISO 14689-1 (2004) and ČSN EN ISO 14688-2 (2005)). The samples were artificially mixed to modify the park paths. This mixture was formed by mixing a gravel-sand skeleton with loamy-clayey filling.

All samples were sieved through a 2 mm sieve. About 1–2 g of air-dried sample was used for LDA. About 40 g of sample was used in the hydrometer – this was sieved through a 0.063 mm sieve and fractions 2–0.063 mm were dried and sieved through a sieve system. For comparative analysis there were taken falls below 2 mm of these materials.

The research was conducted in the Department of Landscape Management laboratory.

2.2 Hydrometer test preparation

For the hydrometer, soil samples sieved through a 2 mm sieve were used. The weight of the samples ranged from 40 g to 80 g. The sample was mixed with distilled water and 20 ml of sodium hexametaphosphate, stirred for five minutes, sieved through a 0.063 mm sieve into a graduated cylinder and made up to 1,000 ml with distilled water. At the specific time intervals (2´, 5´, 15´, 30´, 60´, 120´, 240´ and 24 hours), the values of the actual temperature and relative density were recorded using a Casagrande's densitometer. Subsequently, the fictitious sieves calculation and fractions percentage decrease were performed. These fractions were then used as comparison sieves for the LDA. In combination

Table 1 USCS Classification (ČSN EN ISO 14688-2, 2005)

	V1	V2	V3	V4	V5	V6	V7	V8	V9
USCS	S4-SM	S4-SM	G3-G-F	S4-SM	S4-SM	S3-S-F	S4-SM	S4-SM	S3-S-F
Sieve <0.063 mm	18.50	20.90	13.50	16.50	17.10	9.30	18.80	19.70	11.00

with the sieve analysis, the complete soil sample grain size distribution curve was obtained. For comparison with LDA, histogram data were obtained from these cumulative values.

2.3 Laser diffraction analysis preparation

Laser analyser Mastersizer 3000 (Malvern Instruments) is composed of a optical unit, a dispersion unit, and a measurement cell. The wet dispersion unit (filled with distilled water) was used. The measurement range was 0.01–3,500 μm (Malvern Instruments Ltd., 2013).

The samples for LDA were sieved at 2 mm mesh size. From this amount there was measured about 20 g and quartering was performed. All samples' preparations were the same, without the use of chemicals. Some samples were dried at room temperature and some were dried at 105 °C, but all samples were fully dry when the measurement was performed (the samples were dried for practical reasons because dry soil is better sieved through a sieve with small meshes). After quartering, a small amount of soil (about 1–2 g) was inserted into the laser analyser. Three measurements were performed. First, with manual measurement, second, with entered fictitious sieves from hydrometer (fictitious sieves are imaginary sieves calculated from the hydrometer test). These data were obtained during the previous measurement with a densitometer. The third measurement was performed with SOP (standard operating procedure) measurement with no default sieve sizes (SOP is a predefined measurement sequence). The second measurement was used for comparison with the hydrometer test. The grain size distribution curve is formed by the cumulative volume in percentage. Laser analyser processed the specified sieves, but only for the histogram (percentage of individual sizes). For cumulative volume, the two closest sieves had to be selected (Malvern Instruments Ltd., 2015).

2.4 Data evaluation

Nine samples (V1 to V9) were analysed. Six samples were SM-S4, two were S3 S-F and one was G3-G-F. The analysis was performed by a combination of a sieve and a hydrometer. The falls percentages on the individual sieves are given in Table 3.

Only grain size fractions below 0.063 mm were compared with LDA because the larger fraction was the result of sieve analysis, and this comparison was not the subject of this analysis. Regarding LDA, the histogram data corresponded to the specified sieves from the densitometer, and the data for the cumulative volume worked with fictitious sieves of the diffraction analyser.

2.5 Mastersizer 3000 data outputs

Table 2 shows an example of LDA output. The refractive index is a value determining the light refraction during its transition from an environment to another environment. It is between 0 and 5. The index is constant. For dispersant (distilled water) and sampled material, refraction indices of 1.33 and 1.457 were used, respectively. The absorption index is a measure of the light amount that particles absorb. It is between 0 and 10 and the higher it is, the less transparent the materials are. Weighted residual is an indication of how well the calculated data were fitted to the measurement data. A good fit is indicated by a residual of less than 1%. Obscuration is a measure of the laser light amount lost due to the introduction of the samples into the analyser beam. Obscuration helps the user to set the right sample concentration during the measurement. Concentration is calculated using the Beer-Lambert's law. Span is the width of the distribution measurement. The narrower the distribution, the smaller the span becomes. Uniformity is a measure of the absolute divination from the median. Specific surface area is the particles total area divided by the total weight. D (m, n) are the distribution statistics, they are calculated from the results (Malvern Instruments Ltd., 2015).

Table 2 The example of LDA Mastersizer 3000 output

Analysis	**Result**		
Particle name	sita_V1	concentration	0.07%
Particle refractive index	1.457	span	3.656
Particle absorption index	0.01	uniformity	1.162
Dispersant name	water	specific surface area	188.9 $m^2.kg^{-1}$
Dispersant refractive index	1.33	D [3,2]	11.3 μm
Scattering model	mie	D [4,3]	256 μm
Analysis model	general purpose	Dx (10)	5.51 μm
Weighted residual	0.61%	Dx (50)	176 μm
Laser obscuration	27.11%	Dx (90)	650 μm

3 Results and discussion

Nine granulometric compositions of soils were compared. Granulometric curves were obtained in the form of cumulative fall data on individual sieves and then were converted to histogram data.

Figs 1 and 2 show representative results for samples V1 and V9 for the whole analysed range of fractions 0 to 2 mm. It is a comparison between the hydrometer test (in graphs marked as ARM – areometer) and LDA. The overall behaviour trend in all analysed samples is evident. The falls values on individual sieves determined from the LDA are in 99% of cases higher than from the hydrometer analysis.

The differences in the falls quantity in the individual sieves were determined and the difference between the two methods was quantified. In almost all cases, the amount found for individual fractions was higher for samples analyzed for LDA. The difference between the amount detected by LDA and ARM for all materials and all fractions is shown in Fig. 3.

The magnitudes of the differences between the individual fractions were observed only from comparable sieves, i.e. up to the maximum of 0.063 mm. It can be stated that there is an evident trend in behaviour. Up to the 0.01 mm fraction, the data are more consistent and with less variability, up to the maximum of 4% by volume,

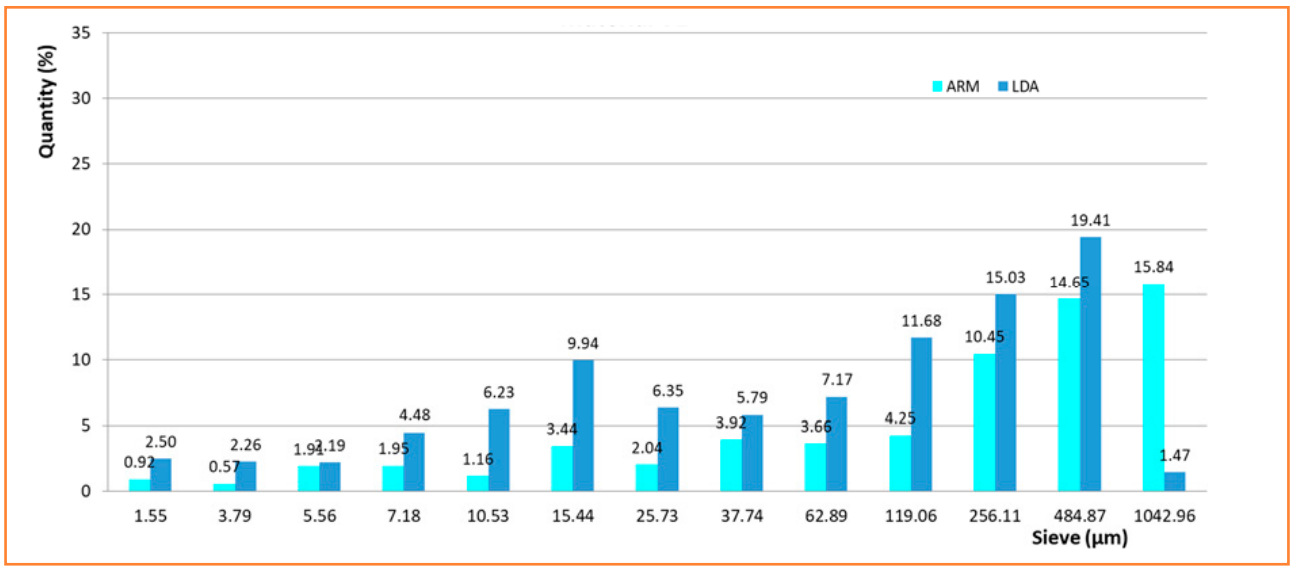

Figure 1 Representative results for materials V1

Table 3 Outputs from the hydrometer

Sieve (µm)	**V1**	**V2**	**V3**	**V4**	**V5**	**V6**	**V7**	**V8**	**V9**
1,41–1,56	0.92	4.10	1.41	1.80	1.51	1.36	0.66	0.55	1.38
3.39–3.77	0.57	1.69	1.34	1.00	1.70	0.38	0.66	0.51	1.34
4.75–5.28	1.91	0.88	1.34	1.66	1.39	0.43	0.35	0.43	0.34
6.68–7.47	1.95	1.61	0.68	0.37	0.85	0.39	1.89	1.65	0.73
9.35–10.47	1.16	2.09	0.69	1.37	2.32	0.71	2.50	3.97	0.69
13.10–14.67	3.44	2.13	1.31	0.70	2.45	0.33	3.68	4.84	1.03
22.44–25.32	2.04	1.46	1.40	2.26	0.89	1.33	3.06	3.20	0.74
35.23–39.81	3.92	2.76	1.97	3.24	2.08	1.07	3.10	2.09	1.99
63.00	3.66	2.94	2.39	2.68	2.26	0.57	0.61	2.14	2.83
125.00	4.25	5.38	4.03	6.03	4.75	3.78	4.49	7.37	5.02
250.00	10.45	7.91	6.62	9.99	8.65	9.33	10.63	12.98	8.46
500.00	14.65	11.25	10.56	14.62	13.16	16.47	14.01	16.81	13.35
1,000.00	15.84	17.90	18.94	23.10	21.79	26.24	15.81	19.74	19.47
2,000.00	23.27	27.62	25.02	20.55	29.25	25.98	23.96	18.47	20.35

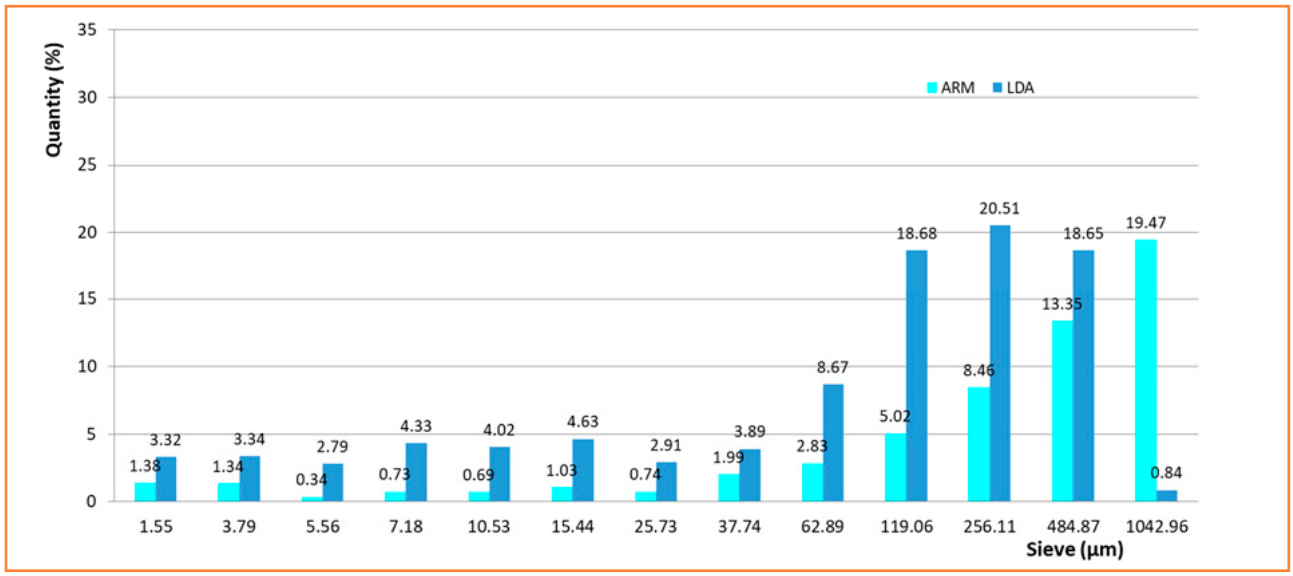

Figure 2 Representative results for materials V9

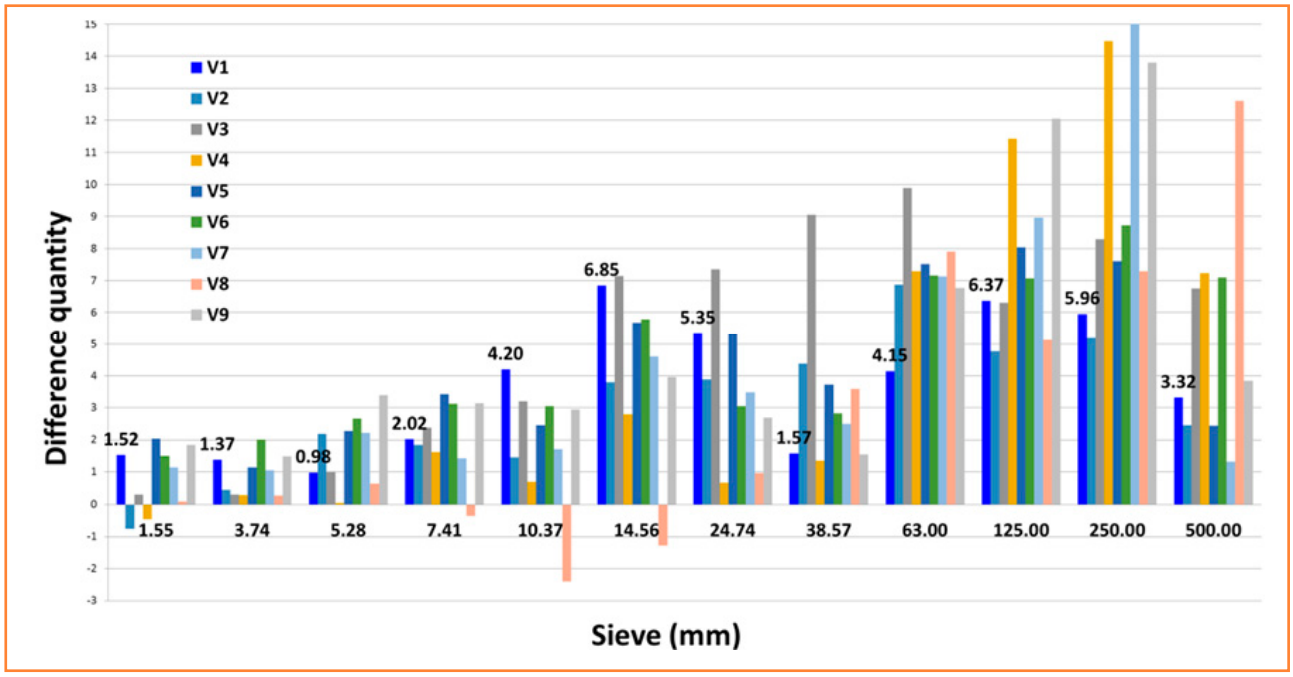

Figure 3 The difference in quantity between the amount detected by LDA and ARM for all materials V1–V9 and all fractions

as shown in Fig. 3. For sieves over 0.01 mm, the differences in the detected volumes between the hydrometer and LDA are already larger, up to 10% of the volume (Fig. 3), and the values show greater variability. Fig. 4 shows drop differences in sieves for each sample.

Several scientific teams have already dealt with the comparison of LDA and the sedimentation methods, especially with the pipetting method for soil science purposes, however, we did not find any work comparing LDA with the Casagrande's sedimentation method for geotechnical purposes.

Yang et al. (2019) compared LDA with the pipetting method and the scanning electron microscopy. They measured over 200 samples. The samples were prepared with hydrogen peroxide and hydrogen chloride. Sodium hexametaphosphate was used for better dispersion. This team used the Mastersizer 2,000 laser analyser and distilled water as a dispersant. Worse results were observed for clay, better for sand grain size fractions. The results of this research confirmed the suitability of the use of LDA instead of the pipetting method, but at the same time pointed out that each soil is different, and research

© Slovak University of Agriculture in Nitra
www.uniag.sk

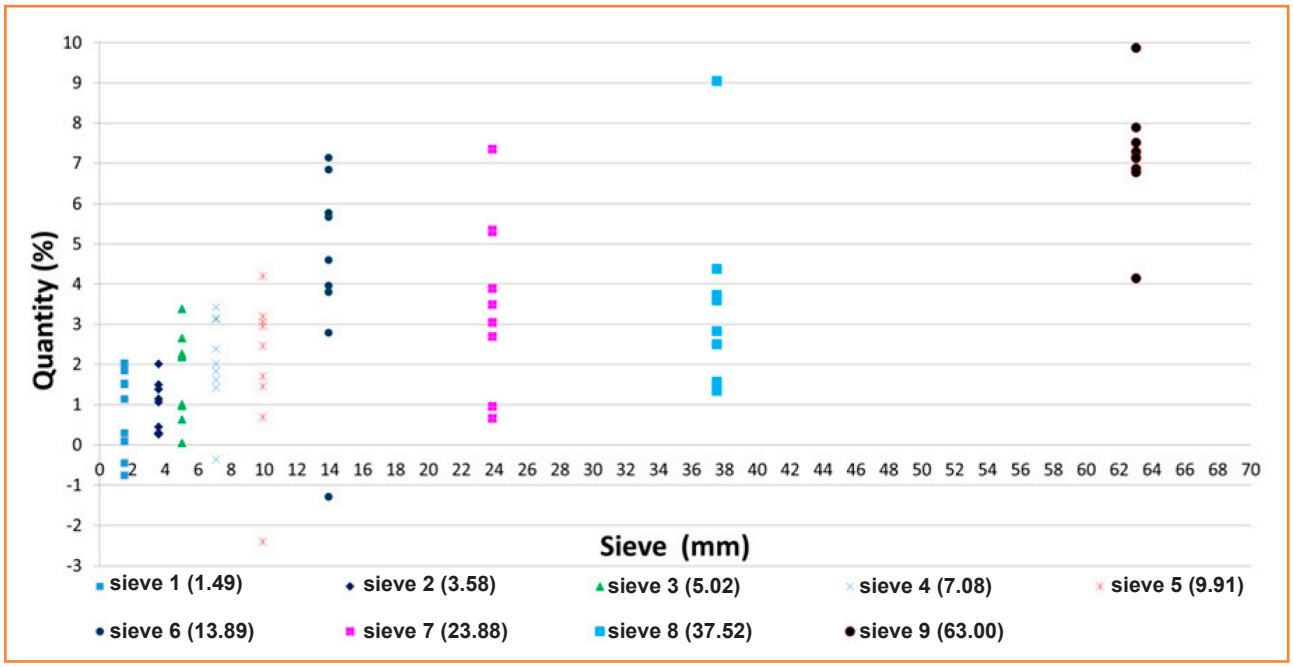

Figure 4 Drop differences in sieves for individual samples

needs to be continued and all other factors addressed (Yang et al., 2019).

The research carried out using the Casagrande's sedimentation method can be used to compare the presented results, but for soil science purposes, i.e. at other sedimentation times (Ryżak & Bieganowski, 2010). Ryżak and Bieganowski (2010) compared LDA with the hydrometer method. They worked with dry samples and with the Mastersizer 2,000 (the previous version of the analyser used in this study). The dispersant was distilled water. They proceeded with 23 samples. Only three fine grain size fractions were compared in the analyses, namely clay and silty up to 0.05 mm and sand up to 2 mm. Although they achieved better correlations for sand fraction, worse correlation than in our study was observed for clay fraction. The conclusion was that the evaluated three particle size fractions should be considered separately and should only be analysed separately from each other (Ryżak & Bieganowski, 2010).

Over 200 samples were processed by Di Stefano et al. (2010). They compared LDA with the sieve-hydrometer method. The hydrometer was carried out with different sample amounts at other times and using other mesh sizes than in our research. They used the laser analyser Analysette 22. Before comparing, some factors affecting the LDA were tested – the ultrasound duration, the sample pre-treatment and the diffraction theory applied. All samples analysis showed that the sand part determined by hydrometer was similar to that obtained by the LDA. The clay percentage was an overestimation to LDA (Di Stefano et al., 2010).

The aim for determining the PSD for all mentioned methods is to determine the fractions percentage for the classification preparation. Soil classification is used in individual disciplines for specific purposes. However, individual methods differ in the methodology of preparation. There are different amounts of soil entering the analysis, differences in the sample preparation procedure, and the times for determining the density of the solution may lead to different absolute values of the percentages for the individual fractions.

The observed difference between the hydrometer and LDA results may be due to the different sample preparation and different amount of sample. Due to the small amount of sample entering the LDA analysis, the samples for LDA were only air-dried, and no sodium hexametaphosphate was used. Therefore, the samples were not perfectly separated for LDA. Very different amounts of the sample also enter both measurements – about 40 g for the hydrometer and about 1–2 g for LDA.

Studies showed good statistical dependencies between methods for soils with prevailing grain size fractions. Significant differences were found in the soils with a wide grain size fraction range (Ryżak & Bieganowski, 2010). Therefore, it can be stated that this first comparison showed interesting relations between LDA and hydrometer, which will need to be subjected to a more detailed analysis.

4 Conclusions

There are various methods for classifying PSD of soils. They are based on different grain sizes of detected fractions, sample preparation methods, and measurement procedures, from which the percentage is determined – the distribution of the individual particles. It is very difficult to make a simple substitution for one method after another because each is associated with a specific purpose and focus to use. The presented results of the first comparison of LDA and the hydrometer method for the geotechnical purposes show significant differences in the detected amounts of falls on the sieves but at the same time, a good trend that could be used to determine the dependencies between the individual sieves.

The analysis clearly shows better correlations between finer fractions. Up to the 0.01 mm fraction, the differences in falls were within acceptable limits. For finer-grained soils, especially clays (which are more difficult for hydrometer processing), the LDA could offer a solution. Furthermore, a careful analysis identified some possible sources of errors that arose during the transformation of procedures. The main reason for the differences is a method of sample preparation for the hydrometer method – the amount of used sample, the maximum fraction, and the use of reagent. In LDA, incomparably smaller amounts enter the analysis, and the sample was prepared without the use of a reagent.

Acknowledgements

The project was supported by the Internal Grant Agency Faculty of Forest and Wood Technology Mendel University in Brno, project IGA LDF_VP_2020044.

References

Beuselinck, L., Govers, G., Poesen, J., Degraer, G., & Froyen, L. (1998). Grain-size analysis by laser diffractometry: comparison with the sieve-pipette method. *Catena, 32*(3–4), 193–208. doi.org/10.1016/S0341-8162(98)00051-4.

Bieganowski. A., Ryżak, M., Sochan, A., Barna, G., Hernádi, H., Beczek, M., Polakowski, C., & Makó, A. (2018). Advances in Agronomy. In Donald L. Sparks (Eds), *Chapter Five – Laser Diffractometry in the Measurements of Soil and Sediment Particle Size Distribution (151*, pp. 215–279). Academic Press. doi.org/10.1016/bs.agron.2018.04.003.

ČSN EN ISO 14688-2 (2005). *Geotechnical Investigation and Testing-Identification and Classification of Soil-Part 2: Principles for a Classification*. Institute for Technology Standardization, Metrology and State Testing.

ČSN EN ISO 14689-1 (2004). *Geotechnical Investigation and Testing-Dentification and Classification of Rock-Part 1: Identification and Description*. Institute for Technology Standardization, Metrology and State Testing.

ČSN EN ISO 17892-4 (2017). *Geotechnical Investigation and Testing-Laboratory Testing of Soil-Part 4: Determination of Particle Size Distribution*. Institute for Technology Standardization, Metrology and State Testing.

Di Stefano, C., Ferro, V., & Mirabile, S. (2010). Comparison between grain-size analyses using laser diffraction and sedimentation methods. *Biosystems Engineering*, *106,* 205–215. 10.1016/j.biosystemseng.2010.03.013.

Hanák, K. (2001). *Soil mechanics with the foundation of buildings. Exercises*. MENDELU, Lesnická a dřevařská fakulta (in Slovak).

Igaz, D., Aydin, E., Šinkovičová, M., Šimanský, V., Tall, A., & Horák, J. (2020). Laser diffraction as an innovative alternative to standard pipette method for determination of soil texture classes in central Europe. *Water*, *12*(5), article number 1232. doi.org/10.3390/w12051232

Igaz, D., Kondrlová, E., Horák, J., Čimo, J., Tárník A., & Bárek V. (2017). *Basic measurements in hydropedology*. Slovak University of Agriculture in Nitra (in Slovak).

Malvern Instruments Ltd. (2013). *Mastersizer 3,000*. user manual.

Rejšek, K., & Vácha, R. (2018). *Nauka o půdě*. Agriprint.

Ryżak M., & Bieganowski A. (2010). Determination of particle size distribution of soil using laser diffraction – comparison with areometric method. *International Agrophysics*, *24*, 177–181.

Ševelová, L., Florian, A., & Hrůza, P. (2020). *Using Resilient Modulus to Determine the Subgrade Suitability for Forest Road Construction*. ID: forests-989232. doi: 10.3390/f11111208.

Šulcová, P., & Beneš, L. (2008). *Experimental methods in inorganic technology*. Univerzita Pardubice (in Czech).

Sławiński, C., Walczak, R. T., & Skierucha, W. (2006). Error analysis of water conductivity coefficient measurement by instantaneous profiles method. *International Agrophysics*, *20*, 55-61.

Taubner, H., Roth, B., & Tippkötter, R. (2009). Determination of soil texture: Comparison of the sedimentation method and the laser-diffraction analysis. *J. Pant Nutr. Soil Sci.*, *172*(2), 161–171. doi:10.1002/jpln.200800085.

Usowicz, B., Lipiec, J., & Usowicz, J. B. (2008). Thermal conductivity in relation to porosity and hardness to terrestrial porousmedia. *Planet. Space Sci.*, *56*, 438–447.

Walczak, R. T., Witkowska-Walczak, B., & Slawiński, C. (2004). *Development of Pedotrasfer Functions in Soil Hydrology* (1st ed). Elsevier Press.

Witkowska-Walczak B., Walczak R. T., & Slawiński C. (2002). Correlation model for water retention prediction with soil structure parameters. *Polish J. Soil Sci.*, *35*(1), 11–18.

Wlodarczyk, T., Stêpniewski, W., Brzezińska, M., & Przywara G. (2008). Impact of different aeration conditions on the content of extractable nutrients in soil. *International Agrophysics*, *22*, 371–375.

Yang, Y. Wang, L., Wendroth, O., Liu, B., Cheng, C., Huang, T., & Shi, Y. (2019). Is the Laser Diffraction Method Reliable for Soil Particle Size Distribution Analysis? *Soil Science Society of America Journal*. doi.org/10.2136/sssaj2018.07.0252

sciendo
Acta hort regiotec, 24, 2021(1): 56–62
DOI: 10.2478/ahr-2021-0024

Research Article

Erodible fraction content change in long term wind erosion duration

Lenka Lackóová[1]*, Jana Kozlovsky Dufková[2]
[1]*Slovak University of Agriculture in Nitra, Slovak Republic*
[2]*Mendel University in Brno, Czech Republic*

Article Details: Received: 2020-12-15 | Accepted: 2021-02-26 | Available online: 2021-05-31

Licensed under a Creative Commons Attribution 4.0 International License

SCREENED BY iThenticate® Professional Plagiarism Prevention

Soil erosion by wind is the primary land degradation process which affects natural environments and agricultural lands. In agricultural lands, soil erosion by wind mainly results from removing of the finest and most biologically active part of the soil richest in organic matter and nutrients. Repeated exposure to wind erosion can have permanent effects on agricultural soil degradation. Knowing spatial and temporal changes in soil conditions and soil erodibility is essential to understand wind erosion processes. There are many methodologies to predict the susceptibility of landscape to erosion. The more complex is the scheme combining multiple factors, the more accurate the estimate is. There are very few studies on mapping the changes in soil grain size and erodible fraction due to wind erosion. Existing studies only deal with eroded soil units (where particles are removed – deflation) and not the eroded units (areas) to which the eroded particles are wound – accumulated. Prevailing wind direction should also be taken into account when mapping changes in erodible fractions of wind-eroded soils and the nature of the soil (whether soil particles accumulate or deflate). In this study the "historical" grain size distribution of the soil in three cadastral areas using data from complex soil survey (1968) and year 2018/2019 was analysed. Erodible fraction change was also calculated and compared for both time periods.

Keywords: grain composition change, wind erosion, erodible fraction, accumulation zones

1 Introduction

Data dealing with the extent and severity of soil degradation by the erosion of wind across the whole Europe is minimal (Chappell & Warren, 2003). Recent EU projects studies (Wind Erosion on European Light Soils (WEELS) and Wind Erosion and Loss of Soil Nutrients in Semi-Arid Spain (WELSONS), Warren, 2003) indicate reasons that there may be more areas potentially threatened by wind erosion than foreseen by the European Environment Agency (EEA, 1998) in the past. Further studies have shown that areas previously identified as only slightly affected by wind erosion (EEA, 1998) are currently experiencing extensive erosive processes (Böhner et al., 2003; Gomes et al., 2003).

Inappropriate land use and landscape management, along with growing intensive crops, increasing mechanization, increasing the size of land areas, and removing shrubs, multiply the impact of wind erosion on Europe's most vulnerable agricultural areas (Warren, 2003; Riksen et al., 2003; Funk & Reuter, 2006). Muchová and Tárníková (2018) quantified the level of anthropogenic impacts on the landscape by detection, measuring, spatial localization, evaluation, and visualization of land use/land cover changes. To better understand the geographical distribution of erosion processes in Europe, in early 2014, the JRC proposed an integrated approach of mapping the susceptibility of soil to wind erosion (Borrelli et al., 2014). Erodible soil fraction (EF) (percentage of aggregates <0.84 mm in diameter) is one of the key parameters for estimating susceptibility of soil to wind erosion (Fryrear et al., 1994; Fryrear et al., 2000). The standard method for EF determination is the dry sieving by means of a rotary sieve. Fryrear et al. (1994) proposed a multiple regression equation for calculating EF in those cases where a rotary sieve is not available. This equation considers the contents of organic matter, sand, silt, clay, and calcium carbonate as predictive variables. The EF value (for the soil surface layer 0–20 cm) was calculated for 18,730 georeferenced samples in Europe (LUCAS data set).

The objective of this ongoing study was to analyse soil grain properties of the areas, where soil erosion causes

***Corresponding Author:** Lenka Lackóová, Slovak University of Agriculture in Nitra, Hospodárska 2, 949 76 Nitra, Slovakia; e-mail: lenka.lackoova @uniag.sk

accumulation of eroded material in long term duration. The results of this work point to the consequences of wind erosion in time (50 years).

2 Material and methods

For the assessment of soil erosion by wind, 3 cadastral areas (Borský Svätý Jur, Kuklov and Kúty) located in the Záhorská Lowland were selected. The Záhorská Lowland lies in the south – west of Slovakia and fills the area between the Morava River in the west and the Small Carpathians in the east. Nowadays, blowing sands present, alongside river deposits, one of the most important phenomena and relief elements of this area. The sands formed during the Pleistocene by wind activity in the Trnava region. The total selected area is 8,278.55 ha. To determine the potential wind erosion threats in the selected area (Fig. 1), the data on climate classification, grain size, and characteristics of the main soil units from the soil information system were used. In the selected cadastral areas, the acreage of no erosion in the 1st category is 11,556.42 ha (32.33%), middle erosion in the 2nd category 38,99 ha (0.81%), strong erosion in the, 3rd category 1,547.01 ha (32.13%), and strong erosion in the 4th category 1,670.99 ha (34.71%).

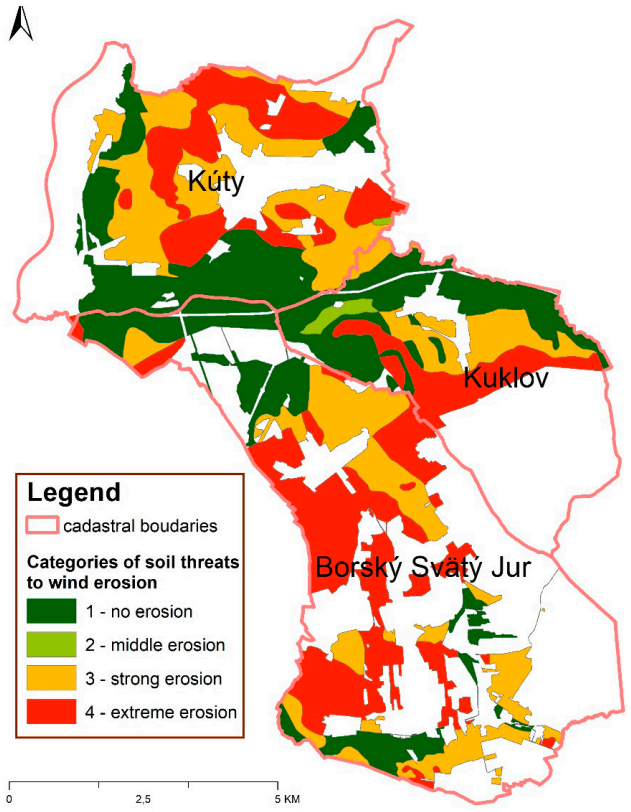

Figure 1 Categories of potential soil threats posed by wind erosion

2.1 Historical soil grain analysis

To analyse the "historical" grain size of the soil in the selected areas there were used electronic data from the Soil Complex Survey (SCS) (% content of sand, dust and clay) from years 1961–1970. Balkovič et al. (2010) created from the sand and clay content profile data at the A horizon spatial model of Slovakia (total 16, 264 georeferenced probes). The regression kriging was used for interpolation and was used as an explanatory variable including coded topsoil grain size from SCS core probes (158.478 georeferenced probes in total). The sand and clay distribution model was calculated for a 20m cell size grid. We used 39 sites (probes) in selected cadastral areas (Fig. 2).

The historical soil grain analysis showed that 43% of the arable soils consists of more than 90% of sand soil particles. 56% of the arable soils consists of less than 10% of clay soil particles.

To calculate erodible fraction of soils, a multiple regression equation developed by Fryrear et al. (1994) based on the soil's texture and chemical properties (Fryrear et al., 2000) was used:

$$EF = \frac{29.9 + 0.31S_a + 0.17S_i + 0.33S_c - 2.59OM - 0.95CaCO_3}{100} \quad (1)$$

where:
– all variables are expressed as a percentage; S_a – the soil sand content; S_i – the soil silt content; S_c – the ratio of sand to clay contents; OM – the organic matter content; $CaCO_3$ – the calcium carbonate content

2.2 Present soil grain analysis

Based on the data gained from SCS, all probes together with S-JTSK coordinates for 3 cadastral areas of interest were selected. Based on a well-defined location from SCS, the handheld GPS Trimble JUNO 3B and the software TopoL MOBILE were used directly in the field, to locate the site of the original SCS probe and took the sample from the soil surface (5 cm). A significant methodological problem associated with determining soil particle distribution is the preparation of soil samples. Kondrlová et al. (2012) discuss the derivation of a quick and simple sample preparation method for determining soil grain fractions by laser diffraction analysis using laser analyser ANALYSETTE 22 MicroTec plus.

During the field mapping, there were identified the locations (Fig. 3) where dust particles were accumulated during wind erosion events which led to a significant change in the soils´ grain composition.

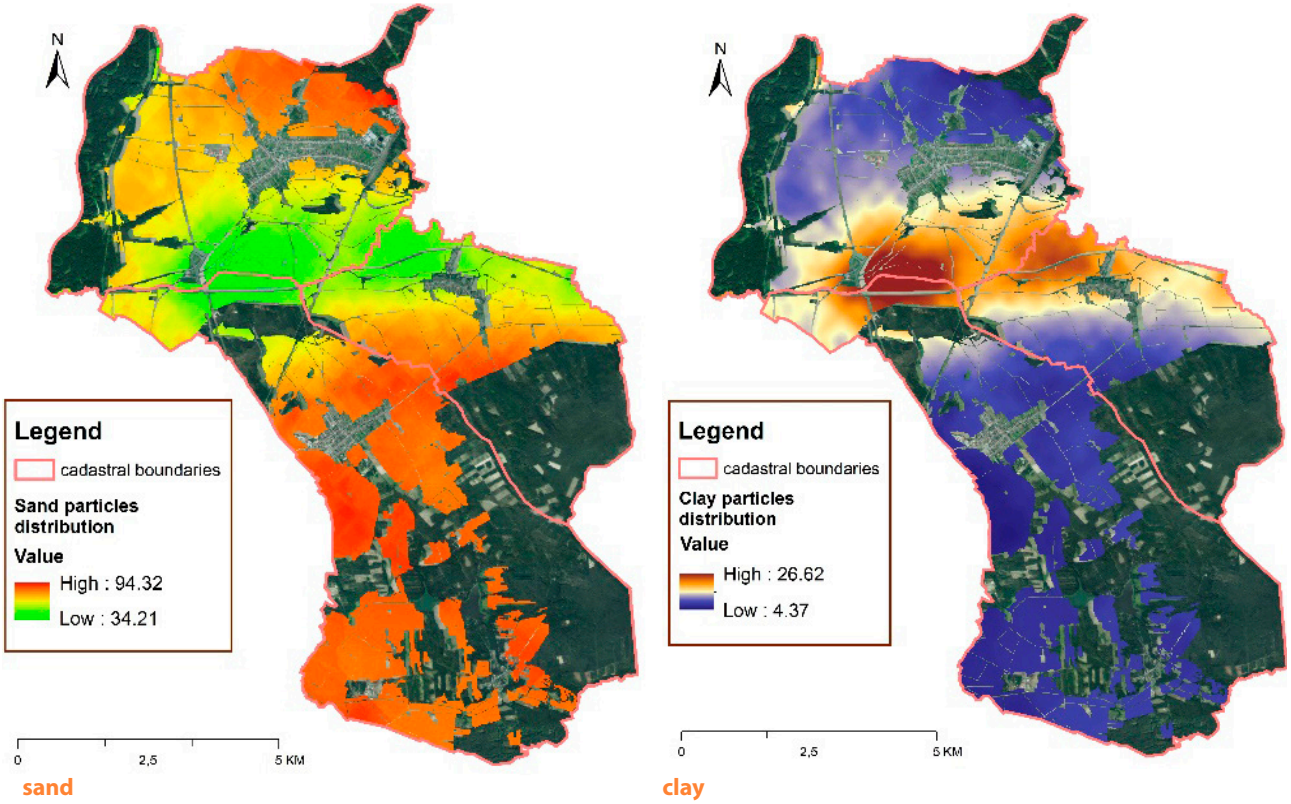

Figure 2 Soil particles distribution based on SCS

Figure 3 Accumulating locations of eroded particles in cadastral areas

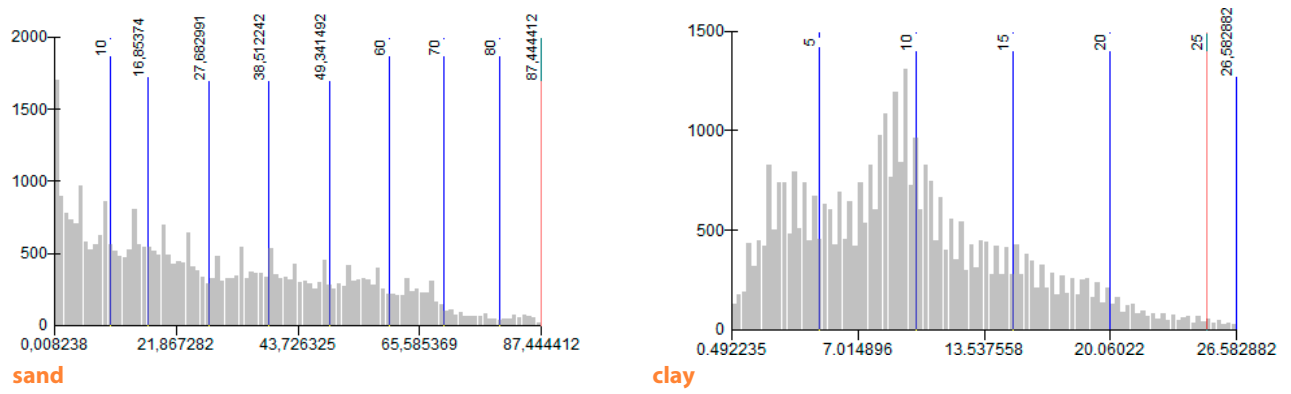

Figure 4 Histogram of grain distribution of present mapping

The histogram (Fig. 4) of measured (2018/2019) grain distribution for sand fraction shows that % distribution of sand content has rapidly decreased. 80% of the selected area has the sand content of up to 50%. Only 3% of the area is covered with the sand fraction content of more than 80%.

3 Results and discussion

The results show that the soil surface has become significantly rougher in 50 years only in a few places. However, in most areas of interest, the erosive phenomenon is manifested in the accumulation of a fraction of silt particles. Analysis of the change in the frequency of soil species occurrence in the monitored time horizon indicates a trend of growth of soil types with a significant proportion of dust particles (silt, silty loam). Sorting by erosion caused changes in soil textural class (Fig. 5). In 15 sites the soils described as loamy sands would now be described as 8× silty loams, 4× sandy loams, 2× silt, and 1× loam. The 17 sites have changed from sand to 12× sandy loam, 3× silty loam, 1× silt and loam. The 6 sites of sandy loams have changed to silty loams. In one case, sandy clay has changed to loamy sand.

Comparing the calculated EF for SCS and present mapping using the raster calculator, we obtained the erodible fraction change map over 50 years (Fig. 6). The erodible fraction values of data from SCS ranged from 28% to 62%, with a mean value of 56%. Erodible fraction of present measured data ranged from 20% to 59%, with a mean value of 49%. Comparing historical and present models, except one site, EF has decreased up to 28.4%. A mean value of EF decrease equals to 13.11%. From 39 sites, only in 2 sand content was higher in present mapping than during SCS (51.5% and 4.1%). The other 37 sites have lower sand content ranging from -20% up to -99%, average -59%. The clay content has increased in 18 sites (from 2.5% up to 68%) and decreased in 20 sites (-2.3% up to 88.3%). One site has not changed at all in clay content. The grates changes occurred in sandy, loamy sandy and sandy loam soils. The rapid increase was monitored in silt content in all sites (Fig. 7).

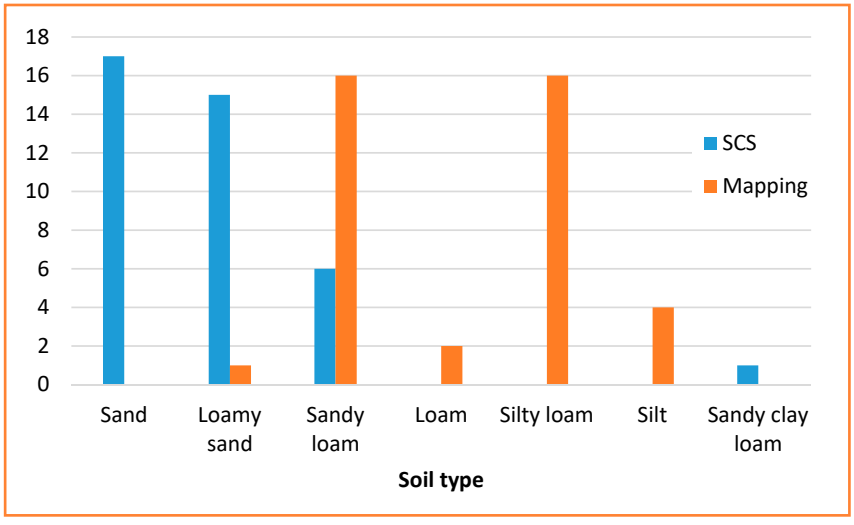

Figure 5 Soil type change between SCS and present mapping

The surface texture changed over the monitored period. Sand – size particles are generally too large to be suspended and transported long distances by wind. The reduction of sand particles does not mean that those were transported, but as the selected locations work as the accumulation zone for eroded particles, the silt and clay particles have been transported to this location over time.

The statistical dependence between SCS and present mapping using the correlation coefficient, which

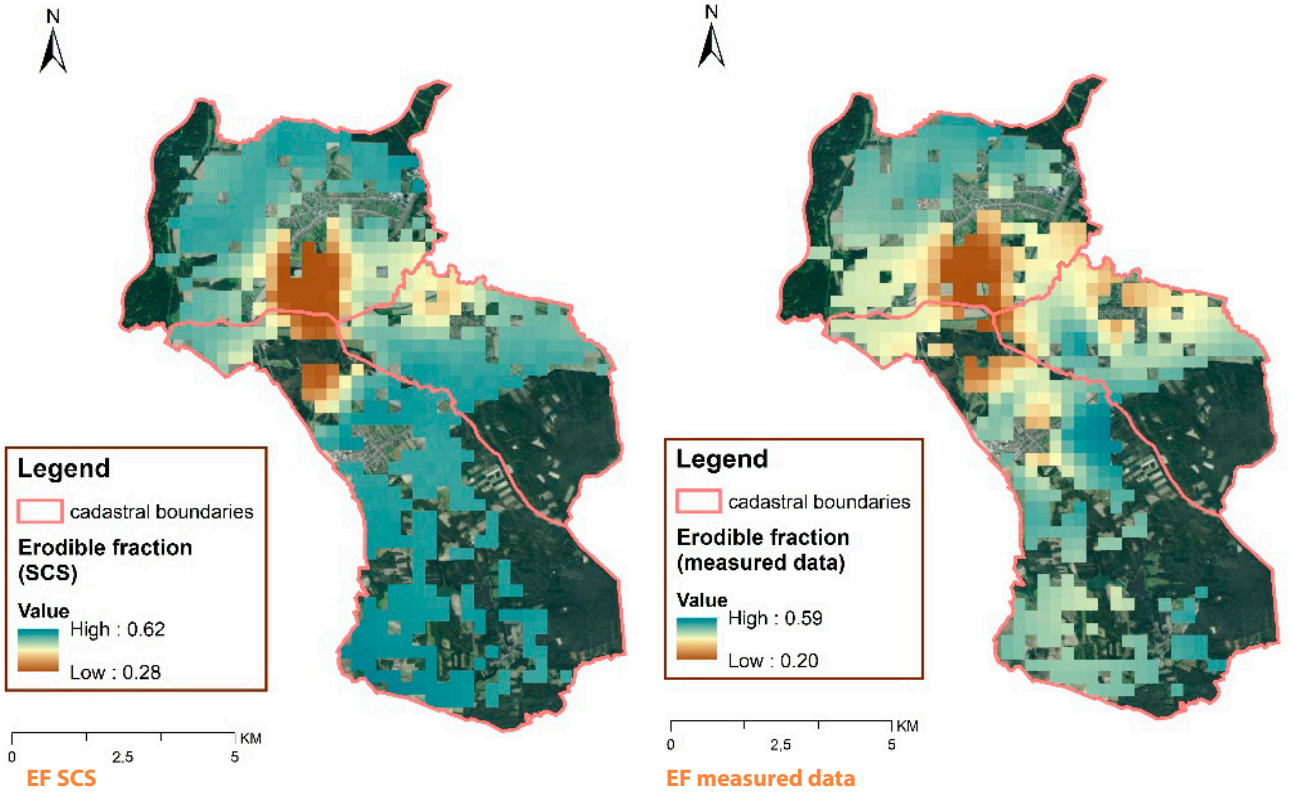

Figure 6 Map of Erodible fraction change over 50 years

measures the statistical linear relationship between the values of the variables *X* and *Y* was used. The correlation coefficient takes values from the interval <-1; +1>. In the case of independence between values of variables *X* and *Y*, correlation coefficient equals zero, there is no linear value between *X* and *Y* values dependence. Positive correlation coefficients indicate direct dependence and negative values correlate with indirect dependence. We modelled the dependence of values on a regression line. The results of the models explain the % of total variability change in grain size fraction. Correlation coefficients are very low and cannot be derived over time. The variance of the values is very high. This phenomenon explained that wind erosion not only acts in one direction (as a deflationary process) by taking away the finest particles, but also vice versa. These particles are taken from one place and transported to other sites, which act as accumulation areas in the long term.

Only a few studies have so far dealt with the quantitative linkage of the effects of wind erosion to analyse changes in grain fractions in the wind eroded soil layer. In this work, the effects of wind erosion on the soil surface due to particle size distribution (changes in sand content, silt, and clay fractions) over 50 years (1968 – data available from comprehensive soil survey and self-mapping and analysis (2018/2019) were investigated. A similar problem was analysed in the work of Li et al. (2007). They found

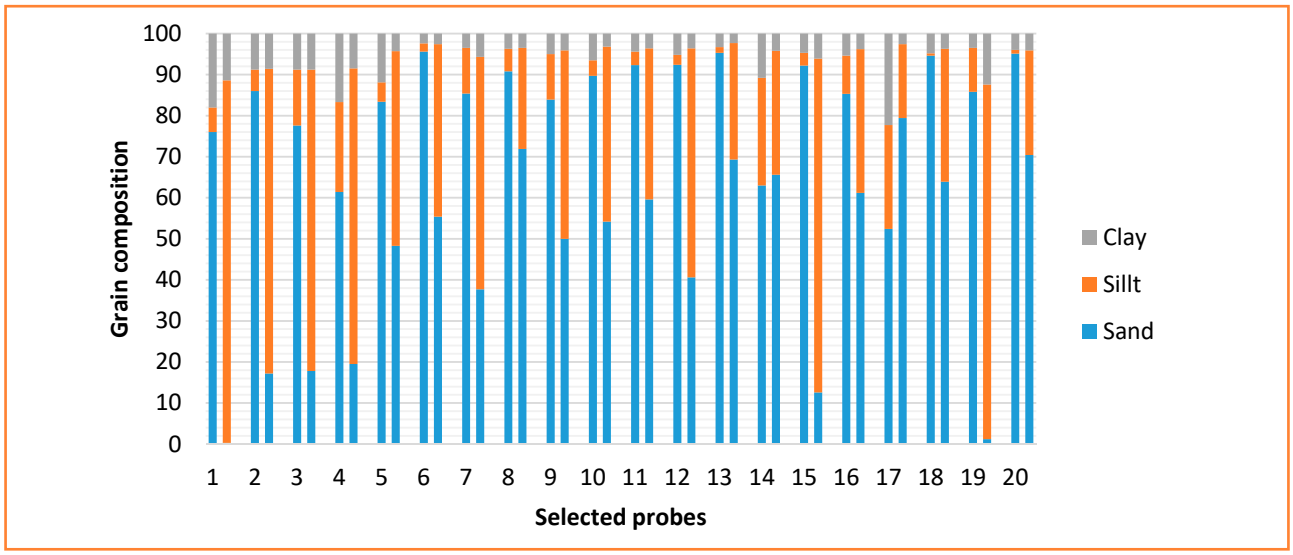

Figure 7 Comparison of grain composition in selected probes between SCS (1st line) and present mapping (2nd line of each probe)

that soil particles with a size of 250–500 μm increased significantly but decreased for particles 50–125 μm and <50 μm. Lyles and Tatarko (1986) show an example of the grain composition of agricultural soils. They compared changes in grain size composition in the top 10 cm layer at 10 sites in Kansas during the 36 years between 1948 and 1984. The proportion of the grain size fraction of sand increased in general. The most significant changes were experienced on medium sandy and sandy (coarse-grained) soils. Lyles and Tatarko (1986) found out that sand content increased over the 36 years due to wind erosion by 6,5% and reduced the silt content by 7.2%. Leys and McTainsh (1994) found out in their research that wind erosion caused increase in particles with a size >250 μm and decrease in particles with a diameter of 75–210 μm and <2 μm for 20 weeks. The process of wind erosion resulted in the effective removal of soil particles with a size of 50–125 μm (very fine sand) and <50 μm (silt and clay) during the 2 years of the experimental period. These observations suggest that fine soil particles were preferably carried away by increased wind erosion intensity (Li et al., 2007).

Comparison of SCS (1968) and present mapping (2018/2019) data revealed the opposite trend of the wind erosion phenomenon. There was a predominant decrease in sand particles´ content and increase silt and clay particles, which may be because it is a territory where transport prevails the finest particles and their accumulation at short distances from the erosion site. The distribution change in the particle size is evident in favour of the silt particle fraction.

4 Conclusions

Wind erosion selectively removes smaller and lighter particles, leaving coarser and denser particles behind. However, there are also locations where the eroded material is accumulated and changes the grain soil properties in favour of silt and clay particles. The objective of this study was to analyse soil grain properties of the areas where soil erosion causes accumulation of eroded material in long term duration. The results of this work point to the consequences of wind erosion in time (50 years). Continuous transport of soil particles during erosion phenomena can cause a dramatic change in soil composition. Authors dealing with this issue have analysed only areas where fine particles are carried away so far. There are also locations where the finest particles accumulate (whether in the windbreak area or forest edges or field inclinations). The results of this work clearly indicate a change in the grain composition of the eroded field. However, it has not been possible to get a trend of the dependence of this change over time yet.

Acknowledgement

This publication results from the project implementation: Scientific support of climate change adaptation in agriculture and mitigation of soil degradation, (ITMS2014+ 313011W580) supported by the Integrated Infrastructure Operational Programme funded by the ERDF.

References

Balkovič, J., Skalský, R., & Nováková, M. (2010). Spatial model of sand and clay distribution in topsoil of agricultural soils in Slovakia. In *Vedecké práce Výskumného ústavu pôdoznalectva*

a ochrany pôdy. Výskumný ústav pôdoznalectva a ochrany pôdy (in Slovak).

Borrelli, P., Panagos, P., Ballabio, C., Lugato, E., Weynants, M., & Montanarella, L. (2014). Towards a Pan-European Assessment of Land Susceptibility to Wind Erosion. *Land Degradation & Development*, *27*(4), 1093–1105. https://doi.org/10.1002/ldr.2318

Böhner, J., Schäfer, W., Conrad, O., Gross, J., & Ringeler, A. (2003). The WEELS model: methods, results and limitations. *Catena*, *52*(3–4), 289–308. https://doi.org/10.1016/s0341-8162(03)00019-5

European Environment Agency. (1998). *Europe's Environment*: The Second Assessment. Copenhagen.

Fryrear, D. W., Krammes, C. A., Williamson, D. L., & Zobeck, T. M. (1994). Computing the wind erodible fraction of soils. *Journal of Soil and Water Conservation*, *49*(2), 183+.

Fryrear, D. W., Bilbro, J. D., Saleh, A., Schomberg, H., Stout, J. E., & Zobeck, T. M. (2000). RWEQ: Improved Wind Erosion Technology. *Journal of Soil and Water Conservation*, *55*(2), 183.

Funk, R., & Reuter, H. I. (2006). Wind erosion. In J. Boardman, J., Poesen. (Eds), *Soil erosion in Europe* (pp. 563– 582). Wiley.

Gomes, L., Arrúe, J. L., López, M. V., Sterk, G., Richard, D., Gracia, R., Sabre, M., Gaudichet, A., & Frangi, J. P. (2003). Wind erosion in a semiarid agricultural area of Spain: the WELSONS project. *Catena*, *52*(3–4), 235–256. https://doi.org/10.1016/s0341-8162(03)00016-x

Chappell, A., & Warren, A. (2003). Spatial scales of 137Cs-derived soil flux by wind in a 25 km^2 arable area of eastern England. *Catena*, *52*(3–4), 209–234. https://doi.org/10.1016/s0341-8162(03)00015-8

Kondrlová, E., Igaz, D., Grešová, L., & Horák, J. (2012). Comparison of methods of soil samples preparation and methods of measurement of grain size fractions of distribution in Nitra River basin. *Acta Horticulturae et Regiotecturae*, *15*, 27–30 (in Slovak).

Leys, J. F., & McTainsh, G. H. (1994). Soil loss and nutrient decline by winderosion-cause for concern. *Aust. J. Soil Water Conserv.*, *7*(3), 30–40.

Li, J., Okin, G. S., Alvarez, L., & Epstein, H. (2007). Quantitative effects of vegetation cover on wind erosion and soil nutrient loss in a desert grassland of southern New Mexico, USA. *Biogeochemistry*, *85*(3), 317–332. https://doi.org/10.1007/s10533-007-9142-y

Lyles, L., & Tatarko, J. (1986). Plant response to topsoil thickness, and to fertilizer on an eroded loess soil. *J. Soil Water Cons.*, *41*, 59–63.

Muchová, Z., & Tárníková, M. (2018). Land cover change and its influence on the assessment of the ecological stability. *Applied Ecology and Environmental Research*, *16*(3), 5169–5182. https://doi.org/10.15666/aeer/1603_21692182

Riksen, M., Brouwer, F., Spaan, W., Arue, J. L., & Lopez, M. V. (2003). What to do about wind erosion. In A. Warren (Ed.), *Wind erosion on agricultural land in Europe, EC, Directorate-General for Research* (pp. 39–52).

Warren, A. (2003). *Wind erosion on agricultural land in Europe: research results for land managers.* Office for Official Publications of the European Communities.

sciendo

DOI: 10.2478/ahr-2021-0025
Acta hort regiotec, 24, 2021(1): 63–70

Research Article

Using the equation for computing the wind erodible fraction of soils in the conditions of the Czech republic

Jana Kozlovsky Dufková*, Vít Procházka, Jan Szturc, Tomáš Mašíček
Mendel University in Brno, Czech Republic

Article Details: Received: 2020-12-15 | Accepted: 2021-02-26 | Available online: 2021-05-31

Licensed under a Creative Commons Attribution 4.0 International License

SCREENED BY iThenticate® Professional Plagiarism Prevention

The erodible fraction (EF) of soil (soil aggregates and particles <0.84 mm) is one of the basic factors according to which the susceptibility of soil to wind erosion can be assessed. The standard method for determining the EF content is the use of a rotary sieve. Nevertheless, its availability is limited by its price and the fact that it is not mass-produced and is necessary to build the sieve to order. An alternative method of determining the EF content is to use an equation based on knowledge of the content of sand, silt, clay, organic carbon, and calcium carbonate. However, this equation has only been tested for US conditions. Therefore, the research focuses on the validation of the equation for the conditions of the Czech Republic, specifically in the territory of Southern Moravia. The results show that the equation validated for the USA cannot be used to determine the EF content in soils of the Czech Republic. Using the statistical program Unistat©, a new equation was proposed with correlation coefficient R = 0.8238 which means good applicability of the equation for the local soils at least in the area of Southern Moravia.

Keywords: erodible fraction, main soil unit, particle size distribution, multiple regression analysis

1 Introduction

The soil is composed of an erodible and a non-erodible soil fraction. The erodible fraction (EF) of the soil easily gets moving due to the wind, while the non-erodible fraction remains practically at rest. The amount of soil transported by wind depends on the ratio of erodible and non-erodible fraction in the surface layer of the soil (Woodruff & Siddoway, 1965). Non-erodible aggregates stand out into the turbulent layer of the air flow, cause greater soil surface roughness, absorb much of the wind energy, and thus protect erodible fraction (Webb & Strong, 2011). The degree of soil erodibility is thus given by the ratio of erodible and non-erodible soil fraction, which was expressed by Chepil (1950) by the value of the soil erodibility factor. The limit size of soil particles, which get moving by the wind, is called the soil erodibility limit or critical minimum (Pasák, 1970). Chepil (1950) further states that relatively few soil particles larger than 0.5 mm become moving by the action of the wind. Based on a wind tunnel research, he set the boundary between erodible and non-erodible soil fraction at 0.84 mm. Pasák (1970) reached the same limit by laboratory measurements in a wind tunnel.

EF can be determined by aggregate analysis. Chepil (1942, 1952, 1962), Chepil and Basil (1943), and Lyles et al. (1970) describe in their works an aggregate analysis using a rotary sieve. It is a device with a nest of sieves placed one behind the other, which, in addition to sifting the soil sample, simulates the abrasion of soil aggregates, which occurs when the aggregates are carried by the wind. However, according to the research of many authors (Kemper & Rosenau, 1986; Kettler et al., 2001; López et al., 2001; López et al., 2007), the availability of the rotary sieve is limited both by its price and by the fact that it is not mass-produced, and it is necessary to build the sieve to order. For this reason, an alternative method for determining individual size categories of soil particles/aggregates was searched. Toogood (1978) modified the method of aggregate analysis so that it could be possible to use flat sieves, or nests of sieves. López et al. (2007) used a standard rotary sieve and a nest of sieves for aggregate analysis, which he placed on an electromagnetic (vibrating) shaker. The comparison of

***Corresponding Author:** Jana Kozlovsky Dufková, Mendel university in Brno, Faculty of AgriSciences, Department of Applied and Landscape Ecology, Zemědělská 1, 613 00 Brno, Czech republic, ☎ +420 545 132 472; e-mail: jana.dufkova@mendelu.cz

both techniques showed that the EF values obtained with the flat sieve were valid and comparable with those obtained using the rotary sieve, and flat sieving can be considered as a suitable alternative to the rotary sieve.

In 1994, Fryrear et al. suggested a different method of determining the wind EF, using a computational model based only on the physical and chemical properties of the soils. Despite the fact that this model is validated only for soil conditions in the USA, it is also used by authors in other areas – e.g. for the Sahelian zone of Africa (Visser et al., 2005), for China (Du et al., 2015), for Europe (Borelli et al., 2016) or for Slovakia (Lackóová, 2016). López et al. (2007) used the Fryrear`s equation (1994) to determine EF in the semiarid regions of Central Aragon (Spain) and the semiarid Pampas (Argentina) and found that the equation could not be used here. Similar conclusions were reached by Guo et al. (2017), who used the equation to determine the EF content in the agro-pastoral ecotone of northern China.

The purpose of this research is to verify whether the equation according to Fryrear et al. (1994) is applicable for determination of the EF content in the conditions of the Czech Republic and if not, to create a new equation that would meet the needs of local conditions.

2 Material and methods

Soil samples for the determination of EF content were taken from ten different main soil units, which, according to the map of potential threat of arable land by wind erosion, that was made by the Research Institute for Soil and Water Conservation (RISWC) (2020), are the most susceptible to wind erosion (Table 1). These were mainly soils located in the south-eastern part of the Czech Republic (Southern Moravia) (Fig. 1).

The main soil unit (MSU) is defined as a synthetic agronomized unit characterized by a purposeful (agronomic) grouping of genetic soil types, subtypes, soil-forming substrates, texture, soil depth, type and degree of hydromorphism, and land relief. The classification system represents 78 MSU (RISWC, 2020). MSU is a part of an evaluated soil-ecological unit.

The evaluated soil-ecological unit (ESEU) consists of a 5-digit numerical code, which expresses the climatic region, the main soil unit, the slope of the land and its orientation to the cardinal points, the soil profile depth, and soil stoniness (RISWC, 2020).

Soil samples of about 5,000 g each were collected with a squared-end shovel from surface layer of the arable land (0 to 25 mm soil depth) (Pansu et al., 2001; Paetz & Wilke, 2005) cultivated by conventional farming in spring 2020. The types of crops grown at individual sampling points are given in the Table 1.

Air-dried soil samples were subject of the grain size distribution (GSD). GSD is used to determine the stability of soil aggregates, to divide the soil sample into individual soil size categories using a nest of sieves and can be performed either dry or wet (McKenzie et al., 2002). For the assessment of EF content, it is recommended to use the dry method, also called the dry aggregate size distribution (DASD) (Zobeck et al., 2003; Chandler et al.,

Table 1 Basic data from sampling sites

Sample	MSU	Soil taxonomy (FAO)	Latitude	Longitude	Altitude (m)	Management
1	01	Chernozems modal	48.927 N	17.119 E	228	triticale (Triticosecale)
2	04	Chernozems arenic	48.926 N	17.112 E	215	winter wheat (*Triticum aestivum*)
3	05	Chernozems modal	48.829 N	16.944 E	186	winter wheat (*Triticum aestivum*)
4	21	Regosols arenic	48.997 N	17.322 E	190	spring barley (*Hordeum vulgare*)
5	22	Cambisols modal	49.054 N	17.394 E	185	spring barley (*Hordeum vulgare*)
6	30	Cambisols modal	49.513 N	16.623 E	356	spring barley (*Hordeum vulgare*)
7	31	Cambisols arenic	49.512 N	16.591 E	363	spring barley (*Hordeum vulgare*)
8	55	Fluvisols psephitic	48.977 N	17.230 E	189	sunflower (*Helianthus annuus*)
9	56	Fluvisols modal	48.953 N	17.081 E	172	maize (*Zea mays*)
10	58	Fluvisols gleyic	48.996 N	16.356 E	277	maize (*Zea mays*)

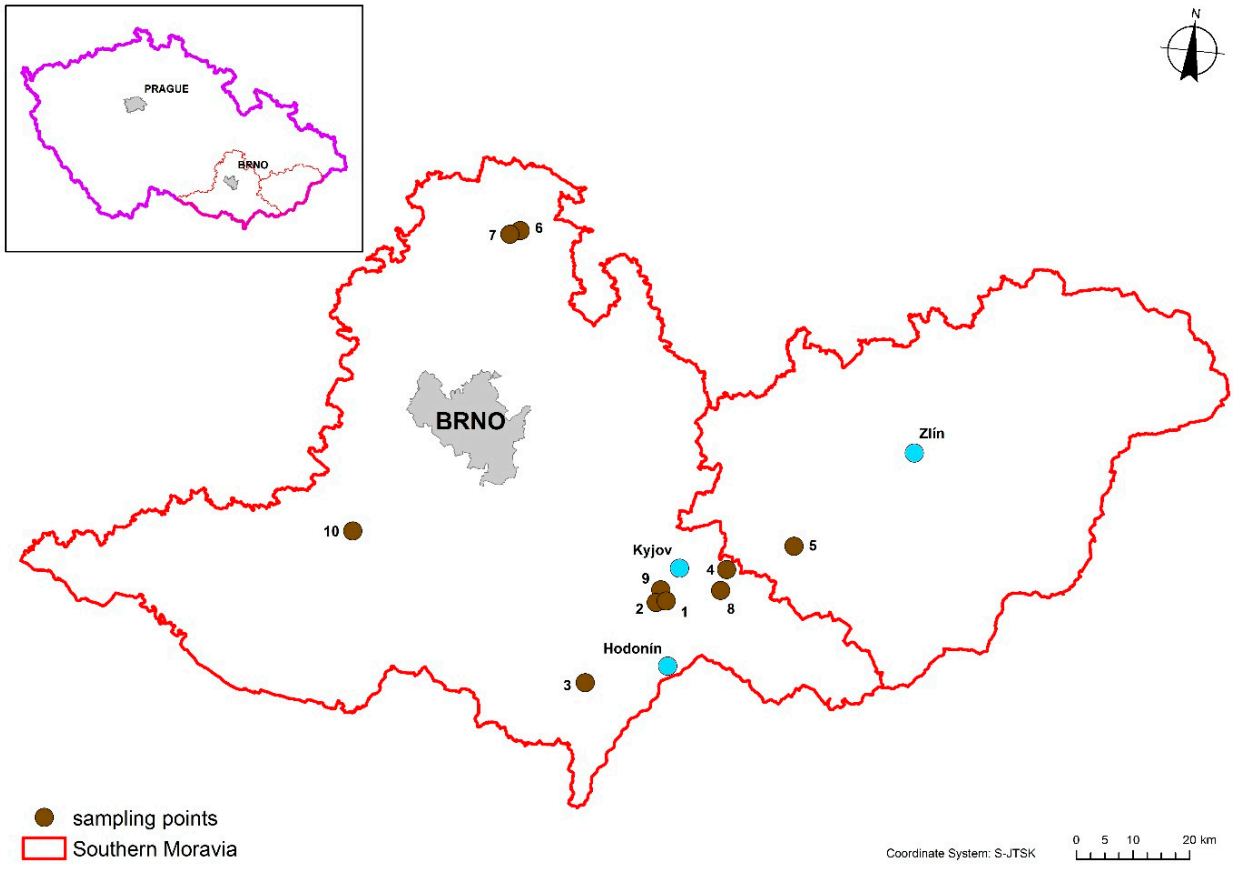

Figure 1 Location of soil sampling points in the territory of Southern Moravia
Source data: Borders of the state, region – © ARCDATA PRAHA, s.r.o., Surveying Office and Czech Statistical Office

2005; Larney, 2008). The use of the wet method leads, according to Marsquez et al. (2004) or Saygin et al. (2012), to intensive disruption of soil aggregates. DASD is one of the primary factors affecting soil susceptibility to wind erosion (Skidmore et al., 1994).

Flat sieves with opening of 2 mm a 0.8 mm were used to obtain the DASD. To eliminate operation error of manual sieving (Diaz-Zorita et al., 2007), electromagnetic sieve shaker (AS 200 Retsch) was used. López et al. (2007) recommends a sieving time of 5 min and an amplitude of 0.1 mm for 100–200 g undisturbed soil mass. After sieving, the amount of EF sieved through the 0.8 mm sieve openings was weighed and the percentage of EF was calculated.

Equation (1) according to Fryrear et al. (1994) can be also used for calculation of EF content (%). It is necessary to know content of sand (S, %), content of silt (I, %), content of clay (C, %), content of organic carbon (OC, %), and content of $CaCO_3$ (CC, %):

$$EF = \frac{29.09 + 0.315 + 0.171 + 0.33\frac{S}{C} - 4.66OC - 0.95CC}{100} \quad (1)$$

$R^2 = 0.67$

Percentage content of sand (0.05–2 mm), silt (0.002–0.05 mm), and clay (<0.002 mm) was determined through particle size distribution (PSD) using PARIO© (Fig. 2). PARIO© is an automated system for the PSD of soils and sediments. The device derives the PSD from the pressure decrease at a measuring depth in a suspension. The theory of the method is published by Durner et al. (2017) and procedure for the sample preparation and analysis can be found in the PARIO© user manual (METERGROUP, 2020). The sedimentation methodology is based on the Stokes' law. PARIO© automatically measures at the interval of ten seconds and continuously records the change of suspension pressure as well as the temperature. This results in highly accurate and continuous PSD curves (METERGROUP, 2020).

Organic carbon content was determined with chromic acid titration procedure (Walkley & Black, 1934), and carbonate content ($CaCO_3$) was determined by a calcimeter. The calcimeter works in accordance with the method of Scheibler, which involves the determination of carbonate content in soil based on the volumetric method (Allison & Moodie, 1965).

Statistical analyses for validation of the Eq. (1) for the conditions of the Czech Republic, as well as other

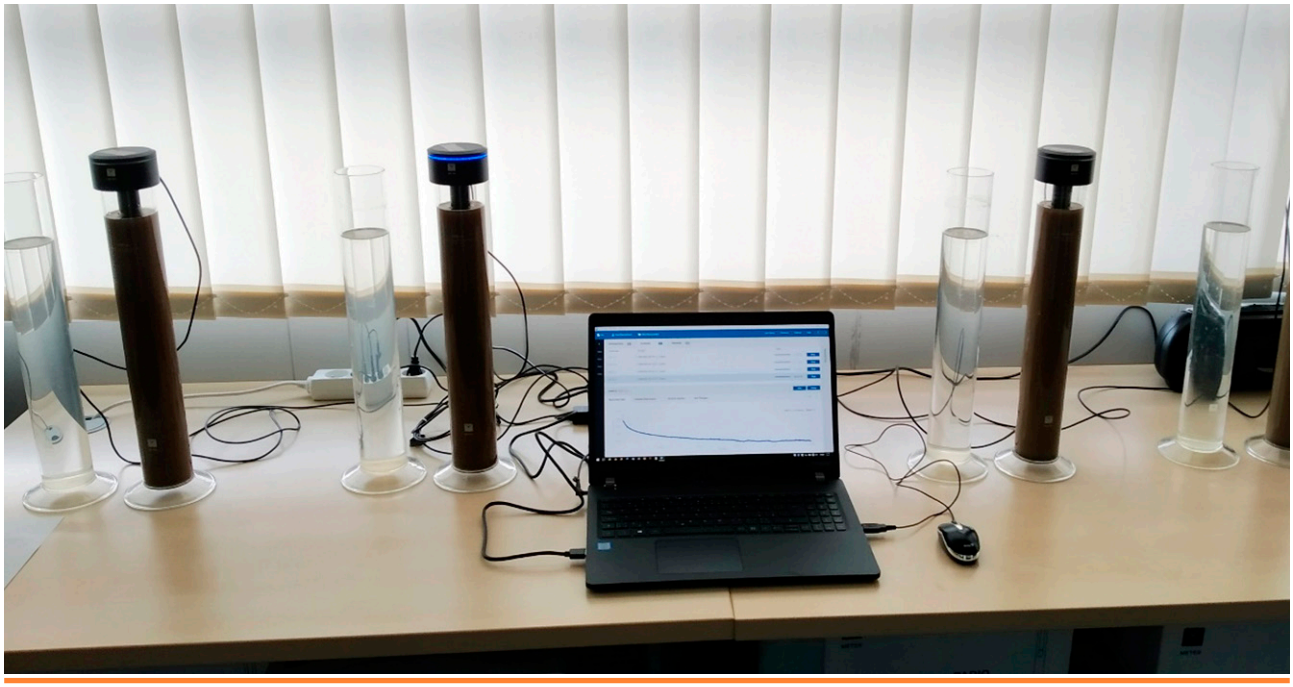

Figure 2 PARIO© devices for automatic determination of particle size distribution of analysed soil samples

statistical analyses, were performer by using the Unistat© Statistics Software (UNISTAT Ltd.).

3 Results and discussion

The results of DASD and PSD analyses are given in the Table 2. The EF content sieved through the 0.8 mm sieve openings (EF-sieve) ranges from 43.14% to 72.28%. According to the erosion classification given by Zachar (1982), nine samples are very erodible because all these soil samples exceed 50% of the EF content. The EF content calculated according to Eq. (1) (EF-equation) ranges from 33.97 to 47.48%.

The relationship between EF-sieve and EF-equation is shown in Fig. 3. The correlation coefficient takes on value 0.5679 (p-value <0.005). According to the statistical analyses, the Eq. (1) underestimates the results by 45% on average.

Used statistical analyses (two-sample F-test for variance and two-sample t-test with equality of variances) show that the content of EF-sieve and EF-equation differ statistically significantly from 95%. It follows that the Eq. (1) cannot be used to calculate the EF content for the soils of the Czech Republic, at least not for the samples analysed.

The reason is probably the lower content of $CaCO_3$ in the Czech soils because other factors entering the Eq. (1) have approximately the same values for soils in the Czech Republic and the soils in the USA for which Eq. (1) was

Table 2 Results of pedological analyses of soil samples

Sample	Sand (%)	Silt (%)	Clay (%)	Organic carbon (%)	$CaCO_3$ (%)	EF-sieve (%)	EF-equation (%)
1	14.04	55.02	30.94	1.10	0.10	60.17	37.72
2	65.32	24.32	10.36	1.70	0.16	68.33	47.48
3	52.36	29.20	18.44	1.83	0.05	71.47	42.65
4	54.64	28.14	17.22	2.32	0	72.28	41.05
5	39.02	37.70	23.28	1.69	0	56.54	40.27
6	35.62	47.00	17.38	1.73	0	58.11	40.74
7	33.08	46.60	20.32	1.38	0.10	57.73	41.28
8	46.28	39.16	14.56	0.97	0	57.07	46.62
9	21.66	57.82	20.52	1.02	0	53.46	41.23
10	33.94	27.58	38.48	2.28	0	43.14	33.97

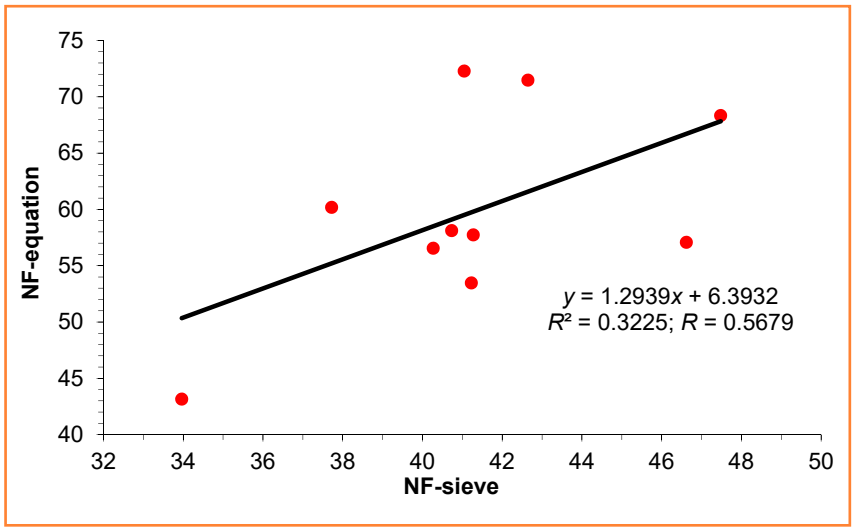

Figure 3 Relationship between EF content measured by sieving (EF-sieve) and calculated from equation (EF-equation)

tested. The range of soil properties for the USA and Czech soils is given in the Table 3.

Another reason for underestimating the EF calculation could be the term of soil sampling. In spring, soil is more susceptible to loss by wind due to the disruption of soil aggregates caused by low temperatures during winter. A larger amount of EF can be found in the surface layer of the soil and, as Kozlovsky Dufková (2010) states, in the area of Southern Moravia this problem occurs every year as a result of the freeze and drying process and the freeze-thawing process.

According to some authors (e.g. Skidmore & Layton, 1992; Tatarko, 2001; Šimanský et al., 2013), the intensity of soil aggregates disruption caused by freeze is also affected by the content of organic matter and $CaCO_3$ in the soil. Lehrsch et al. (1991) reports that soils with a high content of organic matter increase their stability when frozen. The positive effect of organic matter on the stability of soil aggregates is also mentioned by Kavdir et al. (2004) or Arthur et al. (2013). Colazo and Buschiazzo (2010) report that increasing the $CaCO_3$ content in soil up to 5 $g.kg^{-1}$ has the effect on increasing the EF content. If there is more $CaCO_3$ in the soil than this limit, the EF content decreases due to the formation of secondary aggregates. According to Chepil (1954), a 3% $CaCO_3$ content in the soil has no effect on aggregate stability, but an increase in the $CaCO_3$ content to 10% or more will result in an increase in stability. However, the author notes that the mentioned effect is visible only in light soils. Lehrsch et al. (1993) report that the content of 0–4% $CaCO_3$ in soils with a higher content of clay particles increases the stability of soil aggregates but increasing the $CaCO_3$ content to 4–32% increases the content of EF in the soil.

EF content is also influenced by management. Overwinter breakdown of soil aggregates leads to a higher EF content especially after conventionally tilled fallow, which leaves low crop residue or bare soils. Bullock et al. (2001) point out to the fragility of zero tillage soils once the protective layer of surface residue is removed. Soils that were cultivated after several years of zero tillage, were not erodible in autumn, but they were not resilient to overwinter processes, and became susceptible to wind erosion in spring. Conventional tillage forms soil clods and leads to soil aggregate clustering

Table 3 Comparison of soil properties entering Eq. (1) (Fryrear et al., 1994) in the USA and the Czech Republic

Content of (%)	US soils	Analysed soils of the CR
Sand	5.5–93.6	14.0–65.3
Silt	0.5–69.5	24.3–57.8
Clay	5.0–39.3	10.4–38.5
Organic carbon	0.1–2.7	1.0–2.3
$CaCO_3$	0–25.2	0–0.2
SC ratio (sand/clay content)	1.2–53.0	0.5–6.3
EF measured (EF-sieve)	9.0–86.0	43.1–72.3
EF calculated (EF-equation)	7.7–82.3	34.0–47.5
Coefficient of determination (R^2)	0.67	0.32
Mean of measured EF	47.5	59.8
Standard deviation of measured EF	13.4	8.9

Table 4 Matrix of correlation coefficients from different soil properties

	EF-sieve	Sand	Silt	Organic carbon	$CaCO_3$	SC ratio*
EF-sieve	1.0000					
Sand	-0.6977	1.0000				
Silt	-0.9803	0.6401	1.0000			
Organic carbon	-0.5958	-0.0887	0.5728	1.0000		
$CaCO_3$	-0.4166	0.6022	0.3377	0.0286	1.0000	
SC ratio*	0.4181	-0.9088	-0.3451	0.2856	-0.6786	1.0000

*SC ratio – the ratio between sand and clay; clay was omitted due to multicollinearity; significant at P <0.05

which means better resistance to wind erosion (Zobeck et al., 2003). Negative effect of tillage, disk harrow or other cultivation that leads to the disruption of soil aggregates, is evident only within dry soils. Clods are forming during cultivation of wet soil and thus it leads into the decrease of susceptibility to wind erosion (Fryrear et al., 1994).

The correlation analyses were performed between EF-sieve and different soil properties and a correlation matrix was created (Table 4). One factor entering the correlation analysis (clay) was omitted from the correlation matrix due to multicollinearity. It is a strong correlation between the explanatory (independent) variables in which the least squares method cannot be used due to too large estimates of standard errors of regression parameters or too wide confidence intervals. In practice, multicollinearity means that one of the pair of explanatory variables that are strongly interdependent is extra in the model and should be eliminated (Chatterjee et al., 2000).

The Table 4 shows that all soil properties are correlated significantly with EF-sieve. The strongest relations can be found with silt and sand (both negative correlation), weaker relationship with organic carbon, $CaCO_3$ (also negative), and SC ratio (the only positive correlation).

Using multiple regression analysis, a new equation (2) was created with help of the statistical program Unistat©, and it should be able to determine the content of EF in the analysed soils:

$$EF = -40.20 + 1.44S + 1.08I - 5.40\frac{S}{C} + 6.13OC + 84.17CC \quad (2)$$

where:
R = 0.8238 (R^2 = 0.6786) with significance at P <0.001 and EF – calculated content of erodible particles (%); S – content of sand (%); I – content of silt (%); C – content of clay (%); OC – content of organic carbon (%); CC – content of $CaCO_3$ (%)

The amount of analysed soil samples for validation of the Fryrear`s equation (1) for the conditions of the Czech Republic is relatively small. Fryrear et al. (1994) used more than 3000 samples to identify the relationship between EF and physical and chemical properties of soils in the USA. López et al. (2007) used 27 soil samples from Spain and Argentina to validate the Eq. (1) for his conditions, and Guo et al. (2017) used 74 soil samples to establish a new equation that meets the requirements of the conditions of northern China.

For this reason, it will be necessary to carry out further research, ideally to take soil samples from all MSU, so that the equation can be further specified and used universally for all soils in the Czech Republic.

4 Conclusions

Soil samples from 10 sites of the Czech Republic were used for validation of the Fryrear`s equation (1994) for calculation of EF content. Sand, silt, clay, organic carbon, and $CaCO_3$ content were the input parameters which the equation was compiled from. Statistical analyses found out that the Fryrear`s equation (1994) is not applicable to soils in the Czech Republic because it underestimates the results by 45%. New equation was proposed with value of the correlation coefficient R = 0.8238 which means good applicability of the equation for the local soils. For wider use of the equation, it would be appropriate to extend statistical analyses to other soils of the Czech Republic.

References

Allison, L. E., & Moodie, C. D. (1965). Carbonate. In A. G. Norman (Ed.), *Methods of soil analysis: Part 2 Chemical and microbiological properties* (pp. 1379–1396). American Society of Agronomy.

Arthur, E., Schjønning, P., Moldrup, P., Tuller, M., & de Jonge, L. W. (2013). Density and permeability of a loess soil: long-term organic matter effect and the response to compressive stress. *Geoderma*, *193–194*, 236–245.

Borrelli, P., Panagos, P., Ballabio, C., Lugato, E., Weynants, M., & Montanarella, L. (2016). Towards a pan-European assessment of land susceptibility to wind erosion. *Land Degrad. Dev.*, *27*, 1093–1105.

Bullock, M. S., Larney, F. J., Izaurralde, R. C., & Feng, Y. (2001). Overwinter changes in wind erodibility of clay loam soils in southern Alberta. *Soil Science Society of America Journal*, *65*, 423–430.

Chandler, D. G., Saxton, K. E., & Busacca, A. J. (2005). Predicting wind erodibility of loessial soils in the Pacific Northwest by particle sizing. *Arid Land Research and Management*, *19*(1), 13–27.

Chatterjee, S., Hadi, A. S., & Price, B. (2000). *Regression analysis by example.* John Wiley and Sons.

Chepil, W. S. (1942). Measurement of wind erosiveness of soils by dry sieving procedures. *Canadian Journal of Agricultural Sciences*, *23*, 154–160.

Chepil, W. S. (1950). Properties of soil which influence wind erosion: II. Dry agregate structure as an index of erodibility. *Soil Science*, *69*, 403–414.

Chepil, W. S. (1952). Improved rotary sieve for measuring state and stability of dry soil structure. *Soil Science Society of America Proceedings*, *16*(2), 113–117.

Chepil, W. S. (1954). Factors that influence clod structure and erodibility of soil by wind III. Calcium carbonate and decomposed organic matter. *Soil Science*, *77*, 473–480.

Chepil, W. S. (1962). A compact rotary sieve and the importance of dry sieving in physical soil analysis. *Soil Science Society of America Journal*, *26*(1), 4–6.

Chepil, W. S., & Basil, F. (1943). A rotary sieve method for determining the size distribution of soil clods. *Soil Science*, *56*(2), 95–100.

Colazo, J. C., & Buschiazzo, D. E. (2010). Soil dry aggregate stability and wind erodible fraction in a semiarid environment of Argentina. *Geoderma*, *159*, 228–236.

Diaz-Zorita, M., Grove, J. H., & Perfect, E. (2007). Sieving duration and sieve loading impacts on dry soil fragment size distributions. *Soil Tillage Res.*, *94*, 15–20.

Du, H., Xue, X., Wang, T., & Deng, X. (2015). Assessment of wind-erosion risk in the watershed of the Ningxia-Inner Mongolia Reach of the Yellow River, northern China. *Aeolian Res., 17*, 193–204.

Durner, W., Iden, S. C., & von Unold, G. (2017). The integral suspension pressure method (ISP) for precise particle-size analysis by gravitational sedimentation. *Water Resources Research*, *53*(1), 33–48. https://doi.org/10.1002/2016WR019830

Fryrear, D. W., Krammes, C. A., Williamson, D. L., & Zobeck, T. M. (1994). Computing the wind erodible fraction of soils. *Journal of Soil and Water Conservation*, *49*(2), 183–188.

Guo, Z., Chang, Ch., Wang, R., & Li, R. (2017). Comparison of different methods to determine wind-erodible fraction of soil with rock fragments under different tillage/management. *Soil & Tillage Research*, *168*, 42–49. https://doi.org/10.1016/j.still.2016.12.008

Kavdir, Y., Özcan, H., Ekinci, H., & Yigini, Y. (2004). The influence of clay content, organic carbon, and land use types on soil aggregate stability and tensile strength. *Turkish Journal of Agriculture*, *28*, 155–162.

Kemper, W. D., & Rosenau, R. C. (1986). Aggregate stability and size distribution. In A. Klute (Ed.), *Methods of soil analysis: Part I. Physical and mineralogical methods* (2nd ed., pp. 425–442). American Society of Agronomy.

Kettler, T. A., Doran, J. W., & Gilbert, T. L. (2001). Simplified method for soil particle-size determination to accompany soil-quality analyses. *Soil Science Society of America Journal*, *65*, 849–852.

Kozlovsky Dufková, J. (2010). Laboratory analyses of overwinter processes influence on wind erosion. *Meteorological Journal*, *13*(2–3), 63–67.

Lackóová, L. (2016). *Mapovanie zmien zrnitostných frakcií piesočnatých pôd vplyvom veternej erózie v krajine* [Habilitation work]. Slovak University of Agriculture in Nitra.

Larney, F. J. (2008). Dry-aggregate size distribution. In M. R. Carter & E. G. Gregorich (Eds.), *Soil sampling and methods of analysis* (pp. 821–832). Taylor & Francis Group.

Lehrsch, G. A., Sojka, R. E., Carter, D. L., & Jolley, P. M. (1991). Freezing effects on aggregate stability affected by texture, mineralogy, and organic matter. *Soil Science Society of America Journal*, *55*, 1401–1406.

Lehrsch, G. A., Sojka, R. E., & Jolley, P. M. (1993). Freezing effects on aggregate stability of soils amended with lime and gypsum. *Catena*, *24*, 115–127.

López, M. V., De Dios Herrero, J. M., Hevia, G. G., Gracia, R., & Buschiazzo, D. E. (2007). Determination of the wind-erodible fraction of soils using different methodologies. *Geoderma*, *139*, 407–411.

López, M. V., Gracia, R., & Arrue, J. L. (2001). An evaluation of wind erosion hazard in fallow lands of semiarid Aragon (NE Spain). *Journal of Soil and Water Conservation*, *56*, 212–219.

Lyles, L., Dickerson. J. D., & Disrud, L. A. (1970). Modified rotary sieve for improved accuracy. *Soil Science*, *109*(3), 207–210.

Marquez, C. O., Garcia, V. J., Cambardella, C. A., Schultz, R. C., & Isenhart, T. M. (2004). Aggregate-size stability distribution and soil stability. *Soil Science Society of America Journal*, *68*(3), 725–735.

Mckenzie, N., Coughlan, K., & Creswell, H. (2002). *Soil physical measurement and interpretation for land evaluation*. CSIRO Publishing.

METERGROUP (2020, December 5). *Automated particle size analysis PARIO©*. https://www.metergroup.com/environment/products/pario/

Paetz, A., & Wilke, B. M. (2005). Soil sampling and storage. In R. Margesin, & F. Schinner (Eds.), *Manual for soil analysis: Monitoring and assessing soil bioremediation* (pp. 1–46). Springer-Verlag.

Pansu, M., Gautheyrou, J., & Loyer, J. Y. (2001). *Soil analysis: Sampling, instrumentation and quality control.* A. A. Balkema Publishers.

Pasák, V. (1970). *Wind erosion on soils.* Research Institute for Soil and Water Conservation.

RISWC. (2020, December 5). *Geoportál SOWAC GIS*. https://geoportal.vumop.cz/

Saygin, S. D., Cornelis, W. M., Erpula, G., & Gabriels, D. (2012). Comparison of different aggregate stability approaches for loamy sand soils. *Applied Soil Ecology*, *54*, 1–6.

Šimanský, V., Bajčan, D., & Ducsay, L. (2013). The effect of organic matter on aggregation under different soil management practices in a vineyard in an extremely humid year. *Catena*, *101*, 108–113.

Skidmore, E. L., & Layton, J. B. (1992). Dry soil aggregate stability as influenced by selected soil properties. *Soil Science Society of America Journal*, *56*(2), 557–561.

Skidmore, E. L. (1994). Wind erosion. In R. Lal (Ed.), *Soil erosion research methods* (pp. 265–294). CRC Press.

Tatarko, J. (2001). Soil aggregation and wind erosion: processes and measurements. *Annals of Arid Zone*, *40*(3), 251–263.

Toogood, J. A. (1978). Relation of aggregate stability to properties of Alberta soils. In W. W. Emerson, R. D. Bond, & A. R. Dexter (Eds.), *Modification of soil structure* (pp. 211–215). Wiley.

Visser, S. M., Sterk, G., & Karssenberg, D. (2005). Wind erosion modelling in a Sahelian environment. *Environ. Modell. Software*, *20*, 69–84.

Walkley, A., & Black, T.A. (1934). An examination of the Degtjareff methods for determining of soil organic matter, and a proposed modification of the chromic acid titration method. *Soil Sci.*, *37*, 29–38.

Webb, N. P., & Strong, C. L. (2011). Soil erodibility dynamics and its representation for wind erosion and dust emission models. *Aeolian Res., 3,* 165–179.

Woodruff, N. P., & Siddoway, F. H. (1965). A wind erosion equation. *Soil Science*, *29*(5), 602–608.

Zachar, D. (1982). *Soil Erosion.* Elsevier Science.

Zobeck, T. M., Popham, T. W., Skidmore, E. L., Lamb, J. A., Merill, S. D., Lindstrom, M. J., Mokma, D. L., & Yoder, R. E. (2003). Aggregate-mean diameter and wind-erodible soil predictions using dry aggregate-size distribution. *Soil Science Society of America Journal*, *67*, 425–436.

sciendo

DOI: 10.2478/ahr-2021-0026
Acta hort regiotec, 24, 2021(1): 71–76

Research Article

Geospatial model for establishing constructed wetlands for municipal waste water treatment: Case study in South Bačka District, Serbia

Jasna Grabić, Sanja Antić*, Pavel Benka, Boško Blagojević
University of Novi Sad, Faculty of Agriculture, Departmet of Water Management, Serbia

Article Details: Received: 2020-12-31 | Accepted: 2021-03-08 | Available online: 2021-05-31

Licensed under a Creative Commons Attribution 4.0 International License

SCREENED BY iThenticate® Professional Plagiarism Prevention

The process of integration into the European Union (EU) requires from new member states significant efforts; not only harmonizing legislation but also respecting all posed standards. Among numerous issues, wastewater purification represents a significant request. To achieve the goal of discharging good-quality water into natural water bodies as recipients, various methods have been used. The method of constructed wetland (CW) is based on wastewater purification by using wetland plants. The method of CWs shows the best results for small settlements for up to 5,000 inhabitants and can be nicely integrated within the landscape of a plain where waterbodies' banks are overgrown by wetland plants. Such facilities have been used for decades in the territory of the EU, and only a few have been built in the Republic of Serbia. Since the Republic of Serbia is a candidate country for the EU, there is a strong intention to take action focused upon solving wastewater purification from various sources. Therefore, this paper aims to examine favourable locations for CW installations within the rural area of the South Bačka District. Geographic information system was applied for examination of the basic spatial criteria (distance from the settlement, distance from water bodies, elevation, and land use). These were presented in separate maps and finally in one joint map of favourability for establishing CWs in the vicinity of 35 villages within the District. The obtained results have fulfilled the basic spatial preconditions, but further analyses should be conducted to precisely position the location of each CW concerning land ownership criterion.

Keywords: wastewater treatment, constructed wetland, geographic information system – GIS, South Bačka District

1 Introduction

Natural ecosystems are dependent on water, but also ecology and landscape influence water quality and availability (González et al., 2013). The practice of releasing non-purified water into water bodies leads to deterioration of water quality, eutrophic processes (algal blooms), and might have a significant impact on biodiversity. Until now humans have significantly affected water quality and quantity and therefore the goal of ensuring availability and sustainable management of water and sanitation for all is listed on the 6th place in the UN's "The 2030 Agenda for Sustainable Development" (United Nations, 2015). Due to the overall importance of water and its multipurpose use, it has special protection by a set of regulations under the umbrella of Water Framework Directive – WFD (Directive 2000/60/EC, 2000) in the territory of the EU, which is the most important legal instrument in the field of water in the European Union. Concerning wastewater treatment (WWT), its daughter directive Council Directive 91/271/EEC on urban wastewater treatment, is in charge, while some specific pollutants are covered by the Directive 2013/39/EU (2013), regarding priority substances. The method of constructed wetlands (CWs) as a solution for WWT is well known and has wide applicability (Vymazal, 2005). In recent years upon enacting the Directive 2013/39/EU (2013) regarding priority substances in the field of water policy, the role of CWs was also examined (Gorito et al., 2017), but further research is necessary. Currently, when green technologies are taking advantage and in the context of promoting the circular economy, reconnecting urban environment with nature, CWs are seen as a promising solution. Besides water, purification CWs can provide other services such as habitat creation sites, urban wildlife refuges, recreational or educational facilities, landscape engineering, etc. (Stefanakis, 2019).

Harmonizing with the WFD and later on respecting standards posed by its daughter directives is one of the

***Corresponding Author:** Sanja Antić, University of Novi Sad, Faculty of Agriculture, Trg D. Obardovića 8, 21000 Novi Sad, Serbia; e-mail: sanja.antic@polj.uns.ac.rs

core questions for both members and candidate states. Presently, there is a lack of WWT facilities in Serbia. Therefore, it i imperative for the country, on its way toward joining the EU to provide wastewater purification for all pollution sources (Kolaković et al., 2013; SEPA, 2019). It is necessary to treat wastewater as close as possible to the place of origin which for small settlements excludes large, centralized treatment systems. Besides the conventional method of WWT, CW represents a favourable solution for small settlements for up to 5,000 inhabitants. CWs have been in use for decades worldwide and in Serbia from 2004, when the first CW was established (Josimov-Dundjerski et al., 2013, 2015a). Northern Serbia (Vojvodina Province) has been characterized by flat land, being a part of the Pannonian Plain. Numerous water bodies intersect the plain consisting of rivers and drainage canals, as well as natural wetlands adjacent to river meanders, or formed from abandoned meanders. In such a landscape, common reed (*Phragmites australis* (Cav.) Trin. ex Steud.) builds dense stands along riverbeds. Especially, it covers large areas of wetlands, where it represents dominant vegetation. Bearing this in mind CWs are leading nature-based solutions for wastewater purification. Another important fact is that in the Northern Serbia – Vojvodina Province the dominant type of settlements are villages with up to 5,000 inhabitants (Josimov-Dunđerski et al., 2015b), relatively uniformly dispersed within the landscape, where centralized systems are not an appropriate solution.

The paper aims to select favourable locations for CW installations intended for settlements within the rural area of the South Bačka District. During the examination, the most important spatial criteria were analyzed.

2 Material and methods

2.1 Study area

The research area in this paper encompassed the South Bačka District (Fig. 1). The area is characterised by flat land, mostly cultivated as arable land. Besides, an important feature is a dense hydrographic network consisting of artificial drainage canals, which join rivers. Small settlements – villages are the dominant type of settlements and are relatively uniformly dispersed over the District. The average number of inhabitants for 35 examined settlements was 2,485, while minimum and maximum were 738 and 4,831, respectively (Statistical Office of the Republic of Serbia, 2014). The overall population of the South Bačka District according to the census from 2011 was 86968 inhabitants. This assumes the production of 13,045 m^3 of wastewater daily, if calculated as 150l/day per inhabitant equivalent (Dalmacija, 2010).

2.2 Constructed wetlands

The primary function of CWs is wastewater purification. Wastewater can originate from various sources: municipal, industrial, agriculture, etc. The cores of CWs are wetland plants, which are intentionally planted and irrigated by wastewater. Typical plants of CWs are common reed (*Phragmites australis*) and rush (*Typha angustifolia*). Plants feed on nutrients available in

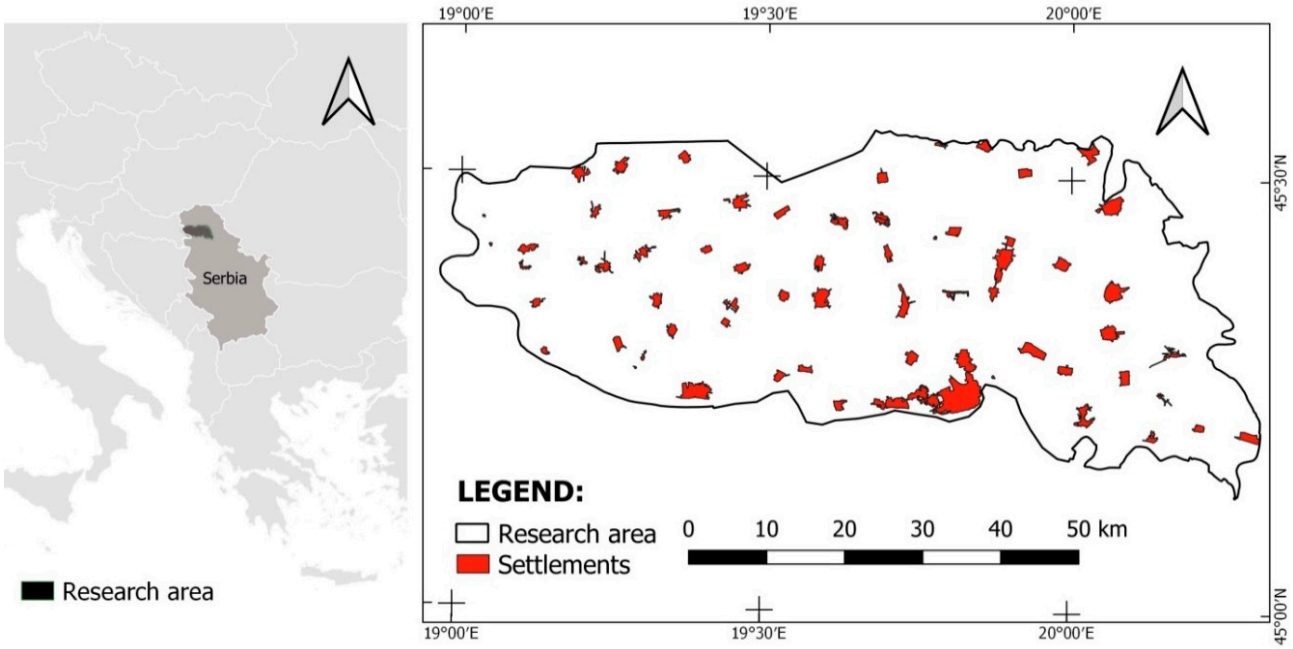

Figure 1 Location of investigated area – the South Bačka District, Republic of Serbia

wastewater and provide oxygen to the root zone. They also enable microorganisms from rhizosphere to conduct nitrification and other processes of degrading organic molecules from wastewater making them available to plants. Additionally, plants absorb and bioaccumulate heavy metals and other toxic compounds (Nikolić et al., 2015). Each CW is composed of several segments/fields which have an impermeable bottom. The segments are placed in line and wastewater flows from one field to another until the end. At the outlet, water is purified up to a level posed by wastewater quality standards. The efficiency of purification depends on a type of CW and can be above 80–90% for total nitrogen, total phosphorus, BOD, COD, and total suspended solids (Vymazal, 2005).

The Pannonian part of Serbia, the Vojvodina Province, is characterized by a flat landscape intersected by the dense hydrographic network. Wetland plants overgrow edges of watercourses and shallow marshy areas, all forming dense uniform stands, providing nesting places for birds and shelter for other organisms. The most represented plant is common reed which is an indigenous species for the region. Therefore, CWs are well-fitting the landscape of the region.

2.3 GIS and analysed data

Presently, for any spatial analysis, support system, such as the geographic information system (GIS) is irreplaceable, where a multi-layered approach facilitates the decision-making process when a land-use prospect is an issue (Muchová et al., 2016). GIS as a spatially oriented information system enables data processing through operations of collecting, storing, handling, analysis, and presentation, which provides the basis for further decision making. Advantage and specifics of GIS in comparison to other databases are the precise definition of the exact place on the Earth's surface to which these data refer. Within GIS, data are organized in layers for easier handling, where each layer is presenting a set of data of the same type. Input GIS data can be in vector format (point, polyline, polygon), or raster format – matrices covering certain space. Each cell of the matrix represents a specific pixel (Benka, 2011).

To fulfil the research aim concerning spatial analyses, free geographic information system (GIS) software QGIS was applied. The main criteria for positioning CWs included following spatial features: distance from a settlement, distance to water bodies, land use, and elevation. For practical reasons, above all satisfying a cost-saving request, a CW had to be in the vicinity of a settlement. For a similar reason, it is important to be close to the watercourse, where purified wastewater will be discharged. For both criteria, the distances of 500 m and 1000 m were chosen and mapped. When building any wastewater facility, it must be positioned at a lower altitude than the settlement. That enables the free low-pressure gravitational flow of wastewater through the sewage network which finishes in the wastewater treatment facility. Therefore, the criterion of elevation was chosen and mapped as a belt surrounding each analysed village. Finally, analysing the land cover after the arable land exclusion, abandoned areas and those covered by grass are assumed as favourable land uses. These data were extracted from CORINE land cover (CLC, 2018). All input data were in vector format except data on elevations – Shuttle Radar Topography Mission (SRTM) 30 (NASA JPL, 2013), which were in raster format.

Additional analysis was focused on grading of individual plots, to obtain a degree of favourability. For this purpose, a system of scoring was set, where points were assigned for each plot according to a level of favourability, i.e. the least favourable – 2 points, less favourable – 3 points, moderately favourable – 4 points, favourable – 5 points

Figure 2 Schematic modelling workflow of the applied processes

and very favourable – 6 points. For each criterion, there were 3 possibilities for grading: 2 points for more favourable, 1 point for less favourable and 0 points for unfavourable. Namely, distances of 500 m from settlement and watercourse were assigned to 2 points, and 1 point if the distance is within 500–1,000 m. Complete schematic modelling workflow, of the processes applied in the paper, is shown in Fig. 2.

3 Results and discussion

After delineation of the study area, GIS layers were formed, where each layer presents one criterion: distances from the settlement (Fig. 3), distances from watercourse (Fig. 4), land use according to the CORINE land cover (CLC) (https://land.copernicus.eu/pan-european/corine-land-cover) (Fig. 5) and elevation SRTM 30. Concerning elevation, all settlements were at the same elevation in comparison to the adjacent area or higher, and therefore this criterion was not further analysed. As for CLC, the analyses were performed only from the attribute tables and were not presented in maps. Finally, all layers were overlapped to form the final map. On this map settlements with more than 5,000 inhabitants were excluded, settlements which have already been connected to centralized wastewater treatment facilities and those already having installed some type of wastewater treatment. Further analysis was orientated towards grading of individual plots, to obtain a degree of favourability. For this purpose, a system of scoring was set, where points were assigned for each plot according to a level of favourability (Table 1). For each criterion, there were 3 possibilities for grading: 2 points for more favourable, 1 point for less favourable and 0 points for unfavourable. Namely, distances of 500 m from settlement and

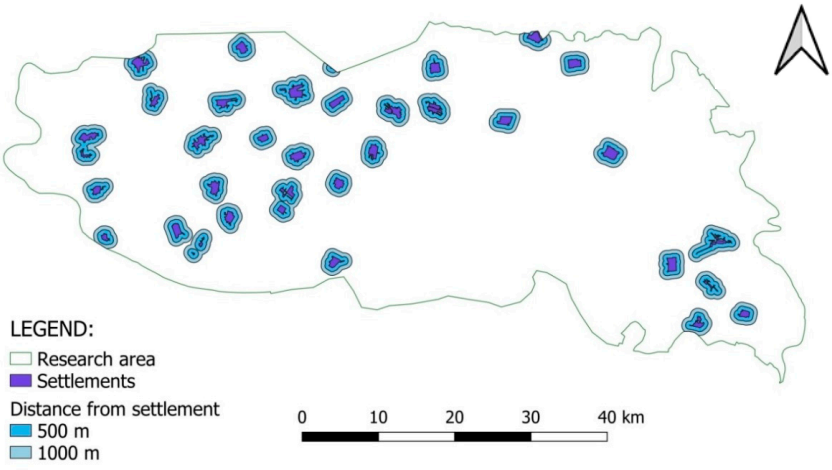

Figure 3 Distance from settlement within the South Bačka District, Republic of Serbia

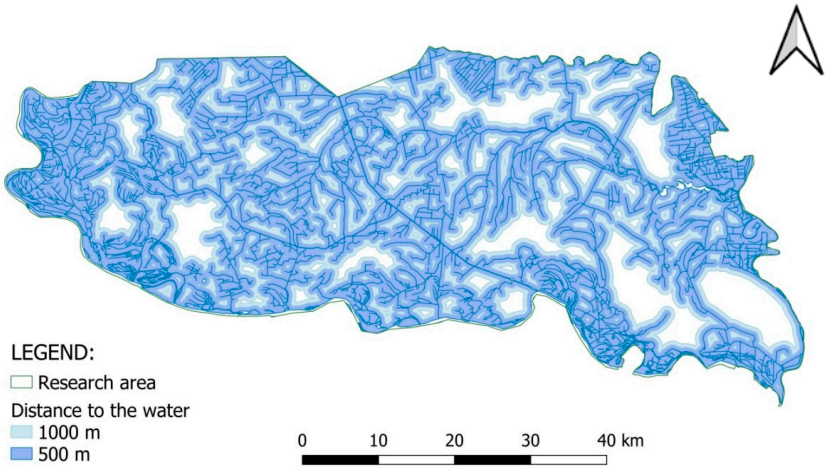

Figure 4 Distance to water bodies within the South Bačka District, Republic of Serbia

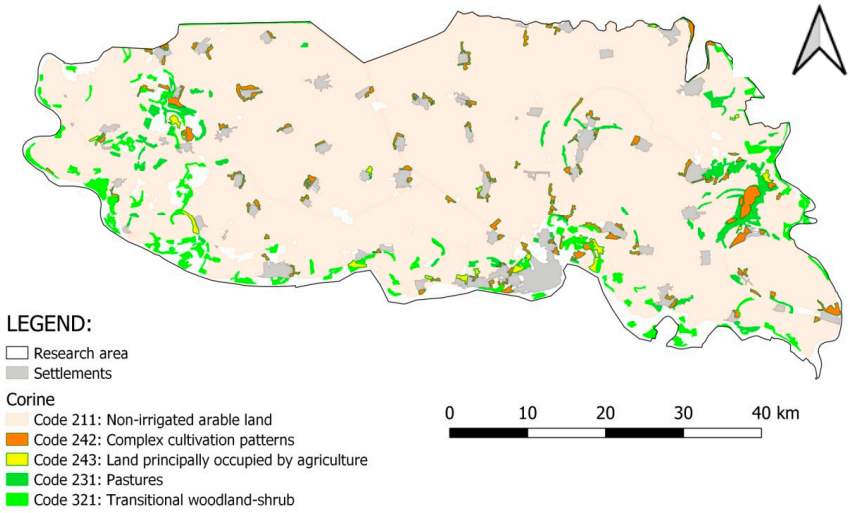

Figure 5 Land use within the South Bačka District, Republic of Serbia
Source: CLC, 2018

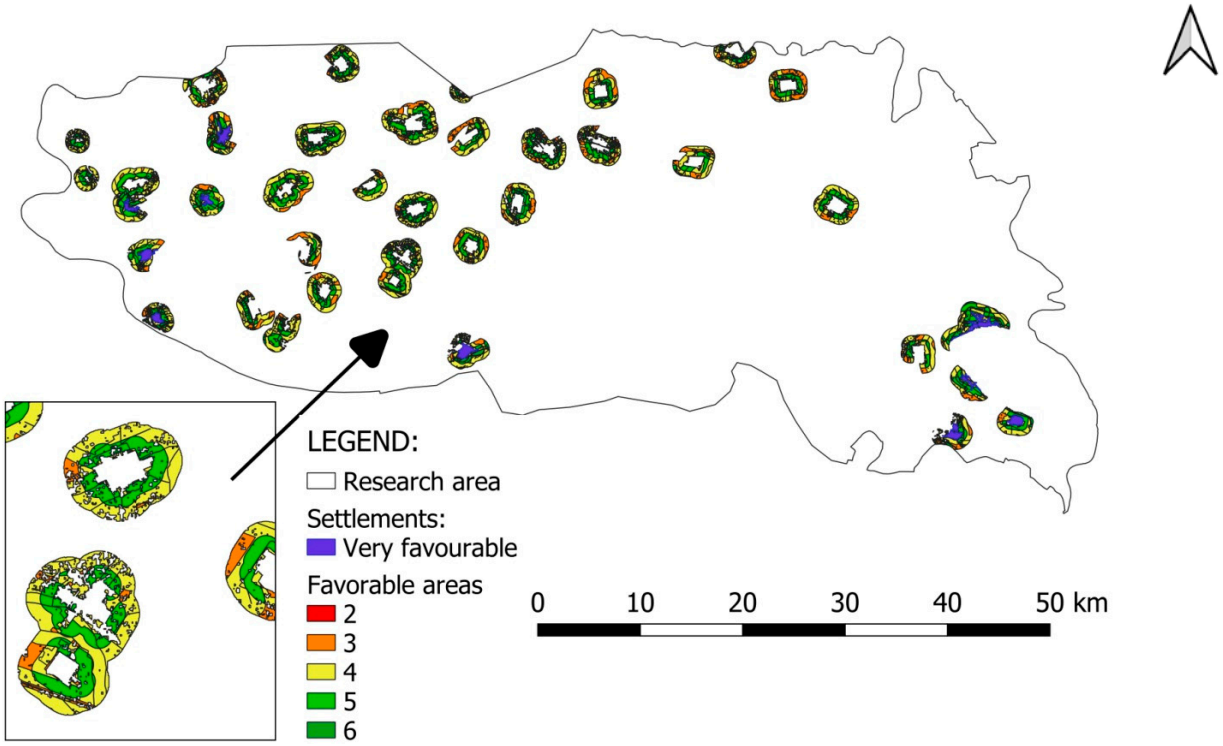

Figure 6 Favourable plots for establishing CWs within the South Bačka District, Republic of Serbia

watercourse were assigned to 2 points, and 1 point if the distance is within 500–1,000 m. Additionally, according to CLC pastures were chosen as favourable areas (code 231) and transitional woodland/shrub (code 324) for which 2 points were assigned. Less favourable areas where 1 point was assigned, were: land principally occupied by agriculture, with significant areas of natural vegetation (code 243), complex cultivation patterns (code 242) and non-irrigated arable land (code 211) (Fig. 5). For this criterion, unfavourable areas were excluded and therefore there was no chance to assign one point to a single plot.

Upon overlapping GIS layers for distances from watercourse and settlement and the land-use layer, the final map was obtained, with grading incorporated. Fig. 6 presents the final result on favourability for positioning CWs in the surrounding area of small settlements within the South Bačka District, Republic of Serbia. According to it, very favourable plots are determined in the vicinity of ten settlements (marked blue in Fig. 6): Bođani, Deronje, Mali Bač, Bačko Novo Selo, Plavna, Čelerevo, Vilovo, Mošorin, Gardinovci and Lok.

4 Conclusions

The problem of untreated wastewater is still present in the South Bačka District, Republic of Serbia, concerning smaller settlements. Thus, this examination focuses upon finding the most favourable locations for positioning CWs in the vicinity of settlements. GIS analyses and further grading of plots revealed that 26,215.32 ha are to some extent favourable for the mentioned purpose. Therefore, the examination proved that in the vicinity of

Table 1 Evaluating plot favourability for positioning CWs

Character of the area upon favourability for positioning CWs	Points	Number of separate plots	Area (ha)
The least favourable	2	12	21.09
Less favourable	3	260	3,757.32
Moderately favourable	4	470	13,897.34
Favourable	5	182	8,207.77
Very favourable	6	22	331.80
Total			26,215.32

© Slovak University of Agriculture in Nitra
www.uniag.sk

35 villages in the South Bačka District, there are spatial preconditions for establishing CWs. The obtained results have fulfilled the basic spatial preconditions. However, further analyses are necessary to be performed for precise positioning of each CW location, taking into account land ownership criterion.

Additionally, the same process could be applied to the whole territory of the Vojvodina Province, covering all its districts. Moreover, it could be utilised even further across the Pannonian Plain stretching to the neighbouring countries (parts of Austria and Slovakia, whole Hungary, and partly Croatia and Romania) since natural features of the terrain and settlements' structure are similar.

Acknowledgments

The research was funded by the Ministry of Education, Science and Technological Development of the Republic of Serbia (Agreement No. 451-03-68/2020-14/ 200117).

References

Benka, P. (2011). Effects of restructuring of land territory by consolidation on the plot suitability for agricultural production, In I. Aleksic (Ed.), *Professional Practice and Education in Geodesy and Related Fields* (pp. 348-355). Faculty of Civil Engineering, University of Belgrade.

CLC – © European Union, Copernicus land Monitoring Service (2018). *Corine Land Cover* [Data set]. European Environmental Agency (EEA). https://land.copernicus.eu/pan-european/corine-land-cover

Dalmacija, B. (Ed) (2010). *Basis of wastewater management.* University of Novi Sad, Faculy of sciences. Department of chemistry, biochemistry and environmental protection (in Serbian)

Directive 2000/60/EC of the European Parliament and of the Council of 23 October 2000 establishing a framework for Community action in the field of water policy. *Official Journal of the European Union, 327*, 1–73.

Directive 2013/39/EU of the European parliament and of the council of 12 August 2013 amending Directives 2000/60/EC and 2008/105/EC as regards priority substances in the field of water policy. *Official Journal of the European Union*, *226*, 1–17.

Directive 1991/271/EEC of 21 May 1991 concerning urban waste-water treatment. *Official Journal of the European Union, 135*, (40–52).

González, H. F., Corvea Porras, J. L., de Bustamante Gutiérrez, I., LaMoreaux, J. W., & Molerio-Leon, L. F. (2013). Management of Water Resources in Protected Areas: An Introduction. In H. F. González, J. L. Corvea Porras, I. de Bustamante Gutiérrez, & J. W. LaMoreaux (Eds.), *Management of Water Resources in Protected Areas* (pp. v–viii). Springer.

Gorito, A. M, Ribeiro, A. R., Almeida, C. M. R., & Silva, A. M. T. (2017). A review on the application of constructed wetlands for the removal of priority substances and contaminants of emerging concern listed in recently launched EU legislation. *Environ Pollution., 227*, 428–443. https://doi.org/10.1016/j.envpol.2017.04.060

Josimov-Dundjerski, J., Belić, A., Salvai, A., & Grabić, J. (2013). Age of Constructed Wetland and Effects of Wastewater Treatment. *Bulgarian Journal of Agricultural Science*, *19*(4), 679–684. http://www.agrojournal.org/19/04-08.pdf

Josimov-Dundjerski, J., Savić, R., Belić, A., Salvai, A., & Grabić, J. (2015a). Sustainability of Constructed Wetland Based on the Characteristics in Effluent. *Agriculture Journals, Soil & Water Resources*, *10*(2), 114–120. http://www.agriculturejournals.cz/publicFiles/152326.pdf

Josimov-Dunđerski, J., Grabić, J., & Belić, A. (2015b). Constructed wetlands in protection of water resources in Vojvodina. *Annals of agronomy*, *39*(1), 24–32. http://scindeks.ceon.rs/article.aspx?artid = 0546-82641501024J

Kolaković, S., Vujović, S., Jeftenić, G., Kolaković, S., & Mašić, B. (2013). Sanitation and waste water management in Vojvodina (Serbia). *The 6th PSU-UNS International Conference on Engineering and Technology* (ICET-2013), Novi Sad, Serbia, University of Novi Sad, Faculty of Technical Sciences, 1–6.

Muchová, Z., Leitmanová, M., & Petrovič, F. (2016). Possibilities of optimal land use as a consequence of lessons learned from land consolidation projects (Slovakia). *Ecological Engineering*, *90*, 294–306. https://doi.org/10.1016/j.ecoleng.2016.01.018

NASA JPL (2013). *NASA Shuttle Radar Topography Mission Global 3 arc second* [Data set]. NASA EOSDIS Land Processes DAAC. https://doi.org/10.5067/MEaSUREs/SRTM/SRTMGL3.003

Nikolić, L J., Maksimović, I., Džigurski, D. & Putnik-Delić, M. (2015). The content of microelements (Cu i Zn) in reed (*Phragmites australis* (Cav.) Trin. ex Steud.) of the constructed wetland system. *Contemporary Problems of Ecology*, *8*(4), 493–498. https://doi.org/10.1134/S1995425515040113

SEPA – Serbian Environmental Protection Agency (2019). *Study in the field of management of municipal waste waters in local municipalities on the territory of the republic of Serbia.* Ministry of environmental protection of the Republic of Serbia. JN 1.2.4/19 (in Serbian)

Statistical Office of the Republic of Serbia (2014). *Comparative overview of the number of population in 1948, 1953, 1961, 1971, 1981, 1991, 2002 and 2011* [Data by settlements].

Stefanakis, A. I. (2019). The Role of Constructed Wetlands as Green Infrastructure for Sustainable Urban Water Management. *Sustainability, MDPI*, *11*(24), 1–19. https://doi.org/10.3390/su11246981

United Nations. (2015). *Transforming Our World, the 2030 Agenda for Sustainable Development.* General Assembly Resolution A/RES/70/1. http://www.un.org/ga/search/view_doc.asp?symbol=A/RES/70/1&Lang=E

Vymazal, J. (2005). Horizontal Subsurface Flow and Hybrid Constructed wetland System for Wastewater Treatment. *Ecological Engineering*, *24*, 478–490. https://doi.org/10.1016/j.ecoleng.2005.07.010

sciendo

DOI: 10.2478/ahr-2021-0027
Acta hort regiotec, 24, 2021(1): 77–79

Short communication

Role of water under the covid-19 pandemic: beneficial or/and detrimental?

Jasna Grabić*, Ksenija Mačkić
University of Novi Sad, Faculty of Agriculture, Departmet of Water Management, Serbia

Article Details: Received: 2020-11-23 | Accepted: 2021-02-22 | Available online: 2021-05-31

Licensed under a Creative Commons Attribution 4.0 International License

SCREENED BY iThenticate Professional Plagiarism Prevention

The COVID-19 pandemic represented a global phenomenon during 2020. It has spread over most of the countries in the world, leading to the infection of millions of people with a death rate of 2-3% simultaneously causing a serious economic crisis. It resulted in significant pollution reduction, but effects to combat COVID-19 led to an increase of some special pollutants. In such circumstances water can be considered as a cleaning and diluting agent for pollutants, providing hygienic conditions, as well as valuable raw material for the production of a variety of goods necessary for combating COVID-19. On the contrary, water can be viewed as a potential threat in relation to the virus spreading. Within the context of the human water cycle, we have identified possible hotspots related to risks of infection spreading. It may occur when contaminated water is reused (grey and black water), or insufficiently purified water enters the environment, which might interfere with drinking water.

Keywords: coronavirus, water resources, public health, wastewater, water reuse

1 Material and methods

The role of water is immense, in particular as it serves as a universal solvent for various substances of inorganic and organic origin from both natural or/and human-made sources. It circulates not only through the hydrological cycle, but also flows through living organisms (Grabić et al., 2020), simultaneously contributing to diverse interactions with living – non-living nature. This complex role of water, which includes the impact of human societies and economies, is presented in Fig. 1. This implicates different or even contradictory roles of water, i.e. clean water vs. polluted water. Especially during the COVID-19 pandemic, water has a dual role. Its positive role is, in the first place, clean drinking water, which keeps supporting general health and good immunity. Another role is keeping hygienic conditions and diluting pollutants. Clean water is an essential raw material for the production of various goods (disinfectants, drugs, etc.) necessary in the fight against COVID-19, as well as for the production of safe food (Grabić et al., 2020).

On the other side, the negative role of water and water-based body fluids (e.g. saliva, urine, blood) during the COVID-19 pandemic is the ability to carry and spread undesired compounds, in this case, coronavirus. It is confirmed that the most common way of spreading infection is by direct contact with an infected person by droplets after sneezing and coughing, and by aerosol (WHO & UNICEF, 2020a). The second question is about the survival of coronavirus in drinking water.

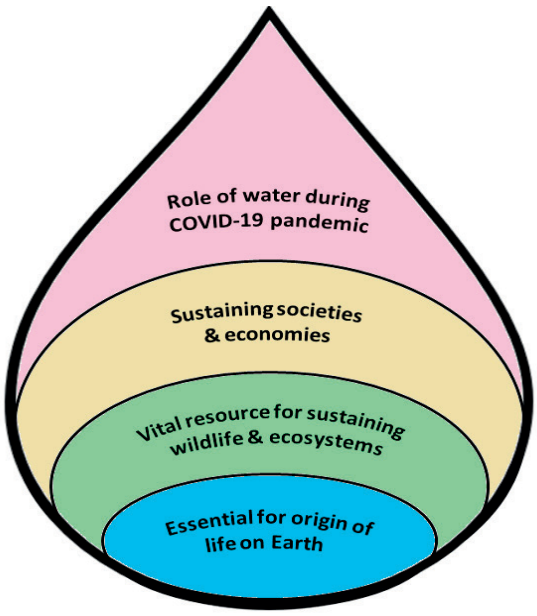

Figure 1 Diverse roles of water apart from and during the COVID-19 pandemic

***Corresponding Author:** Jasna Grabić, University of Novi Sad, Faculty of Agriculture, Trg D. Obradovića 8, 21102 Novi Sad, Serbia; e-mail: grabic.jasna@polj.uns.ac.rs. ORCID: https://orcid.org/0000-0002-6060-5074

A study conducted on other coronaviruses in tap water demonstrated a 99.9% die off within 10 days at 23 °C and over 100 days at 4 °C (Gundy et al., 2009). Bearing in mind that coronaviruses are susceptible to chlorination and UV radiation, there is a predominant opinion that the virus is not likely to be found in drinking water after proper preparation (WHO & UNICEF, 2020b). The third question is related to the presence of the virus in wastewater (WW). Recently, coronavirus has been confirmed in untreated WW in Australia (Ahmed et al., 2020). However, the duration of coronaviruses survival in WW is just 2–4 days (Gundy et al., 2009) and preliminary results showed no infectivity for receiving rivers.

Even efforts to fight pandemics can result in certain water pollution, e.g. remedies used to cure COVID-19 patients (Yang et al., 2020), increased use of disinfectants. Finally, water is also used in the production process of various goods produced exclusively for the prevention of spreading and curing COVID-19 patients, among which are: diverse medical equipment, protective clothes, drugs and vaccines, etc.

2 Results and discussion

The human water cycle is a complex covering all aspects where water is consumed by humans including both clean water uptake and WW generation. Bearing in mind the contradictory role of water during pandemic conditions and to mitigate and overcome the crisis, special attention has to be paid to two aspects:

1. providing sufficient quantities of clean water for drinking and handwashing,
2. adequate treatment or/and management of WW (Fig. 2).

The first aspect addresses water supply services. Namely, it is believed that up-to-date disinfection methods used for drinking water preparation are adequate for coronavirus elimination; nevertheless, water supply services are put to a new challenge, since patterns of distribution have been changed (Cooley et al., 2020). Furthermore, sufficient amounts of water at the required quality are also necessary to satisfy the needs of industry-producing goods intended to suppress the pandemic.

The second aspect is associated with WW management. The research confirmed that the COVID-19 has been found in the faeces of COVID-19 patients, which opens the possibility for fecal-oral transition (Xiao et al., 2020). The duration of the WW treatment process contributes to a decrease in the concentration of coronavirus in the treated WW. However, collateral negative effects may arise from the increased use of disinfectants and antibiotics decreasing the efficiency of the water purification process, especially the biological part of WW treatment.

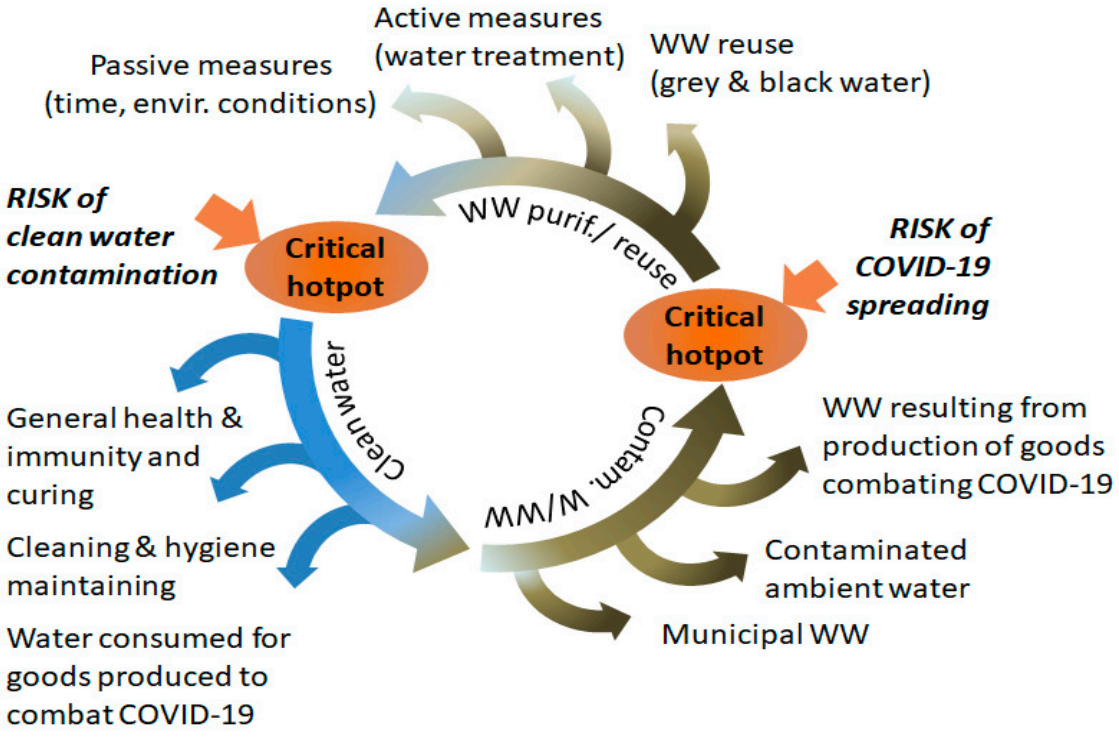

Figure 2 Multiple roles of water during COVID-19 pandemic and critical hotspots

Additionally, there are questions of WW reuse and the use of ambient water where the presence of coronavirus has been confirmed. WHO and UNICEF (2020a) advise never to release "untreated faecal sludge and WW from health facilities... on land used for food production, aquaculture or disposed of in recreational waters". Regarding irrigation, special attention has to be paid to sprinkler irrigation. Namely, this irrigation type produces fine droplets, which are easily turned into aerosols. During the COVID-19 conditions, if there is a concern that water is contaminated by the virus, the application of such irrigation practice should be restricted. Similarly, greywater application has to be restricted only to the irrigation of outdoor greenery, while it should be avoided when it comes to the irrigation of plants intended for food (especially fruits and vegetables) (Grabić et al., 2020). Using contaminated water on farms poses a risk for farmers to get in touch with the virus during harvesting fruits or vegetables, or conducting daily routines related to raising domestic animals. Finally, to conclude, during the pandemic, uncontaminated water – virus-free – is a crucial component in the production of safe food (Grabić et al., 2020). As a precaution measure, wearing protective clothes, gloves, and facial masks for workers, engaged in WW treatment/reuse, must be applied as obligatory (Dabić et al., 2018). Another recommendable measure is WW testing on the presence of COVID-19 and acting according to the results.

In developed countries, obligatory WW treatment enables the elimination of the virus during the process of WW treatment, and only in cases of incomplete WW treatment, a small portion of the virus can survive. Since the problem of water pollution is more pronounced in developing countries (UNESCO & WHO, 2019), there is a risk of coronavirus spread off using contaminated untreated surface water and unprepared drinking water originating from contaminated surface waterbodies.

Acknowledgment

This work was supported by the Ministry of Education, Science and Technological Development of Serbia (Grant No. 451-03-68/2020-14/ 200117)

References

Ahmed, W., Angel, N., Edson, J., Bibby, K., Bivins, A., O'Brien, J. W., Choi, P. M., Kitajima, M., Simpson, S. L., Li, J., Tscharke, B., Verhagen, R., Smith, W. J. M., Zaugg, J., Dierens, L., Hugenholtz, P., Thomas, K. V., Mueller, J.F. (2020). First confirmed detection of SARS-CoV-2 in untreated wastewater in Australia: A proof of concept for the wastewater surveillance of COVID-19 in the community. *Sci. Total Environ*., *728*.

Cooley, H., Gleick, P. H., Abraham, S., & Cai, W. (2020). *Water and the COVID-19 Pandemic: Impacts on Municipal Water Demand.* Issue Brief (Pacific Institute, Oakland, CA, July 2020). Retrieved from: https://pacinst.org/wp-content/uploads/2020/07/Water-and-COVID-19_Impacts-on-Municipal-Water-Demand_Pacific-Institute.pdf

Dabić, B., Mladenović, E., & Grabić, J. (2018). The potential of greywater for irrigation of urban greenery: the situation in the Republic of Serbia. *Glasnik Šumarskog fakulteta Univerziteta u Banja Luci, 1*(28*)*, 103–112 (in Serbian).
DOI: https://doi.org/10.7251/GSF1828103D

Grabić, J., Zemunac, R., Bubulja, S., & Dabić, B. (2020). Importance of water for safe food production and public health protection under COVID-19 pandemic. *XXIV International Eco-Conference, XI Safe Food 2020,* Novi Sad, Serbia, 133–140.

Gundy, P. M., Gerba, C. P., & Pepper, I. L. (2009). Survival of coronaviruses in water and wastewater. *Food Environ Virol., 1*, 10.

UNESCO & WHO (2019). *Progress on Household Drinking Water, Sanitation and Hygiene 2000–2017: Special Focus on Inequalities* (UNESCO & WHO, New York).

WHO & UNICEF. (2020a) *Water, sanitation, hygiene and waste management for the COVID-19 virus.* Technical brief.

WHO & UNICEF (2020b). *Water, sanitation, hygiene, and waste management for SARS-CoV-2, the virus that causes COVID-19*. Interim guidance.

Xiao, F., Sun, J., Xu, Y., Li, F., Huang, X., Li, H., Zhao, J., Huang. J., & Zhao J., (2020). Infectious SARS-CoV-2 in feces of patient with severe COVID-19. *Emerg. Infect. Dis*., *26*, 1920–1922.

Yang, C., Song, G., & Lim, W. (2020). A review of the toxicity in fish exposed to antibiotics. *Comp Biochem Physiol C Toxicol Pharmacol, 237*, 108840.